LAPPEENRANTA UNIVERSITY OF TECHNOLOGY
LUT School of Energy Systems
LUT Mechanical Engineering

Antti Ahola

EFFECT OF LOADING TYPE ON THE FATIGUE STRENGTH OF SYMMETRIC AND ASYMMETRIC WELDED JOINTS MADE OF ULTRA HIGH STRENGTH STEEL

Examiners: Prof. Timo Björk
D.Sc. (Tech.) Timo Nykänen

ABSTRACT

Lappeenranta University of Technology
LUT School of Energy Systems
LUT Mechanical Engineering

Antti Ahola

Effect of loading type on the fatigue strength of symmetric and asymmetric welded joints made of ultra high strength steel

Master's thesis

2016

78 pages, 46 figures, 12 tables, 13 appendices

Examiners: Prof. Timo Björk
D.Sc. (Tech.) Timo Nykänen

Keywords: bending load, fatigue, local approaches, welded joints

In this study, finite element analyses and experimental tests are carried out in order to investigate the effect of loading type and symmetry on the fatigue strength of three different non-load carrying welded joints. The current codes and recommendations do not give explicit instructions how to consider degree of bending in loading and the effect of symmetry in the fatigue assessment of welded joints.

The fatigue assessment is done by using effective notch stress method and linear elastic fracture mechanics. Transverse attachment and cover plate joints are analyzed by using 2D plane strain element models in FEMAP/NxNastran and Franc2D software and longitudinal gusset case is analyzed by using solid element models in Abaqus and Abaqus/XFEM software. By means of the evaluated effective notch stress range and stress intensity factor range, the nominal fatigue strength is assessed. Experimental tests consist of the fatigue tests of transverse attachment joints with total amount of 12 specimens. In the tests, the effect of both loading type and symmetry on the fatigue strength is studied.

Finite element analyses showed that the fatigue strength of asymmetric joint is higher in tensile loading and the fatigue strength of symmetric joint is higher in bending loading in terms of nominal and hot spot stress methods. Linear elastic fracture mechanics indicated that bending reduces stress intensity factors when the crack size is relatively large since the normal stress decreases at the crack tip due to the stress gradient. Under tensile loading, experimental tests corresponded with finite element analyzes. Still, the fatigue tested joints subjected to bending showed the bending increased the fatigue strength of non-load carrying welded joints and the fatigue test results did not fully agree with the fatigue assessment. According to the results, it can be concluded that in tensile loading, the symmetry of joint distinctly affects on the fatigue strength. The fatigue life assessment of bending loaded joints is challenging since it depends on whether the crack initiation or propagation is predominant.

TIIVISTELMÄ

Lappeenrannan teknillinen yliopisto
LUT School of Energy Systems
LUT Kone

Antti Ahola

Kuormitustavan vaikutus suurlujuusteräksisten symmetristen ja epäsymmetristen hitsattujen liitosten väsymiseen

Diplomityö

2016

78 sivua, 46 kuvaa, 12 taulukkoa ja 13 liitettä

Tarkastajat: Prof. Timo Björk
TkT Timo Nykänen

Asiasanat: taivutuskuormitus, väsyminen, paikallismenetelmät, hitsatut liitokset

Tässä työssä tutkitaan FE-analyysien ja kokeellisten tutkimusten avulla kuormitustyypin ja liitoksen symmetrisyyden vaikutusta kuormaa kantamattomien hitsattujen liitosten väsymisominaisuuksiin. Nykyiset ohjeistukset ja standardit eivät anna selkeitä ohjeita siitä, kuinka taivutuksen osuus kuormituksessa ja liitoksen symmetrisyys otetaan huomioon hitsattujen liitosten väsymismitoituksessa.

Väsymisanalyyseissä käytetään tehollisen lovijännityksen menetelmää sekä lineaarielastista murtumismekaniikkaa. Poikittainen ripaliitos ja päällekkäisliitos, analysoidaan käyttämällä 2D tasovenymäelementtimalleja FEMAP/NxNastran- ja Franc2d-ohjelmilla, ja pitkittäiset ripaliitoksen tapaus analysoidaan käyttämällä solidimalleja Abaqus- ja Abaqus/XFEM-ohjelmilla. Määritettyjen tehollisen lovijännitysvaihtelun ja jännitysintesiteettikertoimen vaihtelun avulla lasketaan liitoksen nimellinen väsymislujuus. Kokeellinen osuus koostuu 12:sta kuormaa kantamattoman liitoksen väsytyskokeesta. Testeillä tutkitaan sekä kuormitustyypin että liitoksen symmetrisyyden vaikutusta väsymislujuuteen.

FE-analyysit osoittivat, että epäsymmetrisen liitoksen väsymislujuus on parempi vetokuormituksessa ja symmetrisen liitoksen väsymislujuus taivutuskuormituksessa, kun väsymislujuutta tarkastellaan nimellisen ja rakenteellisen jännityksen menetelmillä. Lineaarielastinen murtumismekaniikka viittasi siihen, että taivutus pienentää jännitysintesiteettikertoimen arvoja, kun särö on suhteellisen suuri, sillä normaalijännitys pienenee särön kärjessä jännitysgradientin takia. Vetokuormituksessa, väsytyskokeiden tulokset olivat yhteneväiset FE-analyysien kanssa. Kuitenkin taivutusväsytyskokeissa havaittiin, että taivutuskuormitus parantaa kuormaa kantamattoman liitoksen väsymiskestävyyttä, ja väsytyskoetulokset eivät täysin olleet FE-analyysien kanssa yhteneväiset. Tulosten perusteella voidaan tehdä johtopäätös, että symmetrisyydellä on selvä vaikutus väsymiskestävyyteen vetokuormituksessa. Väsymiskestävyyden arviointi taivutuskuormituksessa on haastavaa, sillä se määräytyy siitä, onko särön ydintyminen vai kasvaminen määräävää.

ACKNOWLEDGEMENTS

First of all, I would like to thank Professor Timo Björk and Assistant Professor Timo Nykänen from the Laboratory of Steel Structures in Lappeenranta University of Technology for supervising and giving good and valuable advice during this work. I would also like to show my gratitude to the employees of the laboratory for carrying out the experimental tests, not forgetting all the junior researchers of Steel Structures who gave me plenty of great tips for practical work. Moreover, I want to express my gratitude to BSA program for funding this thesis.

Additionally, thanks to my family and my other half for their supportive encouragement during this thesis and my studies.

Antti Ahola

In Lappeenranta, 17th of March 2016

TABLE OF CONTENTS

ABSTRACT
TIIVISTELMÄ
ACKNOWLEDGEMENTS
TABLE OF CONTENTS
LIST OF SYMBOLS AND ABBREVIATIONS
1 INTRODUCTION 10
1.1 Background of the Study 10
1.2 Objectives 13
1.3 Structure and Limitations of the Study 13
2 THEORY 15
2.1 Fatigue Assessment Methods 16
2.1.1 Nominal Stress Method 18
2.1.2 Hot Spot Stress Method 18
2.1.3 Effective Notch Stress Method 19
2.1.4 Linear Elastic Fracture Mechanics 21
2.2 Literature Review 23
2.2.1 Effect of Loading Type 23
2.2.2 Effect of Geometrical Symmetry 27
3 RESEARCH METHODS 31
3.1 FE-analyses of 2-Dimensional Cases 31
3.1.1 Effective Notch Stress Method – 2D-joints 32
3.1.2 Linear Elastic Fracture Mechanics – Crack propagation of 2D-joints 33
3.2 FE-analysis of Longitudinal Gusset Case 34
3.2.1 Effective Notch Stress Method – Longitudinal Gusset 35
3.2.2 Linear Elastic Fracture Mechanics – Longitudinal Gusset 36

3.3 Experimental tests 38
3.3.1 Test Specimens 39
3.3.2 Measurements 41
3.3.3 Test Set-ups and Instrumentations 42
3.3.4 FE-analyses of test specimens 45
4 RESULTS 48
4.1 2-Dimensional Cases 48
4.2 Longitudinal Gusset Case 52
4.3 Results of Experimental Tests 55
4.3.1 Preparing of Test Specimens 55
4.3.2 Fatigue Test Results 57
4.3.3 Numerical Analysis 63
5 DISCUSSION 67
5.1 Conclusions 68
5.2 Further Research 69
6 SUMMARY 71
REFERENCES 73
APPENDICES
Appendix I: Fatigue Classifications – Nominal Stress Method
Appendix II: Fatigue Classifications – Hot Spot Stress Method
Appendix III: Factors of Effective Notch Stress Method
Appendix IV: Procedure of Regression Analysis
Appendix V: Stress Concentration Factor Formulae by Tsuji
Appendix VI: Bending and Thickness Correction Factor by Maddox
Appendix VII: Welding Parameters of Test Specimens
Appendix VIII: Detailed Results of Transverse Attachment Case
Appendix IX: Fatigue Strength Ratios for $t_1/t_0 = 0.5$ and $t_1/t_0 = 1.0$
Appendix X: Detailed Results of Cover Plate Case
Appendix XI: Effective Notch Stresses of Longitudinal Gusset Joints
Appendix XII: Measured Shape Laser Data
Appendix XIII: Fatigue Test Results

LIST OF SYMBOLS AND ABBREVIATIONS

A_5	Elongation [%]
a	Crack depth or throat thickness [mm]
a_f	Final crack depth [mm]
a_i	Initial crack depth [mm]
b	Plate width [mm]
C	Fatigue capacity [MPa^m] or
	Crack propagation coefficient [da/dN in mm/cycle and ΔK in Nmm$^{-3/2}$]
c	Half of crack width [mm]
E	Modulus of elasticity [GPa]
FAT	Fatigue class [MPa]
f_y	Yield strength [MPa]
f_u	Ultimate strength [MPa]
g	Gap [mm]
I	Current [A]
j_σ	Safety factor [-]
k	Factor for the calculation of characteristic value
k_f	Effective stress concentration factor [-]
k_{hs}	Structural stress concentration factor [-]
k_m	Structural stress concentration factor for misalignment [-]
k_t	Stress concentration factor [-]
k_{tb}	Thickness and bending correction factor [-]
L	Length of attachment or gusset length [mm]
l	Half of distance between clamps [mm]
M_k	Stress magnification factor due to nonlinear stress peak [-]
m	Slope of S-N curve or fatigue crack growth exponent [-]
N_f	Fatigue life in cycles [-]
n_i	Number of cycles at the ith stress range [-]
n_t	Thickness correction exponent [-]
Q	Heat input [kJ/mm]
Q_{loss}	Heat input with losses [kJ/mm]

q_{geom}	Fatigue strength ratio for geometrical symmetry [-]
q_{load}	Fatigue strength ratio for loading type [-]
R	Applied stress ratio [-]
$R_{p0.2}$	Yield strength, corresponding with 0.2% strain [MPa]
Stdv	Standard deviation [-]
s	Factor for stress multiaxiality and strength criterion [-]
t	Plate thickness [mm]
$t_{8/5}$	Cooling time (800°C–500°C) [s]
U	Voltage [V]
v_w	Travel speed [mm/s]
v_{wire}	Wire feed speed [m/min]
W1-4	Weld pass ID number [-]
Y	Correction term [-]
α	Angular misalignment [rad]
ΔK	SIF range [MPa$\sqrt{\text{mm}}$]
$\Delta\varepsilon$	Strain range [μStr]
$\Delta\sigma$	Stress range [MPa]
θ	Flank angle [°]
ν	Poisson's ratio [-]
ρ	Actual notch radius [mm]
ρ^*	Substitute micro-structural length [mm]
ρ_f	Fictitious notch radius [mm]
Ω	Degree of bending [-]
σ	Stress [MPa]
σ_{res}	Residual stress [MPa]

Indices

0	Base plate value
1	Attached plate value
a	Crack depth value
asym	Asymmetric joint
b	Bending
c	Crack end value

char	Characteristic value (95 % survival probability)
ens	Effective notch stress
eq	Equivalent value
hs	Hot spot
m	Membrane
mean	Mean value
nom	Nominal value
ns	Notch stress
SG	Strain gage value
SL	Shape laser value
sym	Symmetric joint

BEM	Boundary element method
CVN	Charpy V-notch
DNV	Det Norske Veritas
DOB	Degree on bending
ENS	Effective notch stress
FEA	Finite element analysis
FEM	Finite element method
HFMI	High Frequency Mechanical Impact Treatment
HS	Hot Spot
IIW	International Institute of Welding
LEFM	Linear elastic fracture mechanics
LSE	Linear surface extrapolation
MSSPD	Minimization of the sum of squared perpendicular distances from a line
SIF	Stress intensity factor
S-N	Stress-Fatigue life
TTWT	Through thickness at weld toe
UHSS	Ultra-high strength steel
WPS	Welding procedure specification
XFEM	Extended finite element method

1 INTRODUCTION

The use of high strength and ultra-high strength steels (UHSS) has increased significantly over the last few decades. Along with the development of UHSS manufacturing, the strength of steel can be produced by heat treatments, e.g. by direct quenching, instead of alloying. The less steel is alloyed, the better the weldability of material typically is. By exploiting the strength of UHSS, plate thicknesses of structures can be decreased and payload increased. This master's thesis is a part of FIMECC's BSA (Breakthrough Steels and Applications) program. One of the objectives of the project is to develop new economically and environmentally sustainable steel and cast materials (Fimecc, 2015).

The structures made of UHSS are often under fatigue loading. The fatigue of welded UHSS and fatigue assessment methods have been widely studied in the recent years. Still, more accurate predictions of fatigue capacity require more detailed fatigue assessment approaches and the consideration of structure's local geometry. In this thesis, the effect of symmetry and local geometry on fatigue capacity is studied. The observed non-load carrying welded joint types are presented in Figure 1.

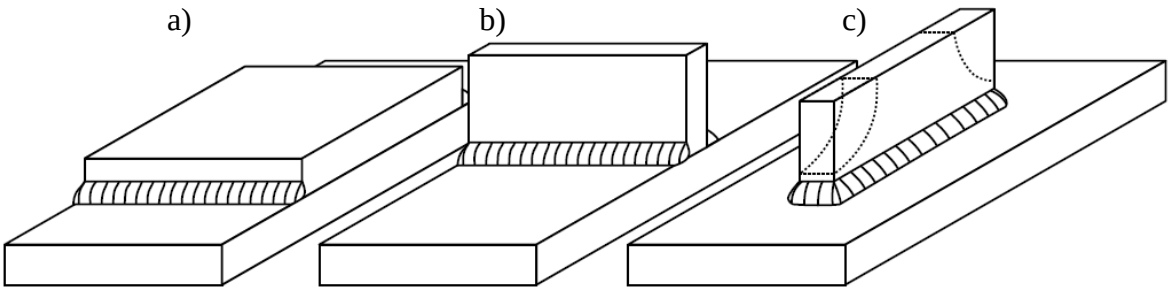

Figure 1. Studied non-load carrying joint types: (a) cover plate (b) transverse attachment and (c) longitudinal gusset with and without smooth transitions.

1.1 Background of the Study

Geometrical symmetry stands for the symmetry of attached plates. In a symmetric case, attached plates are on the both sides of a base plate. Respectively, in an asymmetric case the attached plate is one-sided. The difference between asymmetric and symmetric joints are illustrated in Figure 2. The symmetry of loading can be defined as a degree of bending

(DOB). In a symmetric loading case, structure is tensile loaded and in asymmetric loading, nominal stress distribution through plate thickness is not constant. Bending is an example of asymmetric loading.

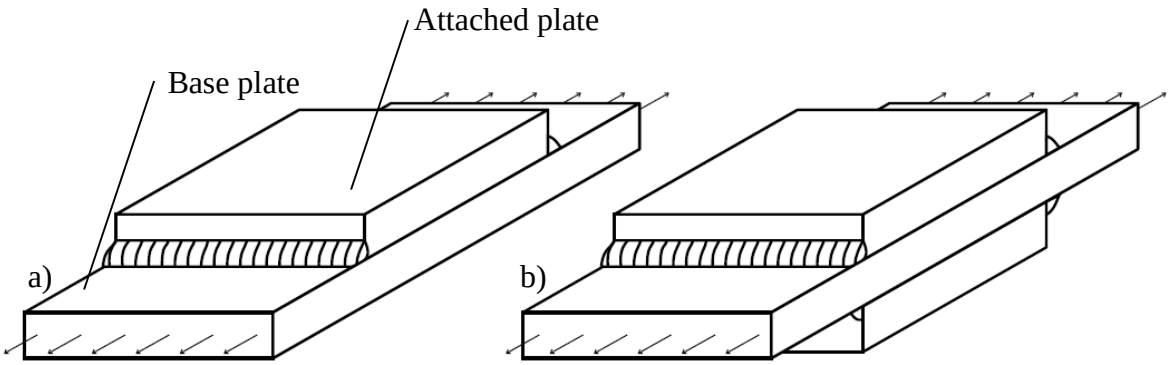

Figure 2. Geometrical symmetry in cover plate joint: (a) asymmetric and (b) symmetric case under symmetric (tensile) loading.

The effect of symmetry on fatigue capacity has not been studied comprehensively yet. However, it has been found that the symmetry has influence on the fatigue capacity. Skriko (2014, p. 16-17) found that the fatigue strength of asymmetric joints was clearly better compared to the capacity of symmetric joints subjected to tensile loading in the fatigue tests of non-load carrying joints. The axial misalignment was studied by Mbeng (2007) and it was discovered that axial misalignment reduces the fatigue strength of symmetric transverse attachment joint to certain point since it develops a secondary bending stress component. When the misalignment is high enough, the fatigue strength increases again since the joint behaves more or less like a T-joint. (Mbeng, 2007, p. 40.) Additionally, computational analyses have shown different fatigue properties in asymmetric and symmetric cases (Salehpour, 2013, p. 53). So far, the symmetry is neglected in International Institute of Welding (IIW) fatigue design recommendations for welded joints (Hobbacher, 2014, p. 63; 76–77).

In real structures, the phenomenon can appear in panels where the stiffness is not constant through the plate width *b*. One example is a bending loaded I-beam with a transverse attachment in the tensile flange, Figure 3. Close to the edge of the flange, the joint corresponds to the asymmetric case. Respectively, on the center line of the flange above the web, the constraint is nearly equivalent with the symmetric case. Nominal stress in the flange

is close to pure membrane stress if the flange is thin with respect to the total height of the I-beam.

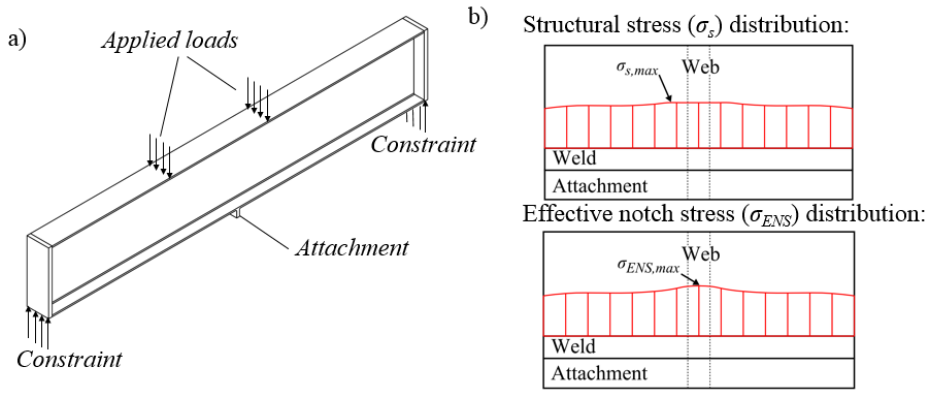

Figure 3. (a) Four-point bending loaded I-beam with transverse attachment and (b) schematic stress distributions described on bottom view (modified: Laamanen, 2013, p. 67–70).

When the fatigue assessment is conducted by structural hot spot (HS) stress approach, the maximum HS stress does not concentrate above the web but aside from the center line. Eventually, the maximum HS point depends on the geometry of the I-beam, and it appears either on the edge of the flange or slightly aside from the center line, as illustrated in Figure 3. When total stress at weld toe is taken into account by utilizing effective notch stress (ENS) approach, the notch stress is highest on the center line. Therefore, it can be found that the notch effect depends on the local constraints of joint. Fatigue assessment based on the total stress is supposedly the most accurate stress based method. Hence, using a HS stress method can lead to conservative assessments of fatigue life or to incorrect assumptions of crack initiation point. The identified phenomenon can appear in other structures where the stiffness of panel alternates locally (e.g. longitudinal or transverse stiffeners of panels).

This study continues the research which was started in the bachelor's thesis of the author. In the bachelor's thesis, the effect of geometrical symmetry on notch stress at weld toe was only studied. (Ahola, 2015, p. 5–8.) In this study, the phenomenon is expanded to the different types of joints. Furthermore, various fatigue assessment approaches are considered. Laboratory tests are typically carried out for the joints subjected to membrane loading. Bending loading is consider in this study, as well.

1.2 Objectives

The main objective of this study is to determine the effect of symmetry in geometry and loading on the fatigue strength of non-load carrying welded joints. The magnitude of the effect for various joints is defined by computational analysis. The observed results of bending loaded joints are compared with experimental tests. Furthermore, the variables influencing the difference in fatigue capacity between the asymmetric and symmetric case are studied. With various geometrical variables, e.g. throat thickness and length of attached joint, the phenomenon is authenticated. The research questions of this study can be formed as follows:

- How does symmetry affect on fatigue capacity and what is the magnitude of the effect?
- Are the result obtained with different fatigue assessment approaches comparable?
- How does the DOB affect on the fatigue capacity of non-load carrying joints?

1.3 Structure and Limitations of the Study

This study is mainly based on structure analysis made by finite element analysis (FEA). The researched joints are modeled and analyzed as geometrically asymmetric and symmetric. Both cases are tensile and out-of-plane bending loaded. The fatigue capacity of the joints are determined by stress based approaches and linear elastic fracture mechanics (LEFM). All analyses are based on finite element method (FEM). The fatigue strength of transverse attachment joints is evaluated in the fatigue tests made at Laboratory of Steel Structures and the results are compared to the FEA results.

Only non-load carrying joint types are studied in this thesis. Welds are assumed to be ideal which means that welds of the FE-models are modeled as filled welds with no penetration. In reality, penetration occurs but usually penetration is neglected in design and calculations according to standards if the weld is not fully penetrated. In addition, flank angle θ is assumed to be 45°. In laboratory tests, all specimens are in as-welded condition which leads to the assumption of high tensile residual stresses σ_{res} when it is justified that all stress ranges are effective.

The influence of welding deformations on structural stresses can be significant in some cases particularly in thin plates. Nevertheless, manufacturing aspects are neglected in the

computational study part because the phenomenon is only slightly researched and the fundamental idea must be understood first. Furthermore, the influences of real structures' constraints are difficult to be quantified exactly so they are neglected. When FEA is conducted for a comparison to test results, also the manufacturing and constraint aspects are taken into account.

2 THEORY

The fatigue of welded structures is caused by fluctuating load. Stress range is typically a result of variation of payload's magnitude and direction, or variation of load's location and position. In addition, load range can be a result of several other things, for example fluctuation of temperature and dynamic response of structure. Although, in these situations stress range is usually lower than in above-mentioned situations and fatigue assessment is not necessarily required in addition to static load designing. (Niemi, 2003, p. 92.)

Fluctuating load and developed stress range can be constant or variable amplitude. In most of real structure cases, loading is somehow irregular so stress range and mean stress level vary. Variable amplitude range can be converted to equivalent stress range by considering single stress ranges. The most common method is rainflow counting method. Constant and variable amplitude stress range is illustrated in Figure 4. (Hobbacher, 2014, p. 37.)

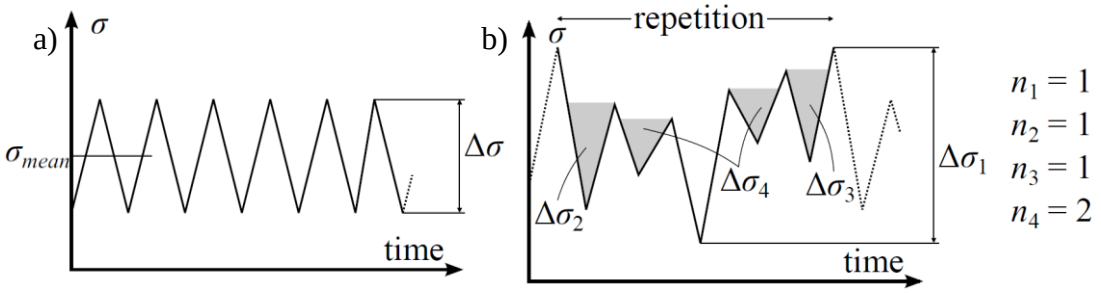

Figure 4. (a) Constant and (b) variable amplitude stress range $\Delta\sigma$ in stress-time history. σ_{mean} is mean stress and n_i is number of cycles at ith stress range.

Variable amplitude stress ranges can be converted to an equivalent constant amplitude range according to Palmgren-Miner rule and the equation can be written as follows if the stress ranges are in the same Stress-Fatigue life (S-N) curve area:

$$\Delta\sigma_{eq} = \sqrt[m]{\frac{\sum[\Delta\sigma_i{}^m \cdot n_i]}{\sum n_i}}, \tag{1}$$

, where $\Delta\sigma_{eq}$ is equivalent stress range and m the slope of S-N curve. Otherwise, stress ranges outside m-slope area must be converted to the same area at first. Furthermore, stress ranges which do not exceed the defined threshold value of stress range, should be neglected. Σn_i can be replaced with 1 if a repetition is considered as one cycle. (Hobbacher, 2014, p. 115.)

2.1 Fatigue Assessment Methods

Fatigue assessment approaches presented in this chapter are based on the recommendations of IIW commission XIII which is specialized in fatigue of welded structures. The designing of steel structures, in Finland and in the rest of the Europe, follows Eurocode 3 which presents instructions for the designing of fatigue. In Eurocode 3, only nominal and structural stress approaches are presented, whereas in the recommendations of IIW, more accurate notch stress and stress intensity factor (SIF) based fatigue assessment methods are also considered. In the case of corresponding instructions, both specifications are mainly consistent. (Hobbacher, 2014, p. iii–iv; EN 1993-1-9, 2009, p. 2.)

The usage of IIW recommendations for assessment of fatigue strength is valid if material and loading fulfil the following requirements:

- Material: pearlitic ferrite or bainitic structural steels, which yield strength f_y is less than 960 MPa, austenitic stainless steels or aluminium alloys.
- Loading conditions: nominal stress range $\Delta\sigma_{nom}$ is less than $1.5 \cdot f_y$ and maximum stress of fatigue loading is less than f_y. Structure is not in corrosive circumstances and creep does not exist.

(Hobbacher, 2014, p. 1).

The material used in this study is SSAB's Strenx® S960 MC UHSS (f_y = 960 MPa). The microstructure of the steel is bainitic martensitic. Stress ranges and maximum stresses applied in this study are kept within allowed limitations mentioned above. (SSAB, 2015.)

In the stress based fatigue assessment approaches (nominal stress, HS stress and ENS methods), the stress is compared to the fatigue classification of the joint type or method. Fatigue class is defined as a stress range which welded joint carries $2 \cdot 10^6$ cycles. (Hobbacher, 2014, p. 6.) Fatigue capacity can be assessed with stress based methods as:

$$FAT^m \cdot 2 \cdot 10^6 = \Delta\sigma^m \cdot N_f = C \quad (2)$$

In Equation (2), *FAT* is fatigue class, N_f fatigue life in cycles and *C* fatigue capacity. LEFM is based on calculation of SIF range which is linearly dependent on stress range. Accuracy and workload of fatigue assessment increases from nominal stress method to LEFM. Details considered fatigue assessment in different concerned methods is illustrated in Figure 5.

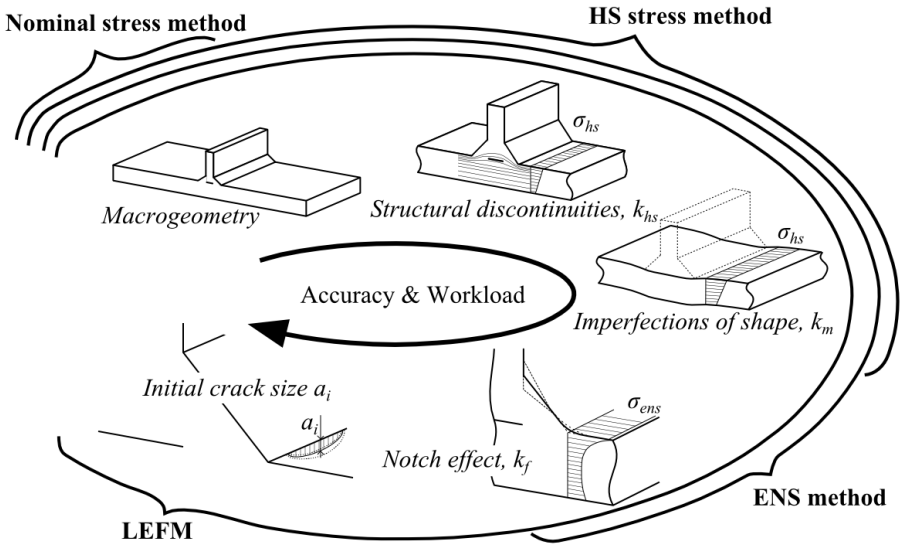

Figure 5. Details included in the observed fatigue assessment approaches according to Niemi (2003, p. 95). σ_{hs} is HS stress, σ_{ens} ENS, k_{hs} structural stress concentration factor, k_m structural stress concentration factor for misalignment and k_f effective stress concentration factor.

IIW recommends that the m = 3 slope is applied in the usage of S-N curves. The slope is based on numerous amounts of fatigue tests but it can be different for various materials and joints. If the slope is defined for certain material and joint, the obtained slope can be used in the fatigue design. Fatigue classes used in practical design, Equation (2), are characteristic values, FAT_{char}, which takes the deviation of service life into account. Characteristic values represent the 95 % survival probability and are determined by means of the standard deviation of large-scale fatigue tests. The procedure of characteristic FAT's calculation is presented in Appendix IV. (Hobbacher, 2014, p. 41; 94; 147–150.)

The standard procedure of IIW is based on the fact that fatigue life (dependent variable) is a function of stress range. Average horizontal distance to assessed curve is evaluated in log-

log coordinate system. Nykänen & Björk (2015, p. 295–296) have presented a more comprehensive method for curve fitting. It is based on minimization of the sum of perpendicular distances from a line (MSSPD), but it is not approved officially, yet.

2.1.1 Nominal Stress Method

Nominal stress approach is based on stress far from the observed area in structure. Although only nominal stress range $\Delta\sigma_{nom}$ is determined, various welded geometries and qualities are considered in fatigue classifications. Furthermore, structural discontinuities, imperfections of manufacturing, notch stresses, and residual stresses are included in fatigue classifications even though they cannot be considered as a parameter in the assessment of fatigue life. The fatigue classifications of the observed joints in this study are presented in Appendix I.

Currently, nominal stress approach does not recognize the effect of geometrical symmetry or the difference between tensile and bending loading. Fatigue classifications are evaluated for an asymmetric joint in longitudinal gusset and cover plate cases and for a symmetric joint in transverse attachment case as depicted in the schematic figures of the fatigue classes, Appendix I. In the both loading cases, the maximum tensile stress range in the base plate is considered as a nominal stress. (Hobbacher, 2014, p. 80–91.)

2.1.2 Hot Spot Stress Method

In HS stress method, the imaginary structural stress at weld toe is calculated. Currently, the HS stress method is not suitable for the assessment of fatigue life in root side cracks. Fricke (2013, p. 761-762) has proposed structural stress method for root side cracks but it is not yet accepted officially. Structural stress at weld toe can be determined by FEA with several methods:

- Linear surface extrapolation (LSE)
- Stress distribution through thickness at weld toe (TTWT)
- Method by Dong
- Method by Xiao & Yamada (1 mm rule)

(Radaj, Sonsino & Fricke, 2006, p. 38–44).

Analytical formulas for the determination of structural stress also exists:

$$\sigma_{hs} = k_{hs} \cdot \sigma_{nom} , \quad (3)$$

, where σ_{nom} is nominal stress. k_{hs} factors can be determined for both structural discontinues (k_{hs}) and shape imperfections of manufacturing (k_m). (Hobbacher, 2014, p. 28.) Although analytical formulas are widely produced in literature, the structural stress concentration factor depends also significantly on global constraints. Hence, numerical analysis is usually a more accurate method to assess the factor. (Poutiainen, Tanskanen & Marquis, 2004, p. 1154.)

In HS stress method, only two different fatigue classifications are used: *FAT* = 90 MPa and *FAT* = 100 MPa. *FAT* = 100 MPa is suitable for the majority of the welded joints, also for the studied joints except for longitudinal gusset (if gusset length L > 100 mm). As illustrated in Tables, in Appendix II, the fatigue resistance of tensile and bending loaded joints are determined with same fatigue classifications and loading type is not consequently taken into account in HS stress approach. (Hobbacher, 2014, p. 76–78.)

2.1.3 Effective Notch Stress Method

Total stress at weld toe or root can be concerned by means of ENS approach where all structural stresses and notch effect are taken into account. Notch effect depends on numerous variables and usually local stress is determined by FEA. Still, analytical formulas exist and notch stresses can be calculated as follows:

$$\sigma_{ns} = k_t \cdot \sigma_{hs} \quad (4)$$

$$\sigma_{ens} = k_f \cdot \sigma_{hs} \quad (5)$$

In Equation (4), σ_{ns} is notch stress, k_t is stress concentration factor. ENS approach is based on the microstructural support of the notch. k_f factor can be defined by means of k_t-factor according to Neuber:

$$k_f = 1 + \frac{k_t - 1}{\sqrt{1 + \frac{s \cdot \rho^*}{\rho}}} \quad (6)$$

In Equation (6), s is factor for stress multiaxiality and strength criterion, ρ^* is substitute micro-structural length and ρ is actual notch radius (Radaj et al., 2006, p. 127). IIW is using hypothesis proposed by Neuber in which local stress is averaged to ENS by applying fictitious radius at notch (Fricke, 2010, p. 4–5).

$$\rho_f = \rho + s \cdot \rho^* \tag{7}$$

In Equation (7), ρ_f is fictitious radius (Fricke, 2010, p. 4). Radaj (1990, p. 219) has proposed the value of 2.5 for the s factor. Neuber has presented the diagram for the factor ρ^*, Appendix III, and ρ^* = 0.4 mm is typically used since weld has been on molten condition. This results in a maximum fatigue notch factor of $k_f = k_{f,max} \approx k_t$ (ρ = 1 mm). The use of fictitious radius at weld toes and roots are illustrated in Figure 6. (Radaj, 1990, p. 218–219.)

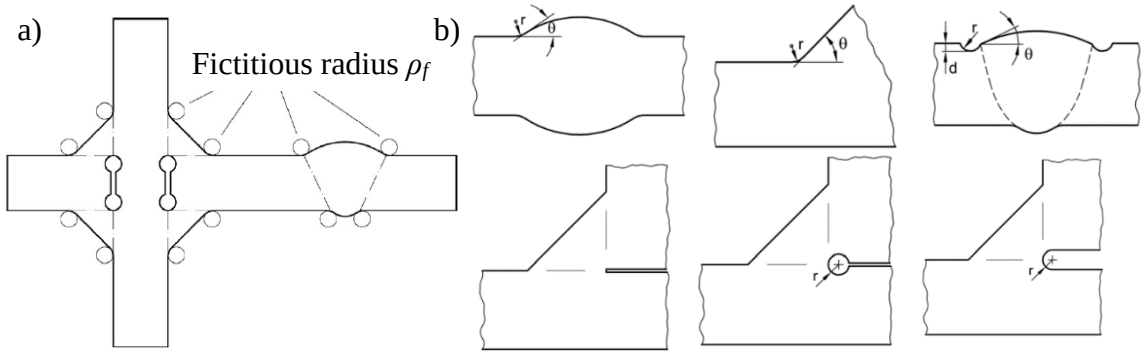

Figure 6. (a) Fictitious radius at weld toes and roots and (b) various styles of modeling the fictitious radius (modified: Fricke, 2010, p. 4; 9).

The most common method to determine the ENS is FEA. Fictitious radius is applied at weld toe or root and the stresses are analyzed. The element size of model, especially at observed spot, is critical and for this reason IIW has given recommended element size at the chamfer. The element sizes' influence on stress concentration is also studied recently. The recommended element sizes are listed in Table 1.

Table 1. Element sizes (modified: Baumgartner & Bruder, 2013, p. 138; Fricke, 2010, p. 12).

Author	No. of elements over 360°	No. of rings	Shape function of used elements	Estimated error
IIW / Fricke	24	3	Quadratic	few %
	40	>3	Linear	-
Gorsitzke et al.	72	6	Quadratic	< 2 %
Eibl et al.	32	6	Quadratic	-
Kranz & Sonsino	125	-	Linear	-

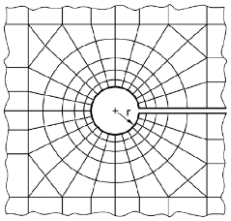

Because of considering the total stress at weld toe or root, only one fatigue classification is needed in ENS approach. *FAT* = 225 MPa is used in maximum principal stress criterion and *FAT* = 200 MPa in von Mises stress hypothesis. (Sonsino et al., 2012, p. 4.)

2.1.4 Linear Elastic Fracture Mechanics

At present, the most accurate method to assess the fatigue life of welded joint detail is fracture mechanics. LEFM makes an assumption of linear elastic material behavior at crack tip (Mettänen, Björk & Nykänen, 2013, p. 3). Typically LEFM can be used with certain conditions:

- Initial crack with infinite small tip radius occurs in structure
- The plastic zone of crack tip is small

(Anderson, 2005, p. 28.)

LEFM is based on calculation of SIF which contains stress state, shape and length of the crack. Crack tip has different modes of loading which are illustrated in Figure 7. (Dowling, 1999, p. 290.)

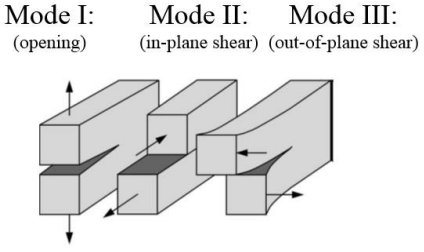

Figure 7. Three modes of loading that can be applied to a crack (modified: Anderson, 2005, p. 43).

Typically the opening mode (Mode I, Figure 7) is predominant and the corresponding SIF K_I is calculated:

$$K_I = \sqrt{\pi \cdot a} \cdot \left[\sigma_m \cdot Y_m(a) \cdot M_{k,m}(a) + \sigma_b \cdot Y_b(a) \cdot M_{k,b}(a)\right] \quad (8)$$

In Equation (8), a is crack depth, σ_m membrane stress, Y_m correction term in tensile loading case, $M_{k,m}$ stress magnification factor due to nonlinear stress peak for membrane loading, σ_b bending stress, Y_b correction term in bending loading case and $M_{k,b}$ stress magnification factor due to nonlinear stress peak for bending loading (Hobbacher, 2014, p. 34). With very small crack depths, the stress magnification factors are equal to stress concentration factor k_t presented in Chapter 2.1.3. Nevertheless, stress magnification factor decreases significantly when crack grows. (Radaj et al., 2006, p. 254.)

The range of SIF is determined in LEFM. By means of the SIF range, the crack propagation rate can be calculated. The most common and simplest formula is Paris' law and it has been included in IIW recommendations:

$$\frac{da}{dN} = C \cdot \Delta K^m \quad (9)$$

In Equation (9), C is crack propagation coefficient, ΔK SIF range and m fatigue crack growth exponent. By separating the variables and integrating from initial crack depth a_i to final crack depth a_f, the fatigue life is produced as cycles. According to IIW a_i = 0.05-0.15 mm is recommended if other test evidence is not assigned. With minor initial crack depths and relatively low stress range, SIF range is below threshold value and crack propagation might not occur. Crack propagation can be divided into three different regions: threshold (I), intermediate (II) and unstable (III) regions, Figure 8. Paris' law is only valid in the intermediate region. (Dowling, 1999, p. 510; Hobbacher, 2014, p. 94.)

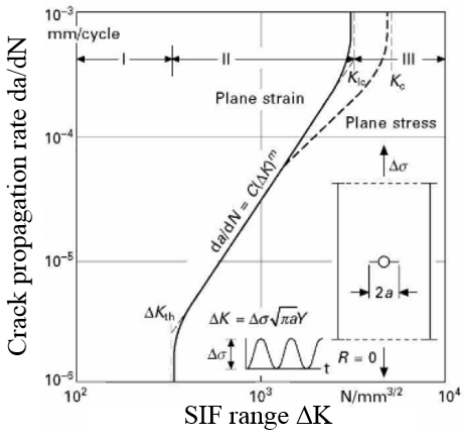

Figure 8. Three regions of crack propagation (modified: Hobbacher, 2011, p. 95).

For a final crack size, a half of plate thickness is estimated. Final crack depth might be larger or smaller but the crack propagation rate is typically much higher at the end crack propagation phase with respect to the early phase, as illustrated in Figure 8. Hence, the final crack size does not have remarkable impacts on fatigue life estimation. (Hobbacher, 2014, p. 93; Hobbacher, 2011, p. 106–107; Leitner, Barzoum & Schäfers, 2015a, p. 8; 11.)

2.2 Literature Review

In this chapter, previous researches concerning the issue are discussed. The effect of geometrical symmetry is almost entirely unexplored while the effect of loading type is already included in certain standards.

2.2.1 Effect of Loading Type

S-N curves are typically determined by means of fatigue tests for joints subjected to tension. Bending fatigue tests are neglected due to more difficult test set-ups and utilization of results. (Maddox, 2015, p. 1; Kang, Kim & Paik, 2002, p. 33.) Still, the influence of loading type on fatigue and beneficial ‘bending effect’ has been noticed already in the last three decades. Recently, the issue has come up again and several studies have been published (i.a. Baik, Yamada & Ishikawa, 2011; Xiao, Chen & Zhao, 2012; Maddox, 2015; Ottersböck, Leitner & Stoschka, 2015). In principal, the conclusion has been that increasing DOB improves the fatigue strength, but the magnification of the effect is not obvious and also completely opposite results and conclusions have been expressed.

Though the recommendations of IIW consider tensile and bending load behavior similarly, various research units have noticed different kind of crack propagation behavior in bending load versus tensile loading. Even Norwegian ship classification society Det Norske Veritas (DNV) has approved a reduction for bending HS stress component in the determination of equivalent HS stress. (DNV-RP-C203, 2011, p. 49.)

$$\Delta\sigma_{eq,hs} = \Delta\sigma_{m,hs} + 0.60 \cdot \Delta\sigma_{b,hs} \quad (10)$$

In Equation (10), $\Delta\sigma_{eq,hs}$ is equivalent HS stress range, $\Delta\sigma_{m,hs}$ membrane HS stress range and $\Delta\sigma_{b,hs}$ bending HS stress range. Membrane HS stress is nominal stress in the two-dimensional cases or determined membrane stress if the stress is distributed through plate width. (DNV-RP-203, 2011, p. 49.) The reduction factor 0.6 is justified by slower crack propagation in bending loading. Crack propagation in tensile and bending loading is illustrated in Figure 9. (Lotsberg & Sigurdsson, 2006, p. 332.)

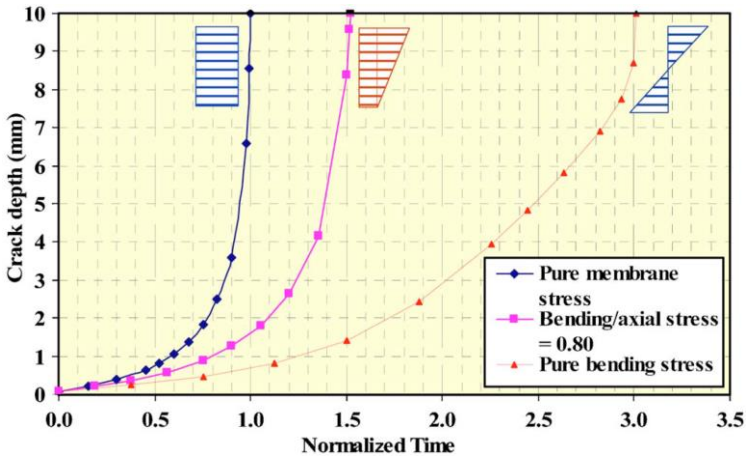

Figure 9. Crack growth curves for same HS stress with different stress gradients (Lotsberg et al., 2006, p. 332).

However, there are some restrictions for the use of the reduction factor, Equation (10), in the DNV-RP-203 standard. The reduction can be used in the areas where localized stress appears. The difference in fatigue resistance between bending and tensile loading is not so remarkable if the stress does not vary along the weld. (DNV-RP-203, 2011, p. 49.)

Maddox (2015) presents that fracture mechanics overestimates the advantageous effect of bending on fatigue strength. In British standard BS 7608:1993, bending effect is included in k_b-factor which considers DOB and plate thickness. The factor is based on results obtained by fracture mechanics and does not correspond well with test results of non-load and load carrying fillet weld joints as well as butt welded joints. New proposal for the formula of the k_{tb} factor given by Maddox agrees better with test results and it is also included in the latest version of the standard, BS 7608:2014. (Maddox, 2015, p. 23.)

$$k_{tb} = \left[1 + \Omega^{1.4} \cdot \left\{\left(\frac{25}{t}\right)^{n_t} - 1\right\}\right][1 + 0.18\Omega^{1.4}] \tag{11}$$

In Equation (11), k_{tb} is the thickness and bending correction exponent, Ω DOB (bending stress divided by total stress), t plate thickness and n_t thickness correction exponent (typically 0.2). Equation is valid for t < 25 mm and transverse fillet or butt welded joints. Test results corrected by the factor are presented in Appendix VI. In Figure 10, the two different test results of non-load carrying joints under bending and tensile loading show the improved fatigue strength of bending loaded joints although Maddox presents also results in which bending effect is practically insignificant. (Maddox, 2015, p. 14; 23.)

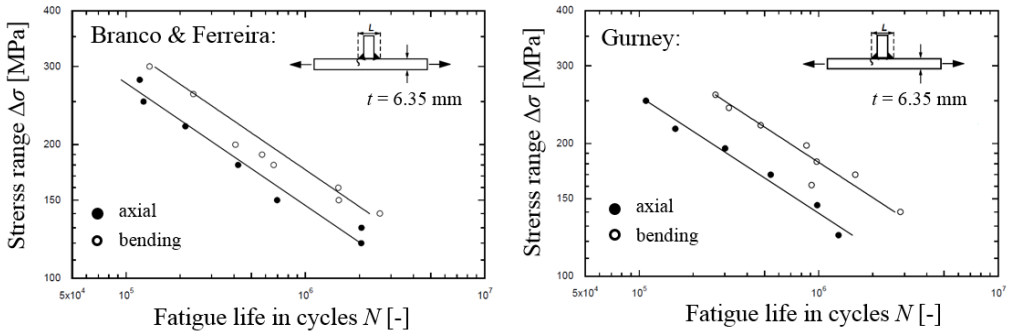

Figure 10. A comparison between tensile and bending loaded joints in which DOB enhances fatigue strength (modified: Maddox, 2015, p. 5–6).

Typically test results have indicated improvement of the fatigue performance in bending loading. The experimental tests conducted by Ottersböck et al. (2015) assign a totally opposite point of view. A rather large test series, in total amount of 125 test specimens (non-load carrying, single-sided transverse attachment joints), indicates loss of fatigue strength in

bending loaded structures if the welds are in as-welded condition. Whereas, in corresponding High Frequency Mechanical Impact (HFMI) treated joints, DOB improves fatigue strength, Figure 11. (Ottersböck, 2015, p. 5–6; 12–13.)

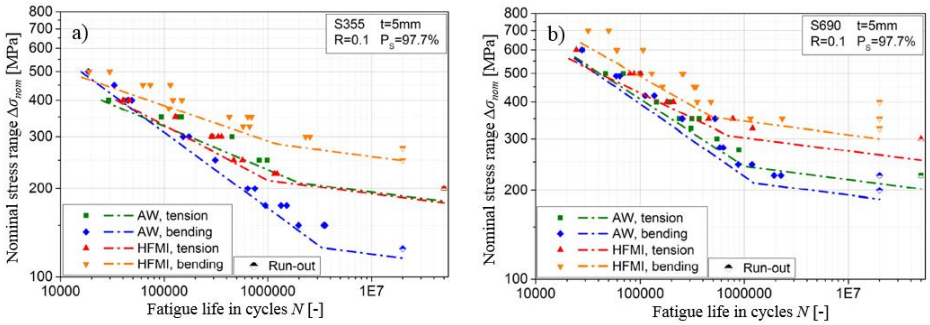

Figure 11. The test results conducted by Ottersböck et al. (2015) for the material (a) S355 and (b) S690 (modified: Ottersböck, 2015, p. 5).

When the bending effect is observed, it is reasonable to consider the level at which the assessment is conducted. It is widely accepted that when crack propagates into lower stress gradient area in bending, SIF range is also lower, respectively. In this fact, Lotsberg et al. (2006) and Maddox (2015) have established their point of view, although Maddox has discover that test results and fracture mechanics do not match in fatigue life estimations. Additionally, it must be noticed that structural stresses are not probably equal in the test results conducted by Ottersböck et al. (2015), since T-joints are under investigation and angular distortion exists more likely which affects increasingly on secondary bending stress component under tensile loading. Geometrically non-linear behavior of asymmetric joint increases also the secondary bending stress in tensile loading.

Chattopadhyay et al. (2011, p. 3) has unequivocally stated that the stress concentration factors are not equal under pure tensile and bending loading. The statement is based on the factors conducted by boundary element method (BEM) and FEM. The results are produced by Japanese research units and introduced in Iida & Uemura (1996, p. 783–785). The results can be estimated to be somehow outdated, while they are still widely used in contemporary studies.

Ottersböck et al. (2015) compared their results to notch stress based fatigue assessment method conducted by FEA, and it seemed to have quite clear agreement in as-welded

condition. Figure 11 shows that the fatigue classifications of the joints were reasonable high, so the welding quality must therefore has been at a high level. When the quality of weld is high, the size of initial defects is minor which leads to the fact that crack initiation affects substantially on fatigue strength. Considering the initiation phase in high quality welds can be difficult but understanding the notch effect is essential. When assessing the total fatigue life of a welded joint, it must be noticed that the crack initiation and propagation phases do not react consistently when loading type is observed, as the foregoing aspects point out. It depends on the weld quality and the size of attachment with respect to structure, whether crack initiation or propagation is dominant.

As a conclusion about the results of previous publications, the effect of loading type is not confirmed. In most of the studies, the fundamental impression has been that the increasing DOB improves fatigue strength but further investigations are obviously required. This study alone is not adequate to establish new revisions for IIW recommendations, since large scale experimental tests are needed, but the study of the phenomenon guides further research.

2.2.2 Effect of Geometrical Symmetry

While the symmetry of loading is relatively widely discussed, the effect of geometrical symmetry on fatigue has been rarely studied. Generally, either asymmetric or symmetric joints are tested or observed. Some studies have dealt with the subject by testing both asymmetric and symmetric joints, but geometrical symmetry has not been paid attention to.

Recently, Lie, Vipin & Li (2015) have published stress magnification factors M_k for British Standards. Stress intensity factors for asymmetric and symmetric transverse attachments with full penetrated welds were determined in the study. The factors cannot be compared with the results of this study because different type of weld is used but the phenomenon can be observed. Stress magnification factors in tensile loading as a function of crack size are presented in Figure 12. (Lie et al., 2015, p. 179–181.)

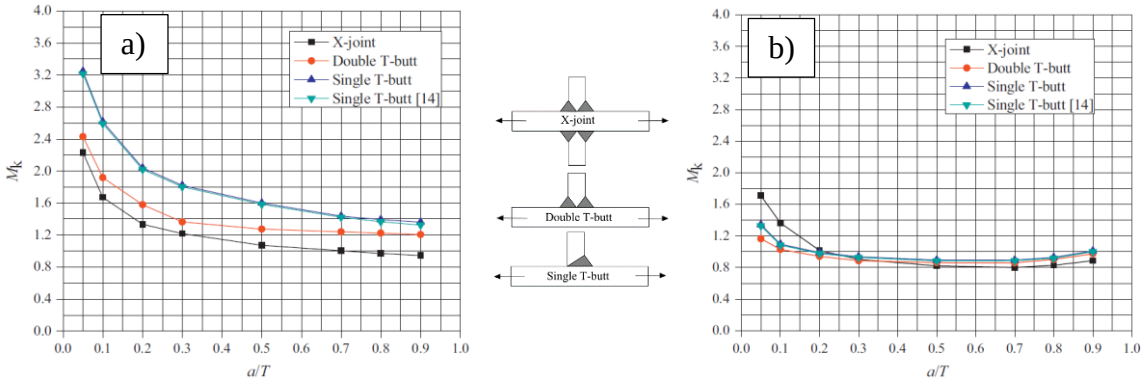

Figure 12. M_k vs. a/T plots in tensile loading at (a) crack end and (b) deepest point (Lie et al., 2015, p. 181–182).

As shown in Figure 12b, stress magnification factor at the deepest point is higher in symmetric X-joint than in asymmetric double T-butt joint with relatively short crack depths. Thus, the notch effect at weld toe is more significant in symmetric case. The difference may be pronounced when smaller crack depths are observed. In the reviewed article, M_k-factors are determined for relatively large flaws. At the crack ends, Figure 12a, the M_k-factors are higher in asymmetric case. Because M_k-factors are determined by the $K_{with\ attachment}/K_{without\ attachment}$ division, the values at crack end and deepest point cannot be compared to each other directly. (Lie et al., 2015, p. 179–182.)

Experimental tests have also showed that the fatigue strength of asymmetric joints is higher than symmetric joints in tensile loading. Kim & Jeong (2013) have conducted test data for one-side and both-side longitudinal gusset joints with L = 150 mm and t = 10 mm or 14 mm. Though the beneficial effect of blast cleaning on fatigue strength was studied, the joints in as-welded conditions indicate improvement of fatigue strength in asymmetric case, Figure 13. In low-cycle fatigue area fatigue strengths are roughly similar but in the high cycle area, the difference is noticeable. (Kim & Jeong, 2013 p. 17.)

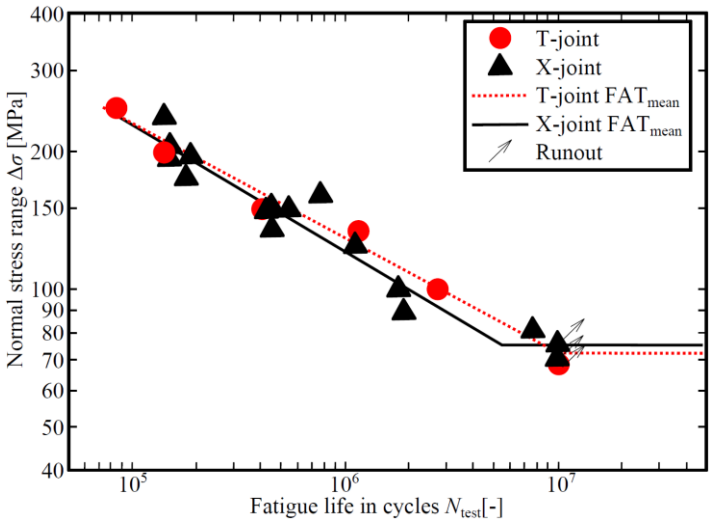

Figure 13. Test results of longitudinal gusset joints subjected to tensile loading in as-welded condition (modified: Kim & Jeong, 2013, p. 17).

Baik et al. (2011) have conducted fatigue tests subjected to bending (i.a. transverse attachment joints, t = 12 mm, applied stress ratio R = -0.23–0.02). In the study, correlation factors for bending load were proposed. Though the aim of the study was to examine bending fatigue behavior, the study showed different kind of fatigue resistance in asymmetric and symmetric case. Test results and fatigue classifications performed by linear regression analysis are presented in Figure 14. (Baik et al., 2011, p. 746–747.)

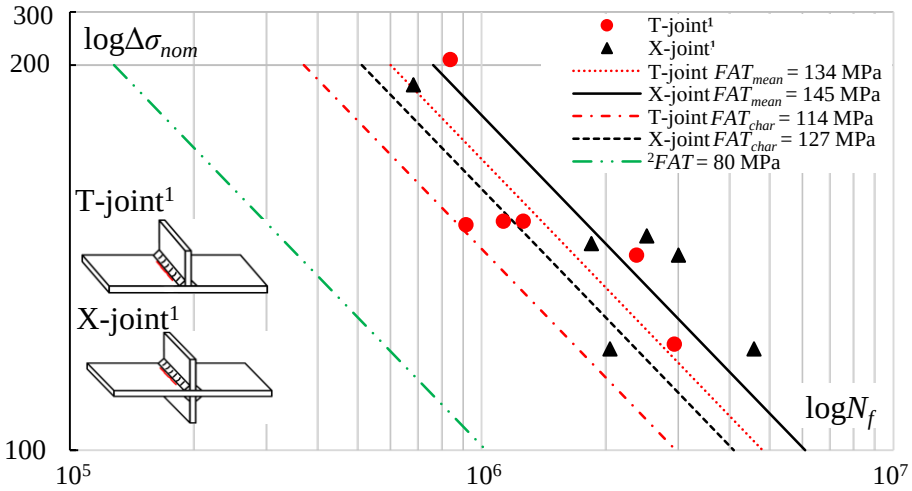

Figure 14. Bending test results conducted by [1]Baik et al. (2011, p. 749–750) in terms of nominal stress system. Mean and characteristic fatigue classes (m = 3) of the tested joints determined by linear regression, Appendix IV, in comparison with *FAT* recommended by [2]IIW (Hobbacher, 2014, p. 63).

Under bending load approximately 10 % higher *FAT* could be estimated based on these fatigue test results. In the fatigue tests carried out by Baik et al. (2011), the external bending loading was applied by using a vibrator which created a constant amplitude loading. Since it is based on the resonance of specimen, it is not convinced how it works in the crack propagation phase. Typically, only one load type or specimen type is studied simultaneously, which makes the analyzing of results problematic. Consequently, further examination is also required about this subject.

3 RESEARCH METHODS

In this study, both computational and experimental methods are used. FEA produces theoretical knowledge about the phenomenon under investigation. Since several factors have an influence on the fatigue behavior of real structures, it is important to study the observed issues by experimental tests. Since large of scale FEAs are conducted, some variables must be fixed in order to reduce the amount of modeling and analyses. Slope of S-N curve and Paris' law $m = 3$ is used since more exact data is not available. Modulus of elasticity $E = 210$ GPa and Poisson's ratio $v = 0.3$ are applied in the material model because the study concerns UHSS and steels in general.

3.1 FE-analyses of 2-Dimensional Cases

The fatigue strengths of two different geometries are assessed with different fatigue assessment methods. The observed joints are a cover plate joint and a transverse attachment joint. The applied fatigue assessment methods are ENS method and LEFM. The analyses indicate the effect of symmetry and loading type on fatigue when manufacturing aspects are ignored and only geometry is observed. Consequently, i.a. welding imperfections and residual stresses are not taken into account. Additionally, only the crack initiation and propagation starting from weld toe is under consideration, although the stress state at the weld root is calculated by the ENS method.

The fatigue strength is usually dependent on the proportions of a joint. Accordingly, certain dimensions are modified in order to study the effects more widely. The variables: throat thickness a, thickness of attached plate t_1 and length of attachment L (in the cover plate case) are taken under observation. The other variables concerning the geometry of the joint, e.g. the base plate thickness $t_0 = 20$ mm, flank angle $\theta = 45°$, gap $g = 0.1$ mm remain constant. The studied joint types are illustrated in Figure 15 and the test matrix in Table 2.

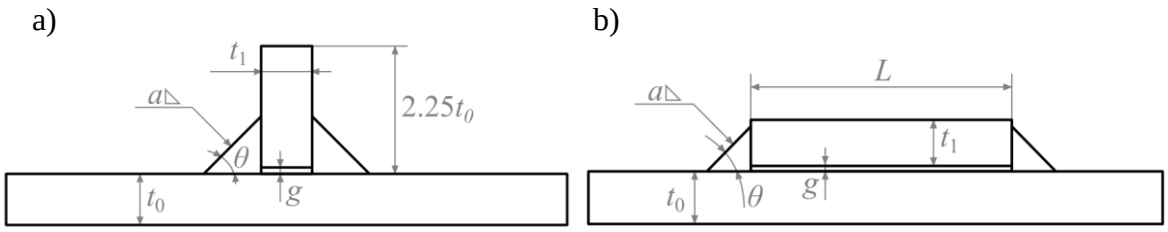

Figure 15. Basic geometries of the studied (a) transverse attachment and (b) cover plate cases and the chosen variables. In the symmetric case, dimensions are similar but attached plates are on both sides.

Table 2. The test matrix of the cover plate and transverse attachment joints.

a) Transverse attachment joint			
Variable	1	2	3
Symmetry	Asymmetric	Symmetric	
Loading type	DOB = 0	DOB = 1	
Thickness of attached plate t_1	10 mm ($0.5t_0$)	20 mm ($1.0t_0$)	40 mm ($2.0t_0$)
Throat thickness a	3 mm	$0.3t_1$	$0.5t_1$
b) Cover plate joint			
Variable	1	2	3
Symmetry	Asymmetric	Symmetric	
Loading type	DOB = 0	DOB = 1	
Thickness of attached plate t_1	10 mm ($0.5t_0$)	20 mm ($1.0t_0$)	40 mm ($2.0t_0$)
Throat thickness a	3 mm	$0.3t_1$	$0.5t_1$
Length of attachment L	100 mm ($5t_0$)	200 mm ($10t_0$)	400 mm ($10t_0$)

Due to the symmetry of the geometry, only a half of the joint is modeled and the symmetry constraints are applied on symmetry line. Once DOB = 0, uniform load equal to 50 MPa is set on the edge line of base plate. In the case of DOB = 1, maximum tensile stress is equal to 50 MPa and linearly distributed through plate thickness. Parabolic plain strain elements with a thickness of 1 mm are used in both of the applied methods.

3.1.1 Effective Notch Stress Method – 2D-joints

Analyzing ENS at weld toe in the joints under investigation was a part of the former phase of this study. The results obtained by ENS method are still essential for the comparison of different methods. Hence, only the basic principle of ENS models is described in this chapter. Femap v11.1 was used as a preprocessor and postprocessor and the models were

calculated by using Nx Nastran software. In the ENS method, most critical actual weld toe radius $\rho = 0$ was assumed, and thus a fictitious notch radius $\rho_f = 1.0$ mm was applied at weld toe. Also $\rho_f = 1.0$ mm was applied at the weld root according to the recommendations even if root side crack propagation is not observed. The mesh size at the notch is approximately 0.05 mm. A typical mesh and boundary conditions are depicted in Figure 16.

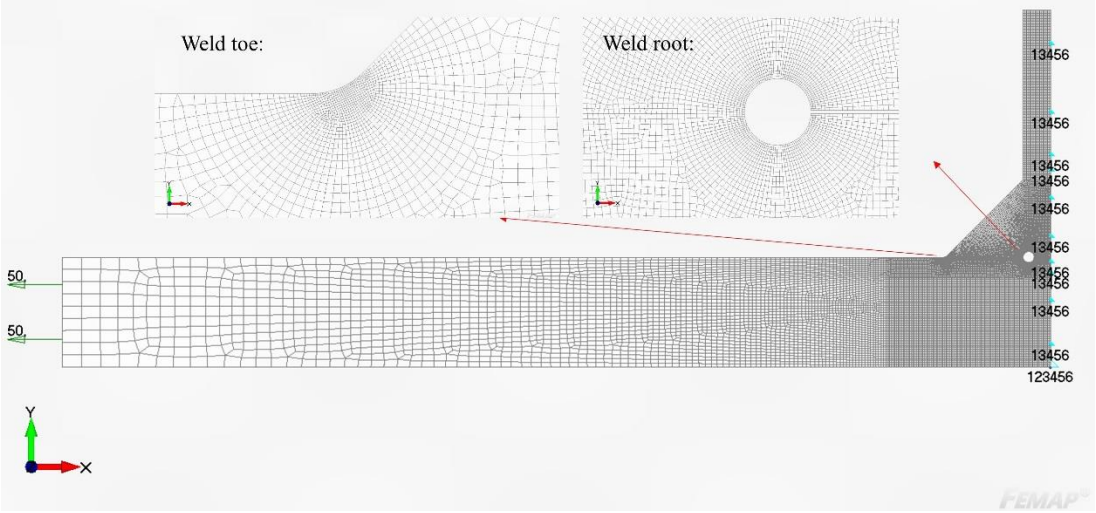

Figure 16. Typical mesh used in the ENS models and boundary conditions.

3.1.2 Linear Elastic Fracture Mechanics – Crack propagation of 2D-joints

The joints analyzed by using ENS method are taken under closer examination. In principle, LEFM is the most accurate method to analyze the fatigue performance of a cracked joint. Using LEFM is also reasonable since loading type (DOB) should have some effects on fatigue as discussed in Chapter 2.2.1. Franc2D (v4.0) is used as a calculation software. Franc2D is a free software provided by Cornell Fracture Group from Cornell University and enables crack propagation in 2D cases. (Cornell Fracture Group, 2014.)

CASCA is the elementary pre-processor of Franc2d. Geometry modeling, meshing and creating input-files for Franc2D is made by using CASCA. Since CASCA's meshing properties are not very effective for boundaries with irregular shape, a gap between base plate and attached plate is modeled as a triangle shape near weld root and sharp edge is received as a result at root notch. Franc2D remeshes the geometry when an initial crack is applied to FE-model. Remeshing is done for every crack propagation step in order to get efficient mesh for the calculation of SIF values.

In the observed joints, an initial crack with size of a_i = 0.05 mm is placed at weld toe. The selected initial crack size is relatively small but to the final calculation of fatigue endurance, the lower limit of the definite integration (a_i) can be set larger which reduces the endurance. The purpose of the crack propagation analysis is to form $\Delta K(a)$ function whereby fatigue life in cycles can be calculated. Since the nominal stress loading the joint is known, the life estimation can be transformed to nominal *FAT*. Figure 17 illustrates a typical FE-model of LEFM.

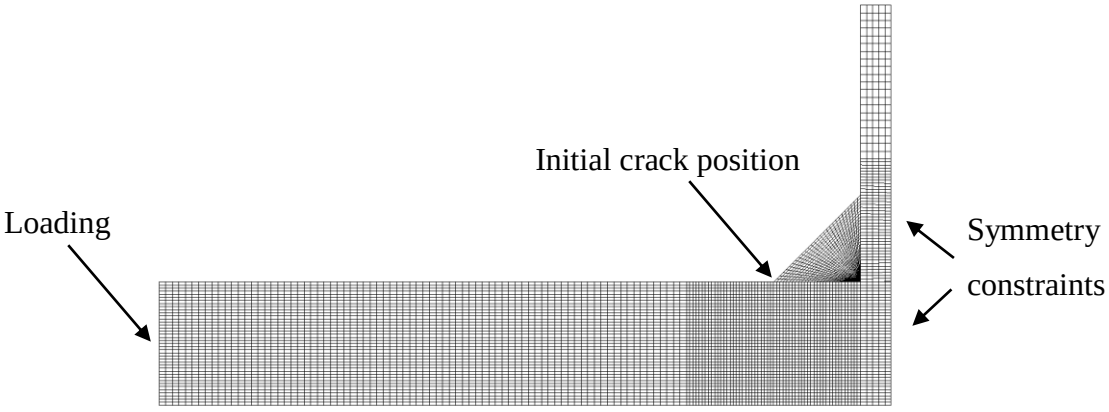

Figure 17. A typical FE-model of Franc2D.

3.2 FE-analysis of Longitudinal Gusset Case

Two different fatigue assessment methods are applied to determine the effect of loading type and symmetry on fatigue in the longitudinal gusset case. Fatigue strength is assessed for the joint, Figure 18, with a few different geometry variations. Since the effect of different geometrical variables on the stress concentration factors of longitudinal gusset joints were evaluated in the previous studies, it is more appropriate to concentrate on the symmetry aspect in different loading cases. A basic geometry is similar in every model but throat thickness and gusset length vary. The test matrix of the variables is presented in Table 3.

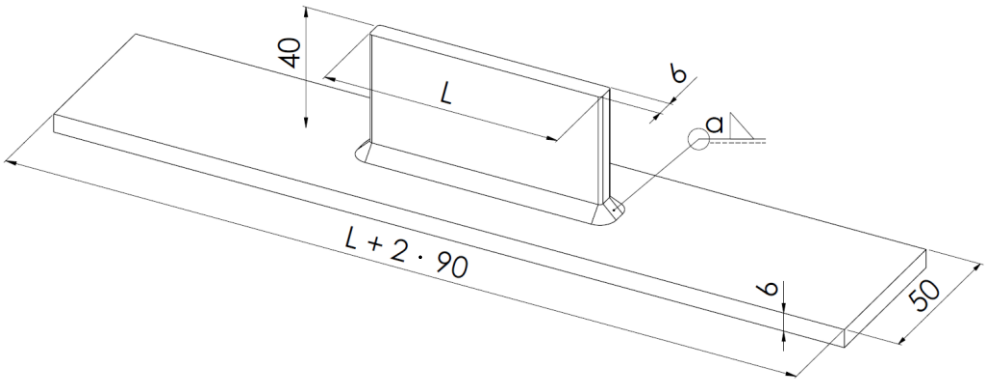

Figure 18. Geometry of the studied longitudinal gusset and the chosen variables.

Table 3. Test matrix of the longitudinal gusset case.

Variable	1	2	3
Symmetry	Asymmetric	Symmetric	
Loading type	DOB = 0	DOB = 1	
Throat thickness *a*	3 mm (0.5*t*)	4.5 mm (0.5*t*)	6 mm (0.5*t*)
Gusset length *L*	75 mm (12.5*t*)	150 mm (25*t*)	300 mm (50*t*)

3.2.1 Effective Notch Stress Method – Longitudinal Gusset

The ENS at weld toe is determined by using the fictitious notch radius ρ = 1 mm at weld toe and root. Although weld toe is under closer examination, also weld root is modeled with fictitious notch radius. The root side does not have an influence on the stress state at weld toe, most likely (Aygül, Al-Emrani & Urushadze, 2012, p. 138). The ¼-model of the part is used since the geometry is symmetrical. FEAs are done by using Abaqus 6.14.1 software. Sub-modeling technique is utilized to conduct more accurate results of notch stresses. In sub-modeling technique, the global deformations of the structure are calculated in the model with relatively coarse mesh. The nodal displacements of the global model are applied to the sub-model, which consists of fine elements and produces more accurate stress values in the observed area. Figure 19 depicts a global model and a sub-model used in the study. (Abaqus, 2014.)

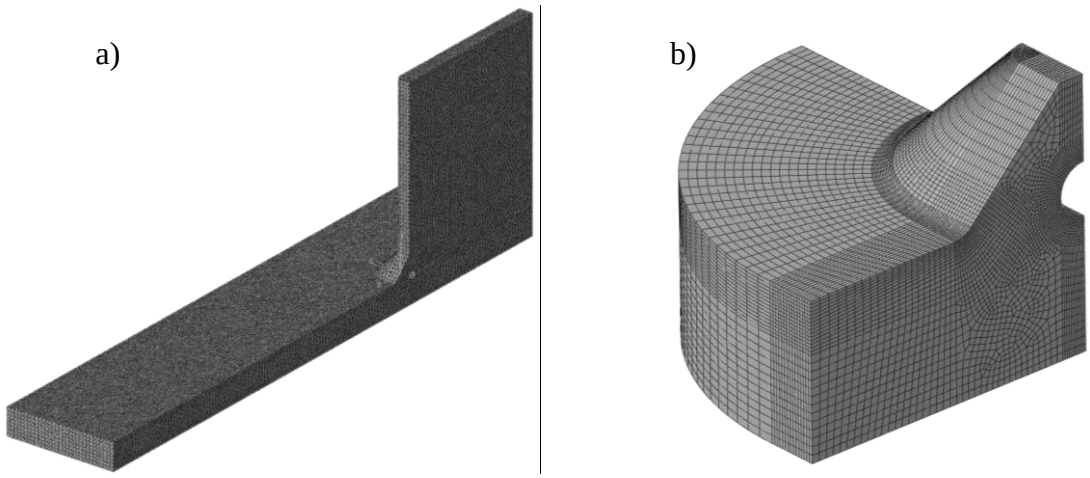

Figure 19. (a) A global model and (b) a sub-model of the ENS method in an asymmetric joint case.

Tetrahedral elements are used in the global model. More accurate hexahedral elements are employed in the sub-model. In both cases, the shape function of the elements is parabolic. At weld toe, which is under investigation, number of elements is 15 with the absolute size of 0.05 mm. The recommendation of IIW is only three elements for the 45° arc. Hence, the used mesh size exceeds the recommendation and the model should give the accurate value of notch stress. Also rings which regularly increase the mesh size were applied near weld toe. Figure 20 shows a typical mesh applied in the sub-model.

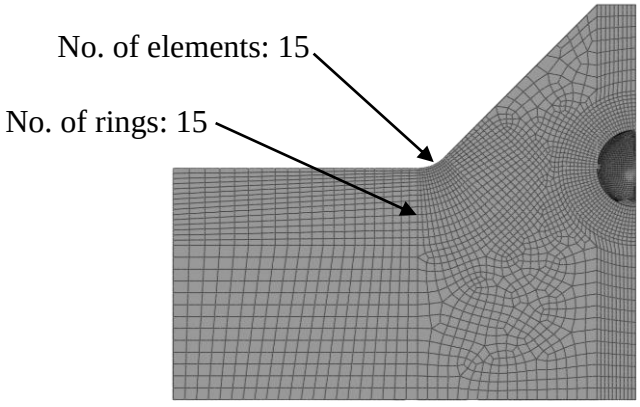

Figure 20. A typical fine mesh used in the sub-model in symmetry plane.

3.2.2 Linear Elastic Fracture Mechanics – Longitudinal Gusset

In order to compare different fatigue assessment methods, LEFM is used also in the 3D-case under investigation. For the practical reasons, after the analyses of ENS method, Chapter

3.2.1, are done, the most critical geometrical variables are established and consequently the chosen variables are changed in the LEFM models. The LEFM analyses are carried out by using Abaqus/XFEM -software. XFEM is an extended finite element method, which allows analyzing joints with cracks and produces SIF values. Remeshing is not performed in XFEM but instead the crack front is enriched with additional nodes. (Abaqus, 2014.) Since the observed geometry is not directly compared with certain test specimens, the effect of residual stresses are neglected, although they may have remarkable influence on fatigue life estimation (Barzoum & Barzoum, 2009, p. 464; Leitner et al., 2015b, p. 872).

However, Abaqus/XFEM has some limitations, and e.g. it is not suitable for parabolic (20-node) hexahedral elements. Hence, linear (8-node) hexahedral elements are used because it was noticed in the preliminary analyses that hexahedral elements converge quicker and are not so mesh sensitive as tetrahedral ones. Additionally, Abaqus/XFEM is not capable of propagating fatigue crack, therefore a semi-elliptic planar crack is inserted in the weld toe manually as follows:

$$\frac{a}{2c} = \begin{cases} 0.5, a < 0.062 \text{ mm} \\ 1/(6.34 - \frac{0.27}{a}) \\ 0, a > 3 \text{ mm} \end{cases}, 0.062 \text{ mm} < a < 3 \text{ mm} \quad (12)$$

$$\frac{dc}{da} = \left(\frac{\Delta K_c}{\Delta K_a}\right)^m \quad (13)$$

In Equation (12), c half of crack width (Engesvik & Moan, 1983, p. 749; Berge, 1985, p. 429). In Equation (13), ΔK_c is SIF range at crack end and ΔK_a SIF range at crack depth. Equation (12) is valid only for continuous welds (e.g. transverse attachment) and for that reason it is utilized only when the crack propagates on the tip of the gusset. After the crack has propagated outside the tip, the free evolution of the crack shape is used, Equation (13). In the free evolution, a crack shape is determined from the proportional propagation of crack end and crack depth points.

Crack increment size is adjusted during the analysis by means of plotted $K(a)$ diagraph. When the notch effect vanishes, the increment size can be enlarged without any significant

effects on fatigue endurance. Thus, the crack increment size is minor when the crack is small, and grows when the crack is propagated. The symmetry of the joint is utilized and only a ¼-model is analyzed. In order to keep model calculation time in reasonable limits, sub-modeling technique is also applied. Basically, the sub-model is used when the crack is on the tip area and the global model when the crack is larger. Figure 21 depicts typical models used in LEFM.

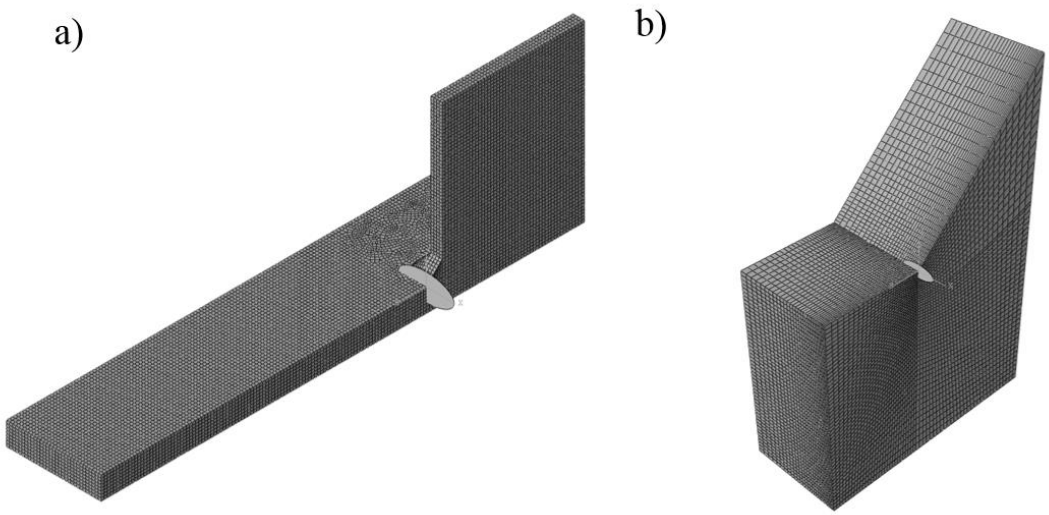

Figure 21. (a) A global model with crack a = 1.2 mm and (b) a sub-model with the crack a = 0.2 mm.

3.3 Experimental tests

Experimental tests are conducted since computational methods must be verified. It is not reasonable to test all the geometries analyzed by ENS and LEFM methods but fatigue assessment is compared to test results with a certain joint type.

Transverse attachment case with fillet welds was determined to be under investigation since a relatively large amount of similar specimens have already been tested subjected to tension. This aspect assists comparability to previous test results. The test matrix includes both asymmetric T-joints and symmetric X-joints, Table 4. Overall 12 specimens are fatigue tested to determine the effect of loading type and geometrical symmetry on fatigue strength.

Table 4. Established test matrix of laboratory tests.

Loading type	Type of joint	No. of specimens	No. of strain / stress levels	Specimen IDs
Tension	T-joint	2	2	AAT5–AAT6
Tension	X-joint	2	2	AAX5–AAX6
Bending	T-joint	4	2	AAT1–AAT4
Bending	X-joint	4	2	AAX1–AAT4

In the both load cases, two different strain or stress levels are utilized to determine the fatigue strength in relatively low-cycle and high-cycle regime. The target value for low-cycle and high-cycle endurances are 10^5 and 10^6 cycles, respectively. The mean fatigue classification values of previous fatigue tests with similar geometry and weld parameters are used to assess the required strain levels of the tests.

3.3.1 Test Specimens

Specimens were made of SSAB Strenx® S960 MC UHSS, which has a nominal yield strength of 960 MPa and nominal ultimate tensile strength is 980-1250 MPa. The mechanical properties and chemical compositions of the base and filler material are presented in Table 5. (SSAB, 2015.)

Table 5. Typical mechanical properties and chemical compositions of the base and filler material used in experimental tests (SSAB, 2015; Böhler, 2013, p. 250).

Mechanical properties												
Material	Yield Strength f_y [MPa]			Ultimate Strength f_u [MPa]			Elongation A_5 [%]			Charpy V-Notch CVN [J]		
S960 MC	960			980-1250			7			27		
Union X96	930			980			14			47		
Chemical compositions [weight-%]												
Material	C	Si	Mn	P	S	Al_{tot}	Nb	V	Ti	Cr	Mo	Ni
S960 MC	0.12	0.25	1.3	0.02	0.01	0.015	0.05	0.05	0.07	-	-	-
Union X96	0.12	0.8	1.9	-	-	-	-	-	-	0.45	0.55	2.35

The dimensions of the joints are presented in Figure 22. The dimensions of the T- and X-joints are similar except for in T-joints attachment is only on the other side.

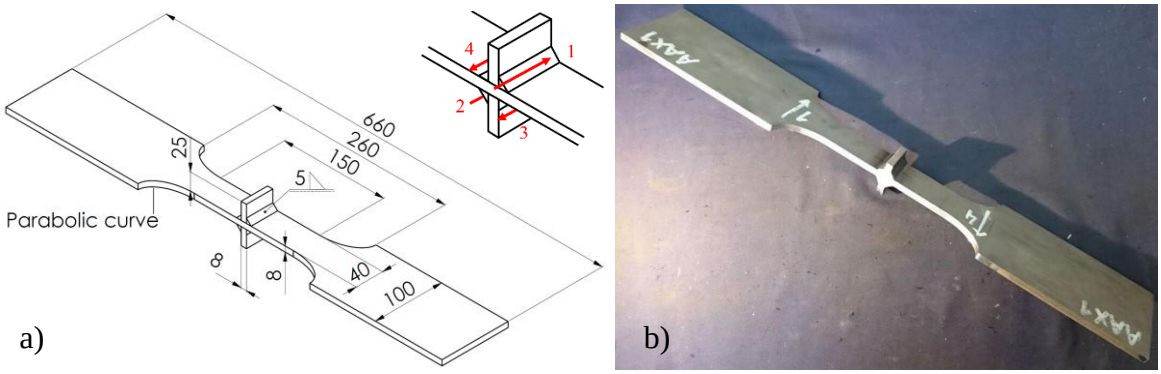

Figure 22. (a) Dimensions of X-joint test specimens and (b) a fabricated specimen. The red arrows signify the welding directions.

The specimens were welded by a GMAW process with one pass per each fillet weld. The welding parameters were effectively identical in each pass. A welding robot was used to get similar quality for all passes and specimens. The main parameters of welding procedure specification (WPS) are listed in Table 6 and parameters of each pass are presented in Appendix VII.

Table 6. The average values of the WPS' main parameters. In total 36 passes were welded. Stdv is standard deviation.

	Current I [A]	Voltage U [V]	Travel speed* v_w [mm/s]	Wire feed speed* v_{wire} [m/min]	Heat input Q [kJ/mm]	Heat input with losses Q_{loss} [kJ/mm]	Cooling time $t_{8/5}$ [s]
Average	229.6	28.8	5.9	13.2	0.90	0.79	7.4
Stdv	1.9	0.1	-	-	0.007	0.006	0.1

*Constant value

Welding position was leading approximately 18° (around the y-axis) and specimen was fastened into bench vice with 4° angle (around the z-axis) to produce a slightly smoother transition at weld toe. Additive wire length was 22 mm in every pass. In order to eliminate the welding imperfections, ignition and ending points of passes were shifted outside the proper specimen, as illustrated in Figure 23. Ignition and ending parts of specimen were sawed and machined after welding.

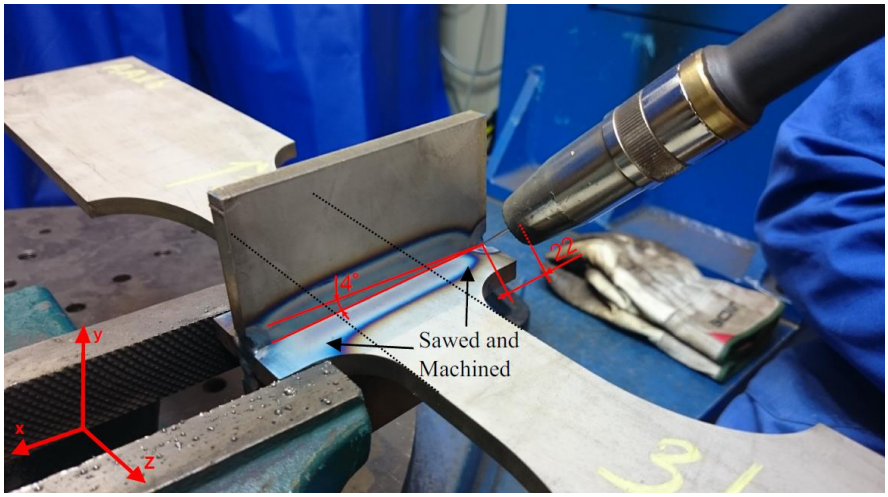

Figure 23. The fastening of the test specimen in welding.

3.3.2 Measurements

Before fatigue tests, certain measurements for specimens are conducted. The polished sections of the joint are made of the ignition and ending part, which are sawed after welding. By the polished section, the nominal and effective throat thickness of the joint can be determined. Furthermore, it is possible to assess the weld toe radius from the polished section. Since the variation of the quality in welds is minor, the polished sections are taken only from one specimen of each symmetry type (AAT3 and AAX6). Figure 24 illustrates the evaluated values of the nominal and effective throat thickness.

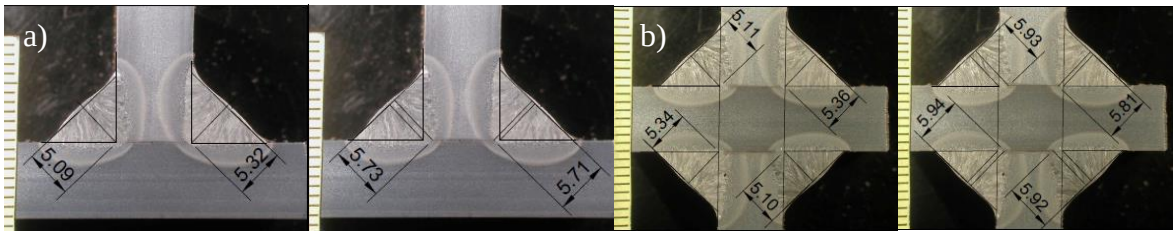

Figure 24. The nominal and effective throat thicknesses of test specimens in (a) T-joint and (b) X-joint. The throat thicknesses are determined according to EN 1993-1-8 (2005, p. 42).

As Figure 24 shows, the nominal throat thickness is slightly larger on the ignition sides than on the ending sides. The reason for this is the warming of the specimen during the welding process. Consequently, the penetration is better when the specimen is at higher temperature, which leads to the fact that the equivalent throat thicknesses are approximately equal on both

of the sides. As well, throat thicknesses are slightly greater than the throat thickness assessed in the WPS beforehand, Figure 22.

The profiles of the weld passes are measured by the shape-laser measurements. The measurements are conducted in every single pass on the middle line of the specimens, Figure 25. To define the angular distortion due to welding, the global shape of the specimen is also measured.

Residual stress in a joint under fatigue loading has a great impact on fatigue performance. Thus, residual stress state is determined by Stresstech Xstress 3000 G3 device, which is based on X-ray diffraction in material and is capable of measuring residual stress at the surface of a specimen (Stresstech, 2014). Since the measurements are quite time-consuming, only the critical points are measured. A distribution along test specimen away from weld toe is determined in a one of each type specimen (AAT1 and AAX1). In the other specimens, only the stress states of weld toes are measured. All the measurements are conducted on the middle line of the specimen. Figure 25 depicts the measurements conducted for the specimens.

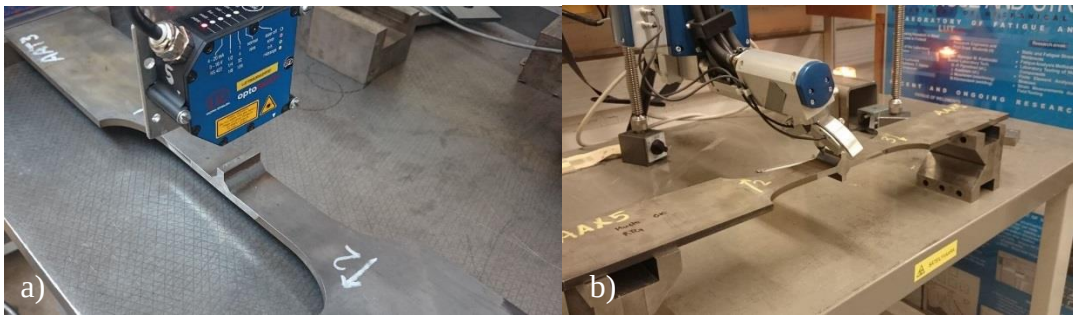

Figure 25. Measurement of (a) weld shape and (b) residual stress.

3.3.3 Test Set-ups and Instrumentations

The fatigue tests are carried out in the laboratory of steel structures at Lappeenranta University of Technology. Two types of loads are applied: tensile load and pure bending load. In both of the joint types, constant amplitude loading with a recommended $R = 0.1$ is used (Hobbacher, 2014, p. 94). A hydraulic actuator produces the load and the cylinder is equipped with a force cell and a displacement transducer which measure the minimum and maximum value of concerned quantities during the fatigue tests.

A strain gage positioned at 0.4*t* distance from weld toe, Figure 26, is exploited in the establishing of required maximum and minimum force. It has been discovered empirically in the previous studies that one strain gage gives reasonable results for structural stress since the nonlinear stress component vanishes at that distance. If the HS stress is determined experimentally more precisely, two strain gages should be placed at 0.4*t* and 1.0*t* distances and HS stress can be evaluated by linear extrapolation. Consequently, structural stress range determined with one strain gage gives slightly conservative results when S-N curves are defined with HS stress method since the linear extrapolation component is neglected. Furthermore, the measuring length of strain gage (i.e. grid size) should be less than 0.2*t*. In this study, strain gages with 1.5 mm grid size are used and thus 1.6 mm requirement for maximum allowed grid length fulfilled. (Takeuchi, 2012, p. 561–563; Hobbacher, 2014, p. 26.)

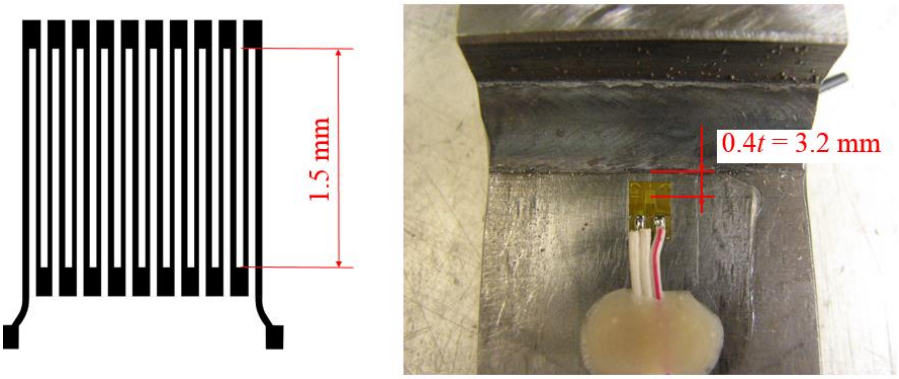

Figure 26. Grid size of the used strain gage and positioning in the specimen.

By measuring a maximum and a minimum value of strain, structural stress range in the uniaxial loading case can be calculated by using the simple Hooke's law as follows:

$$\Delta\sigma_{SG} = E \cdot \Delta\varepsilon_{SG} \tag{14}$$

In Equation (14) $\Delta\sigma_{SG}$ stress range at strain gage and $\Delta\varepsilon_{SG}$ strain range at strain gage (Niemi, Fricke & Maddox, 2006, p. 13).

In the tensile load case, the stress state is not completely only tensile due to angular distortion and the fastening of specimens. Nevertheless, DOB in the loading is low and membrane stress σ_m is predominant, particularly in the X-joints in which angular distortion is minor. Since the strain gage is placed to the concave side of specimen, it takes into account the

bending component and bending stress σ_b can be derived by means of structural and nominal stress. The failure criterion is a rupture of specimen, i.e. fatigue crack is propagated so large that either ductile or brittle failure appears due to the maximum load. Figure 27 depicts the test rig used in the tensile load case.

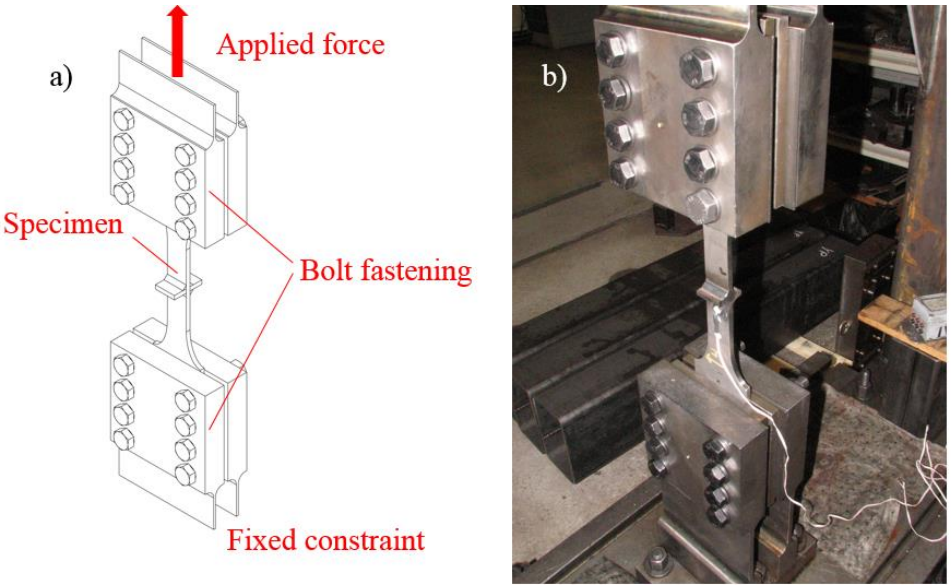

Figure 27. (a) Schematic test set-up and (b) actual test rig in the joints subjected to tension.

In order to study fatigue behavior in bending loading, four-point bending device is used to apply a constant bending moment and zero shear over the length of joint. Hence, a crack can initiate and propagate at both of weld toes. The test set-up is illustrated in Figure 28. In order to finish a fatigue test systematically and safely, the test is stopped when maximum displacement has approximately duplicated and the crack tip depth is greater than a half of plate thickness. As noted, final crack has not great influence on fatigue endurance and hence the result represents well the definitive fatigue endurance.

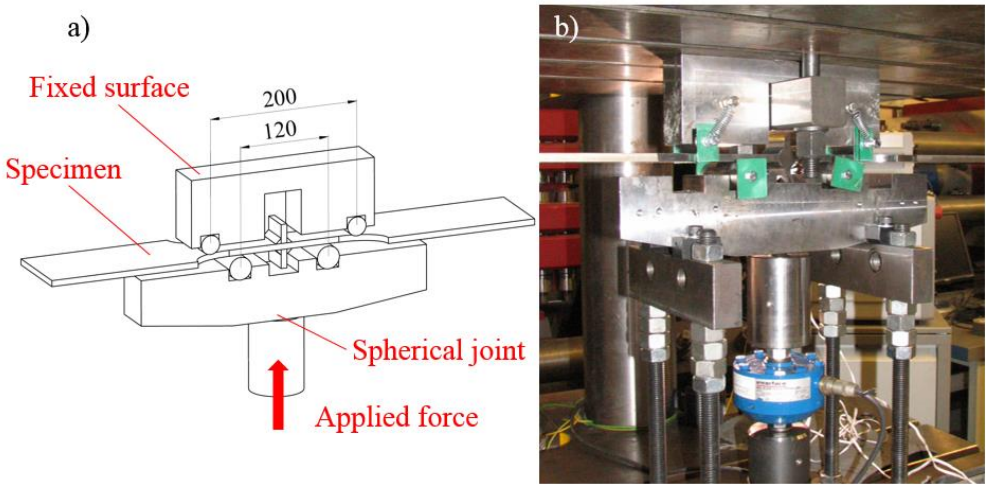

Figure 28. (a) Schematic test set-up and (b) actual test rig in the joints subjected to bending.

Since some errors in loading might occur (e.g. frictions and mounting of specimen), in the first fatigue tests, additional strain gages are positioned on the specimen's compression side and on the other side of the attachment. These strain gages are used to clarify the actual DOB in the tests and the constancy of moment between the press rolls.

3.3.4 FE-analyses of test specimens

Due to the fact that the dimensions of the test specimens are not similar with the analyzed geometries, FEAs are conducted also for the joints under investigation for a comparison. Stress based (HS stress and ENS) methods and LEFM are utilized when analyzing the test specimens by FEM. In the analyses, the actual throat thickness and specimen shape are used in order to reach comparable results.

The angular distortion is assessed by means of the shape laser and strain gage measurements, Chapters 3.3.3–3.3.4, and it is added to the geometry, Figure 30. Consequently, a bending stress component appears in the T-joints subjected to tension. Since the loading type has an influence on notch effect, it is reasonable to assess the stress components. Thus, also a model by using HS stress method is adapted. In the HS stress model, geometrically non-linear analysis is applied since the loading has a decreasing effect on the angular distortion of specimen and it needs to be taken into account. Tensile load is applied by using a linear ramp function with 20 time steps. Also fixed constraint due to the mounting is taken under consideration in the boundary conditions of tensile loading case. Both LSE and TTWT

methods are used in the analyses, Figure 29. The total number of elements through plate thickness is 100 with biased node spacing when the smallest element absolute size is roughly 0.05 mm at weld toe.

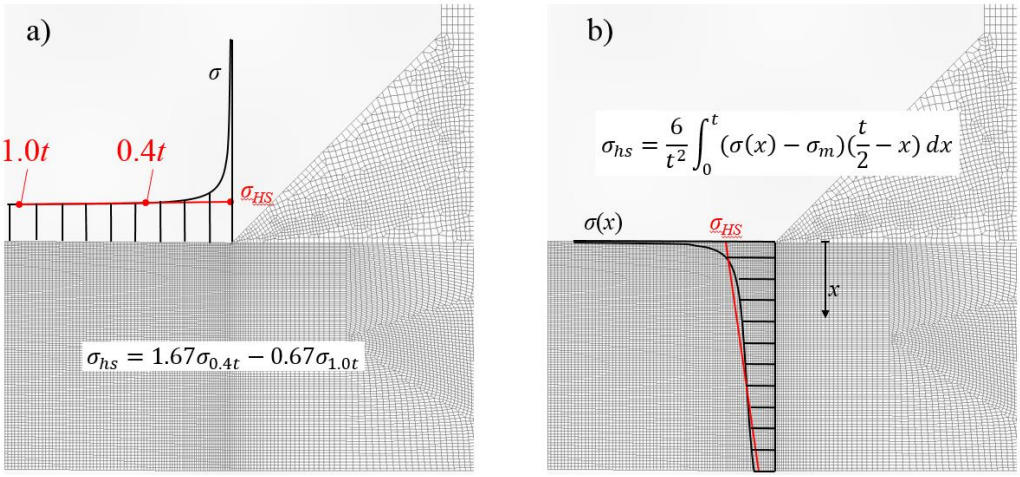

Figure 29. (a) LSE method and (b) TTWT method in a HS stress model (modified: Hobbacher, 2014, p. 15; 24).

As mentioned, angular distortion has a non-linear effect on structural stress concentration factor. However, analytical formula exists which considers also the non-linear behavior.

Analytical formula of structural stress concentration factor for misalignment k_m due to angular distortion can be written as follows:

$$k_m = 1 + \frac{3 \cdot \alpha \cdot l}{2 \cdot t} \cdot \frac{\tanh\frac{\beta}{2}}{\frac{\beta}{2}}, \tag{15}$$

where

$$\beta = \frac{2l}{t} \cdot \sqrt{\frac{3\sigma_m}{E}} \tag{16}$$

In Equation (15), α is angular distortion and l half of distance between clamps. In Equation (16) σ_m is membrane stress. (Hobbacher, 2014, p. 145.) The latter division of Equation (15) estimates the effect of straightening on k_m factor. After assessing the angular distortion correctly, it is applied in the ENS and LEFM models, Figure 30. In both approaches, linear

analysis is utilized. In the ENS models, fictitious ρ_f = 1 mm radius is used, and initial crack size a_i = 0.05 mm is applied in the LEFM model since a_i = 0.05 mm has given an excellent agreement with test data (Nykänen, Marquis & Björk, 2007, p. 142; Nykänen, Marquis & Björk, 2009, p. 84). Otherwise, the modeling is done similarly as discussed in Chapter 3.1.

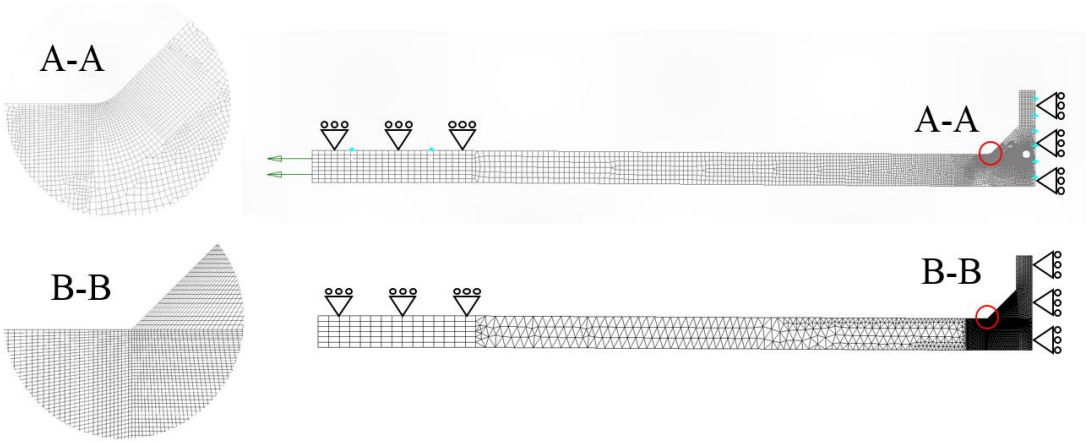

Figure 30. A typical (a) ENS and (b) LEFM model used in the analysis with the evaluated angular distortion. The schematic roller constraints at the loading ends illustrates the constraints of the tensile load case, Figure 27.

When assessing the fatigue endurances of tested joints, the mean values of approaches' coefficients are used by applying minus two standard deviation proposed by IIW (Hobbacher, 2014, p. 40). Hence, safety factor j_σ = 1.37 is received. By means of j_σ = 1.37, the following mean FAT classes are evaluated, Table 7. (Sonsino et al., 2012, p. 7.)

Table 7. Evaluated mean values of stress based methods obtained by using j_σ = 1.37.

Method	Nominal stress	HS	ENS
FAT_{char} [MPa]	80	100	225
FAT_{mean} [MPa]	110	137	309

In the LEFM, the mean value for crack propagation coefficient is not unambiguously given. Nykänen et al. (2005, p. 1582) have proposed $C_{mean} = 1.7 \cdot 10^{-13}$ (da/dN in mm/cycle and ΔK in Nmm$^{-3/2}$) when the former IIW recommendation $C_{char} = 3.0 \cdot 10^{-13}$ exists. Due to the lack of more detailed data, this value is used in the calculation of fatigue life.

4 RESULTS

The purpose of this study was to determine the effect of symmetry and loading on the fatigue strength of various non-load-carrying joint types. For asymmetric and symmetric joints with similar dimensions, both tensile and bending loading cases were studied. For comparison, the following fatigue strength ratio coefficients are established:

$$q_{geom} = \frac{FAT_{asym}}{FAT_{sym}} \tag{16}$$

$$q_{load} = \frac{FAT_m}{FAT_b} \tag{17}$$

In Equation (16), q_{geom} is fatigue strength ratio for geometrical symmetry, FAT_{asym} fatigue class of asymmetric joint, FAT_{sym} fatigue class of symmetric joint, and it is utilized in both loading cases. In Equation (17), q_{load} is fatigue strength ratio for loading type, FAT_m fatigue class of tension and FAT_b fatigue class of bending. Equation (17) is used separately for asymmetric and symmetric joints.

4.1 2-Dimensional Cases

Transverse attachment and cover plate joints were studied. FEAs were conducted by using ENS and LEFM methods. The fatigue strength of weld toe was under determined by both approaches. The fatigue life estimations assessed by the methods are transformed to nominal FAT class in order to obtain comparable results, Figure 31. The ENS results were quantified in terms of maximum principal stress criterion. In total, 168 different geometries were analyzed.

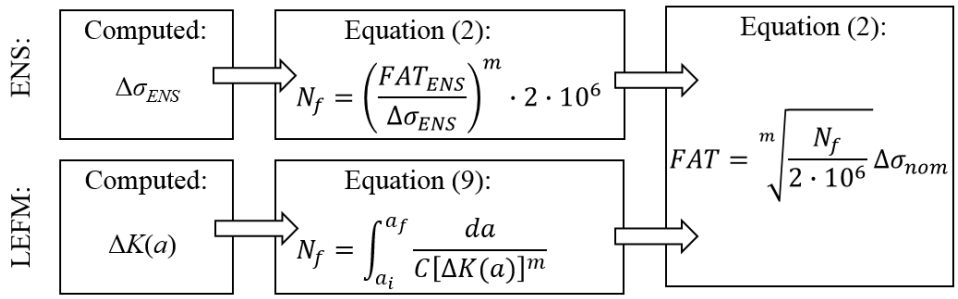

Figure 31. Calculation procedure of nominal FAT class in the ENS and LEFM approaches.

The effect of symmetry on fatigue strength is shown in Figure 32 for the transverse attachment case. The obtained results assign the improvement of fatigue strength in tensile loaded asymmetric joints with respect to the fatigue strength of symmetric joints. In contrast, in bending load case, the fatigue strength of symmetric joints improves compared to asymmetric joints. The ratios obtained by the ENS and LEFM methods have a clear accordance with each other. Although according to ENS method, the effect is more remarkable. The results have better agreement with smaller throat thicknesses.

The geometrical dimensions affect evidently on the ratios. The increase of throat thickness magnified the significance of the symmetrical effect when $a/t < 0.5$. For larger throat thicknesses, the ratio was not as remarkable as for smaller ones. Enlarging the attached plate thickness affected on the ratio with small throat thicknesses, Figure 32.

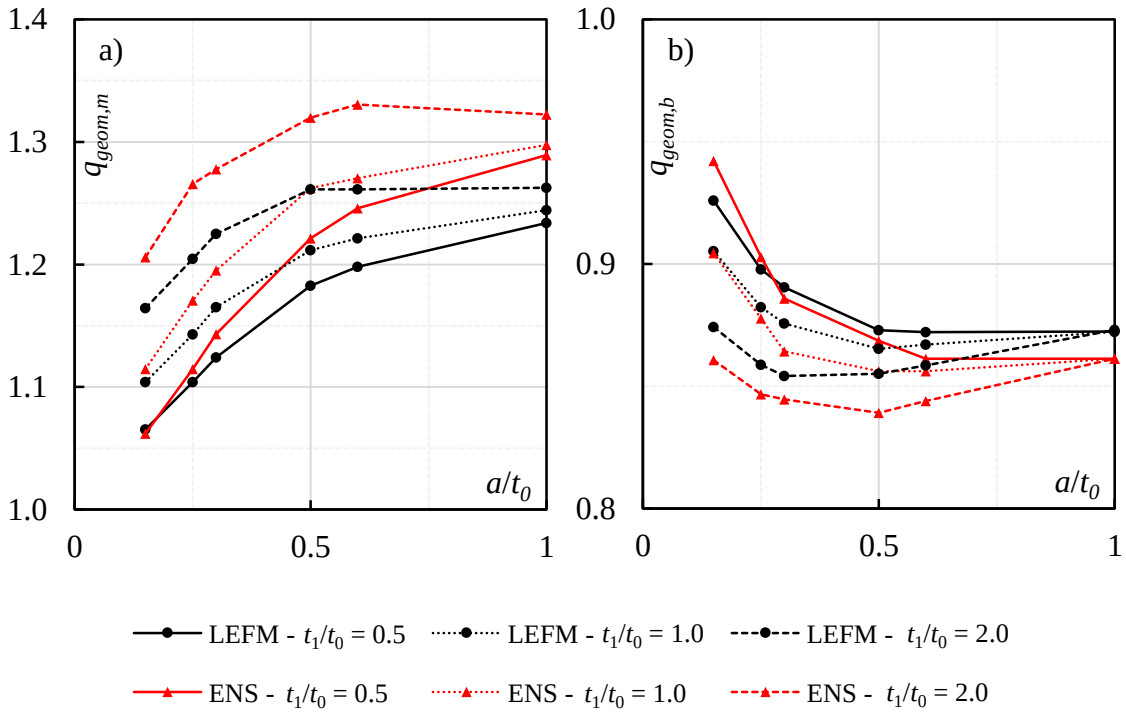

Figure 32. Obtained fatigue strength ratios (q_{geom}) of the transverse attachment joints under (a) tensile and (b) bending loading.

The effect of loading type on fatigue cannot be discovered explicitly. In the asymmetric joint case, ENS method estimated a 1.1–1.2 times higher fatigue strength for joints under tensile loading. The ratios obtained by using LEFM method, instead, pointed out the negligible

effect of loading type, Figure 33a. In the symmetric joint case, Figure 33b, ENS and LEFM methods gave approximately a ratio coefficient of 0.75-0.95 and 0.70-0.85, respectively. Therefore, LEFM estimated slightly more significant effect, but still had good agreement with ENS results.

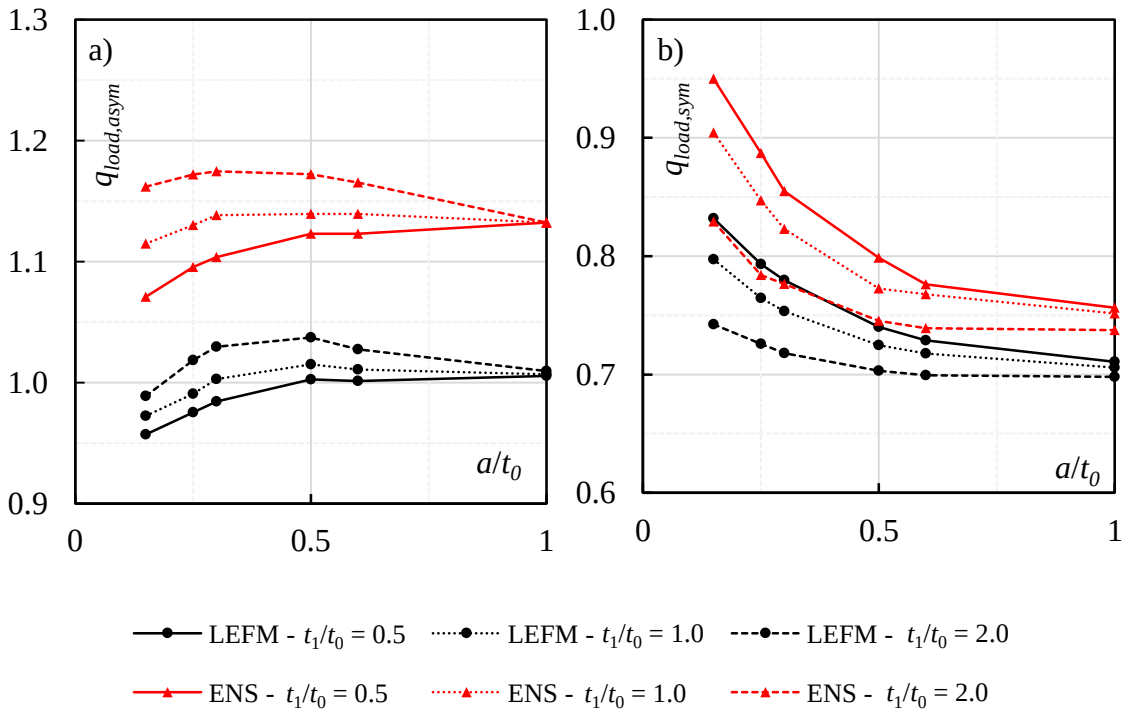

Figure 33. Obtained fatigue strength ratios (q_{load}) of the transverse attachment joints in (a) T-joint and (b) X-joint cases.

The dimensions of joint do not affect significantly on the fatigue strength ratios in the asymmetric case, unlike in the symmetric case. In the symmetric case, the increase of throat thickness and attached plate thickness emphasize the effect of loading type. More detailed results of transverse attachment joints are presented in Appendix VIII.

A clear agreement between transverse attachment and cover plate cases can be discovered. However, in the cover plate case, the magnitude of the effect is highlighted. According to ENS method, the fatigue strength of tensile loaded asymmetric joint is approximately double when the cover plate is long. The fatigue classes obtained by LEFM reduce the effect of geometrical symmetry compared to ENS method in the tensile load case. Still, the both approaches agree well. In bending load case, the magnitude of effect is not emphasized.

Figure 34 shows the fatigue strength ratios of $t_1/t_0 = 2$. Fatigue strength ratios for $t_1/t_0 = 0.5$ and $t_1/t_0 = 1.0$ are shown in Appendix IX. In the case of $a = 0.15t_0$ and $L = 20t_0$, LEFM estimate very low fatigue strength for bending loaded asymmetric joints, Appendices IX–X. For these joints, several crack propagation analyses with different crack increments were carried out but always the crack turned towards the attached plate. This might be a result of computational error.

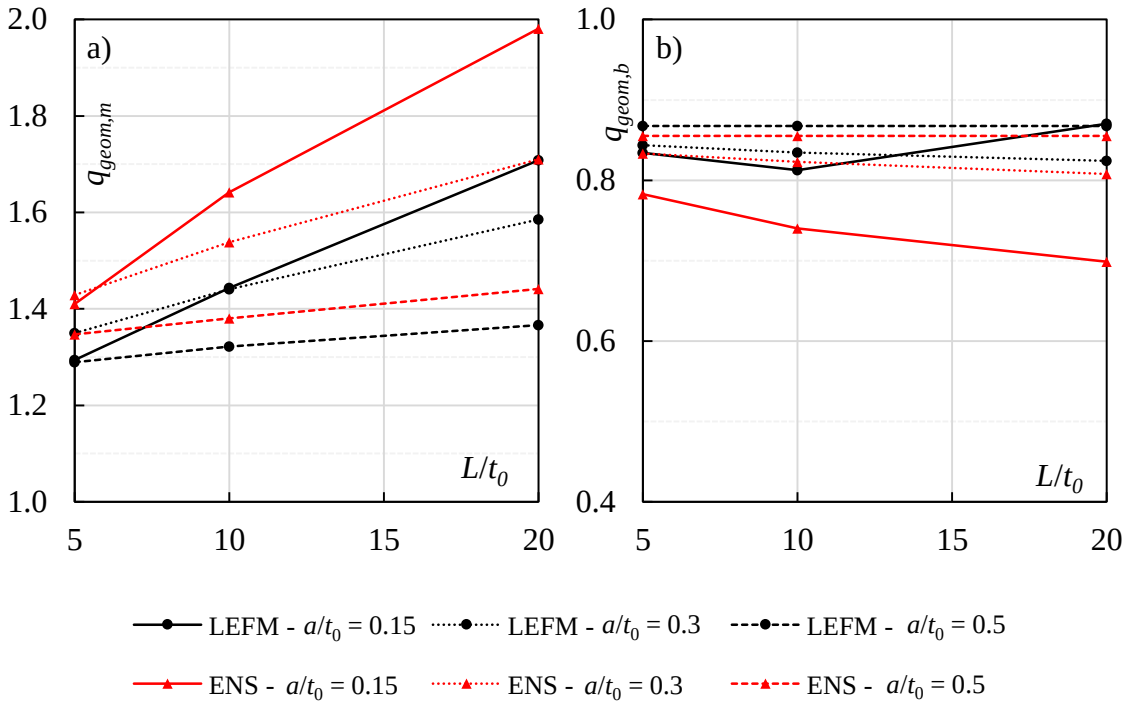

Figure 34. Obtained fatigue strength ratios (q_{geom}) of the cover plate joints under (a) tensile and (b) bending loading for $t_1/t_0 = 2$.

The effect of load type in asymmetric joints is ambiguous. ENS method estimated 1.1–1.7 times higher fatigue strength in tensile loading compared to bending load. According to LEFM, only 1.0–1.1 times higher fatigue class could be allowed for bending, Figure 35a. In the symmetric joints, both approaches have better agreement and estimate a fatigue strength ratio of 0.6–0.7 for tensile loading with respect to bending loading, Figure 35b.

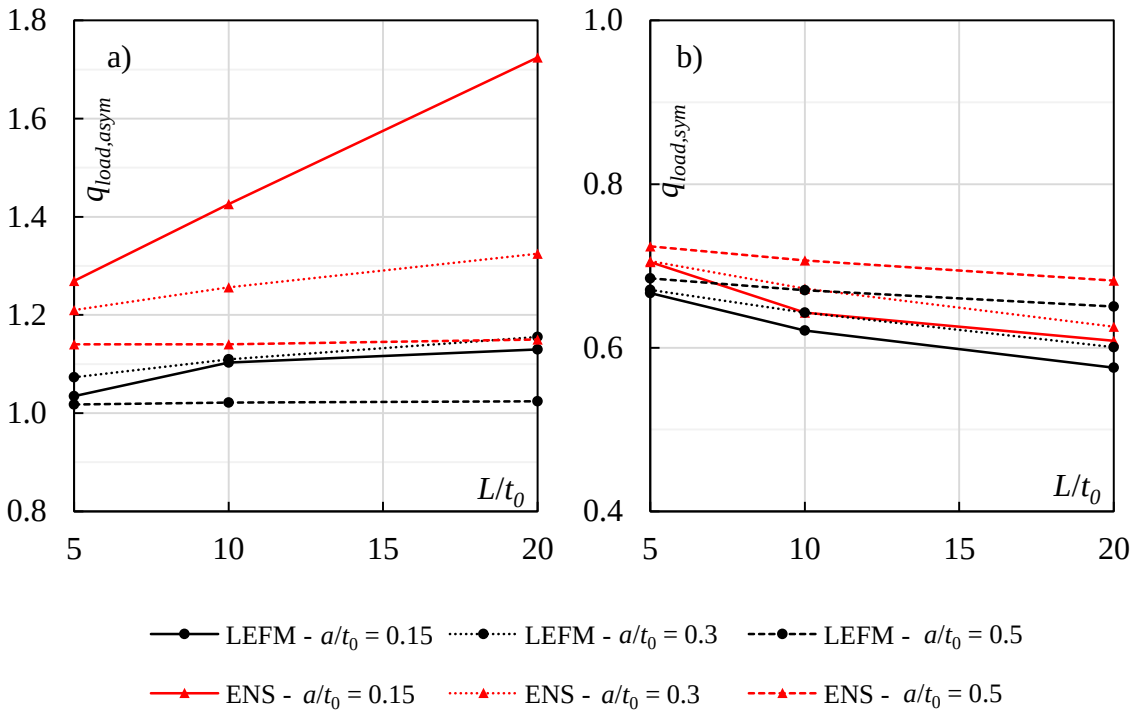

Figure 35. Obtained fatigue strength ratios (q_{load}) of the cover plate joints in (a) asymmetric and (b) symmetric joints for $t_1/t_0 = 2$.

Generally, increasing the length of attached plate emphasizes the effect of geometrical symmetry and loading type. A larger throat thickness decreases the influence of attached plate's length as illustrated in Figures 33–35. With respect to the transverse attachment case, the increase of throat thickness reduces the effect in the cover plate joint case. More detailed results of cover plate joints are presented in Appendix X.

4.2 Longitudinal Gusset Case

By means of ENS method, total number of 13 different geometry options were analyzed. For each geometry, both asymmetric and symmetric cases were analyzed under tensile and bending loading. The FEAs of longitudinal gusset joints point out similar fatigue behavior to 2D joints. The prime geometry consists of b = 50 mm wide and t = 6 mm thick plate. The gusset length and throat thicknesses were alternated.

According to the obtained results, the gusset length does not have a great influence on ENS value at weld toe, Table 8. This was unexpected since IIW recommends to reduce the fatigue strength when the gusset length increases, Appendices I–II. For this reason, the ENS

analyzes were conducted also for wider, b = 200 mm plates with a = 3 mm. Otherwise, the evaluated ENS values follow the phenomenon introduced in Chapter 4.1: ENS is higher for symmetric joint in tensile loading and for asymmetric joint in bending loading. The increase of throat thickness reduced the ENS and improved the evaluated FAT_{nom}, as assumed. Figure 36 shows an example of notch stresses in sub-models. The effective stress concentration factors for analyzed joints are presented in Appendix XI.

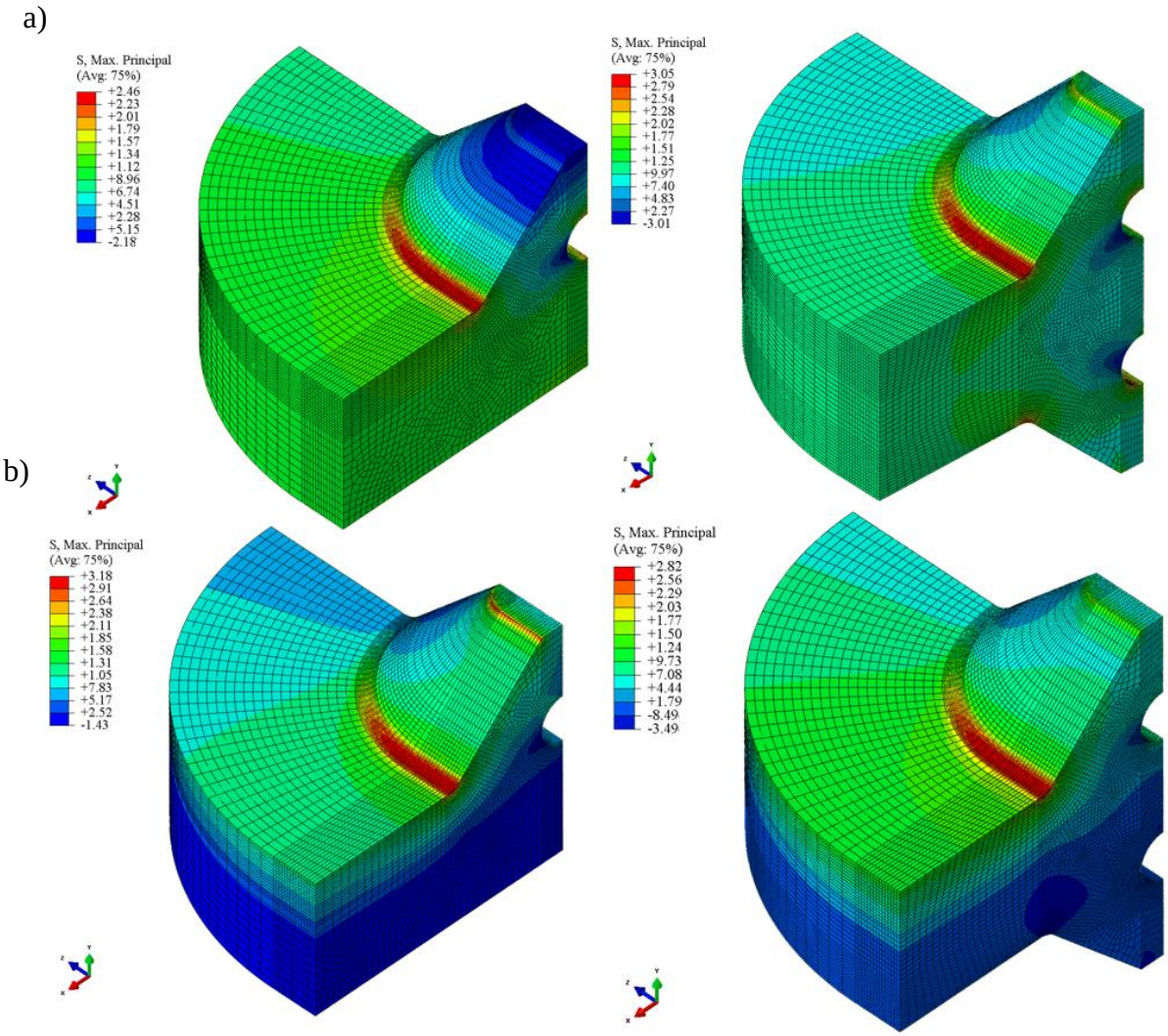

Figure 36. Effective stress concentration factors, k_f in terms of max principal stress criterion under (a) tensile and (b) bending load in the asymmetric and symmetric cases of longitudinal gusset, when a = 3 mm and L = 75 mm.

Table 8. Calculated FAT_{nom} values by means of ENS method. The evaluation has been done according to Figure 31. The highlighted geometries were analyzed by LEFM, Table 9.

Geometry			Nominal FAT class			
b [mm]	L [mm]	a [mm]	$FAT_{nom,t,asym}$ [MPa]	$FAT_{nom,t,sym}$ [MPa]	$FAT_{nom,b,asym}$ [MPa]	$FAT_{nom,b,sym}$ [MPa]
50	75	3	91.6	73.8	70.8	79.7
50	150	3	91.3	70.8	71.7	79.8
50	300	3	91.3	70.3	71.7	79.7
50	75	4.5	95.0	77.6	74.6	82.8
50	150	4.5	94.9	76.0	74.7	82.8
50	300	4.5	94.9	75.8	74.7	82.8
50	75	6	98.4	80.0	77.1	85.5
50	150	6	98.0	79.1	77.1	85.4
50	300	6	98.3	79.0	77.1	85.5
200	37.5	3	83.3	80.1	55.7	57.8
200	75	3	76.3	66.6	42.3	45.7
200	150	3	74.8	59.5	39.7	43.9
200	300	3	74.5	55.7	40.8	45.1

It is noticeable that plate width/gusset length seems to have more significant influence on the notch stress than the gusset length itself. Particularly in bending loading, the width increases the notch stresses consistently in both asymmetric and symmetric joints. Consequently, ENS method predicts that the fatigue strength of longitudinal gusset joints decreases notably when external loading is bending. The gusset length reduces the fatigue strength more distinctly in the wider plates. Actually, the symmetric joint follows fairly the FAT_{nom} given by IIW, Appendix I.

After conducting the ENS results, it was determined that throat thickness and plate width were alternated in LEFM. XFEM analyses were applied for L = 75 mm joints, with three different options. The evaluated FAT_{nom} and test geometries are presented in Table 9. When comparing the results presented in Table 8 and 9, both methods have reasonable accordance. Still, the LEFM slightly reduces the effect of both symmetry and loading type. Additionally, in the LEFM, the increase of plate width does not affect as diminishingly on fatigue strength as ENS method estimates.

Table 9. Calculated FAT_{nom} values by means of LEFM. The evaluation has done according to Figure 31.

Geometry			Nominal FAT class			
b [mm]	L [mm]	a [mm]	$FAT_{nom,t,asym}$ [MPa]	$FAT_{nom,t,sym}$ [MPa]	$FAT_{nom,b,asym}$ [MPa]	$FAT_{nom,b,sym}$ [MPa]
50	75	3	85.2	72.5	81.9	88.2
50	75	6	89.1	79.0	88.0	95.0
200	75	3	70.3	64.2	54.0	57.4

4.3 Results of Experimental Tests

The experimental tests were carried out for non-load carrying, transverse attachment joints. Eight specimens were tested under pure bending and four specimens under tensile loading. In the following chapters, the preparation of test specimens, results and FEAs are presented.

4.3.1 Preparing of Test Specimens

Residual stress distributions along specimen were measured in one specimen of each joint type. Figure 37a illustrates the distribution in the asymmetric joint type and the measured residual stress points at weld toe. In Figure 37b, the corresponding results are presented for the symmetric X-joints.

Compressive residual stresses occurred at weld toes. However, residual stresses were not considerable high, typically $0.1–0.2 \cdot f_y$ and any significant difference in the residual stress state between asymmetric and symmetric joints could not be found in the measurements. Consequently, residual stress did not affect on the effect of symmetry in the fatigue tests, most likely. Specimen global and weld shapes were measured before fatigue tests.

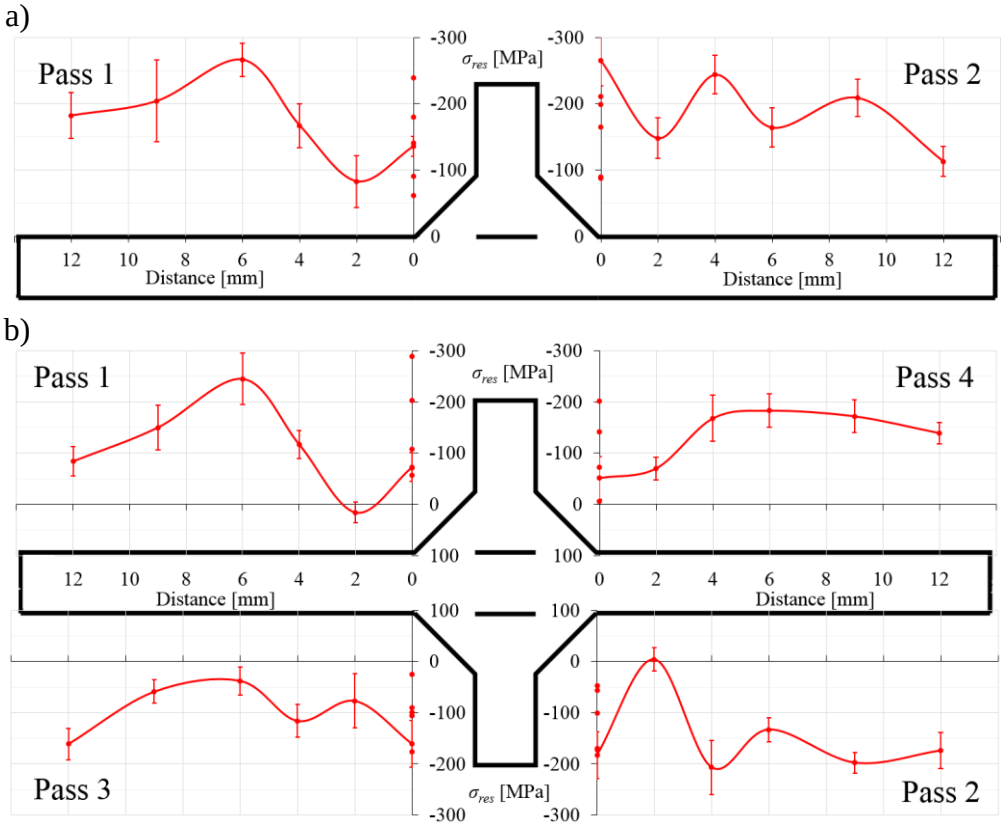

Figure 37. Measured residual stress distribution and single residual stress points at weld toe in (a) the asymmetric T-joint specimens and (b) symmetric X-joints.

All geometrical data are presented in Appendix XII. Nominal throat thickness a_{mean} = 5.2 mm (*Stdv* = 0.16 mm) was evaluated which corresponds well with the values of the polished sections, Figure 24. For the actual notch radius, values of ρ = 0.2–0.4 mm were measured. Since the actual notch radii were only measured on the center line of specimen and the values were quite low, it is reasonable to assume conservatively ρ = 0 in ENS method, as it is also recommended by IIW (Hobbacher, 2014, p. 29–30). Figure 38 depicts the principle of evaluating the measured data.

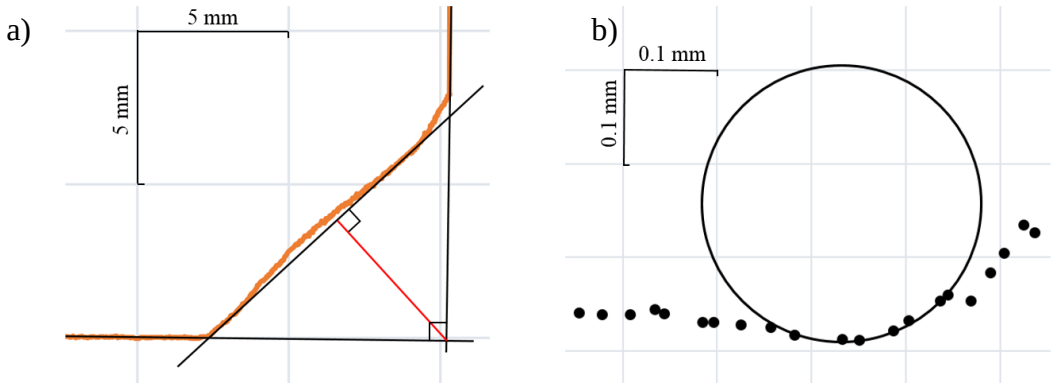

Figure 38. Evaluation of (a) nominal throat thickness and (b) actual notch radius.

4.3.2 Fatigue Test Results

The single test results are presented in Appendix XIII. The resulting data of the tension loaded specimens and the obtained fatigue classes in terms of HS stress method are presented in Figure 39. In order to improve the comparability of the results, the recommended m = 3 and shallower m = 5 slopes were consistently applied. m = 5 was used since it had good agreement with the T-joint test data. Fatigue classes are determined by means of standard procedure recommended by IIW, Appendix IV. In the calculation of characteristic values, factors k = 2.808 and k = 2.486 for tension and bending are derived, respectively. Alternative curve fittings are discussed later in this chapter.

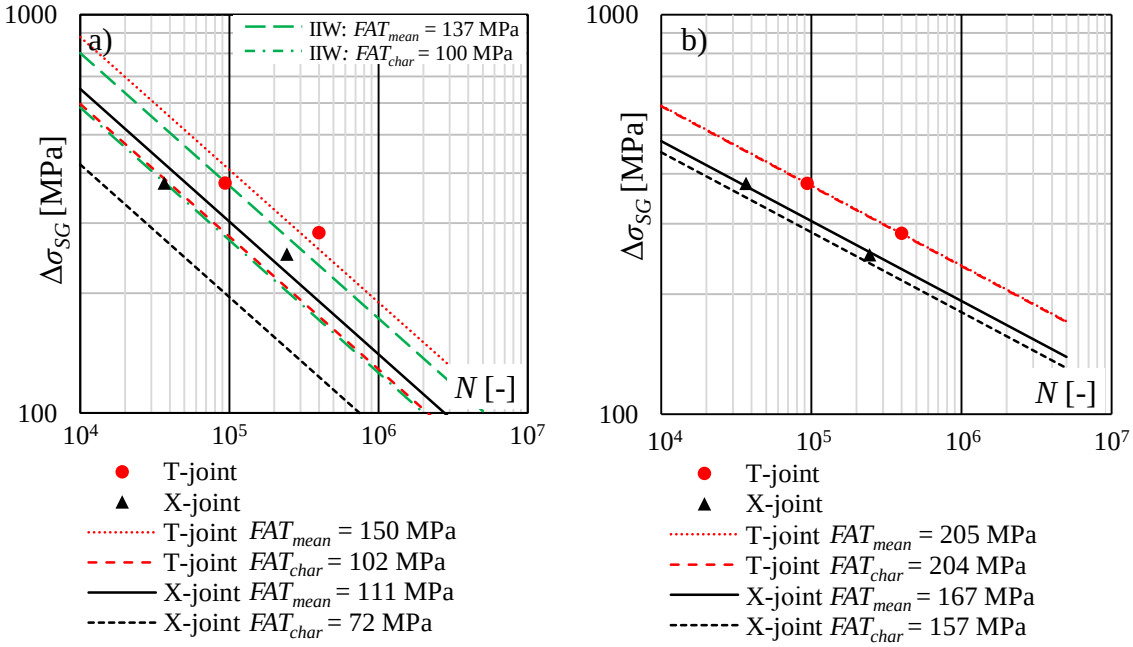

Figure 39. Obtained test results and determined fatigue classes of the tensile loaded joints with a slope of (a) m = 3 and (b) m = 5 in terms of HS stress method.

Figure 39 shows the improvement of fatigue strength in the asymmetric T-joint specimens under tensile loading. When mean values (m = 3) are observed, the FAT class of the T-joints was 35 % higher than the X-joints. Due to the higher standard deviation of the X-joints, the difference increases if the characteristic values are used. In comparison with the mean FAT class of IIW, the FAT class of the T-joints is higher and the FAT class of the X-joints is lower.

As shown in Appendix XII, the angular distortion of the T-joints was clearly higher compared to the X-joints. In the X-joints, shape laser measurements indicated small angular distortions. Although, during the test, it was discovered that stress range at strain gage was identical with nominal stress range calculated by means of measured force range. Also in the T-joints, the strain gage measurements showed lower structural stresses than expected according to the measured shape. Consequently, the specimens straightened due to clamping. Because of secondary bending stress component in the T-joints, the nominal stress ranges did not correspond directly with HS stresses. Additionally, in real structures, nominal loading is typically observed. Based on these facts, it is reasonable to compare the results also by means of nominal stress approach, Figure 40.

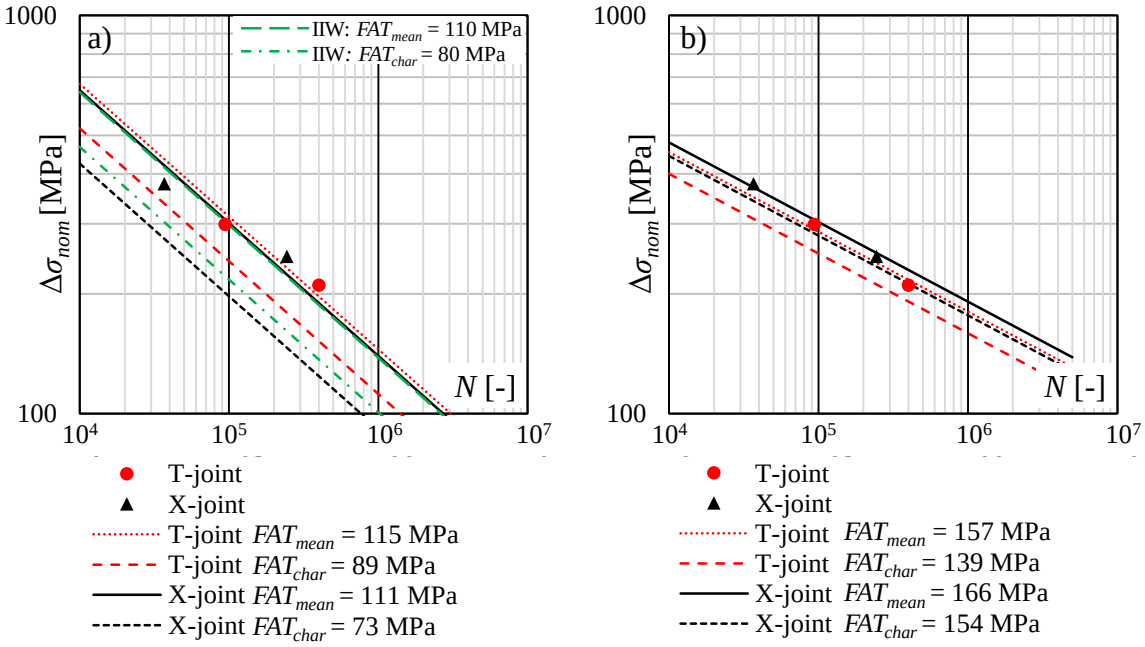

Figure 40. Obtained test results and determined fatigue classes of the tensile loaded joints with a slope of (a) m = 3 and (b) m = 5 in terms of nominal stress method.

In the nominal stress method, the evaluated fatigue classes of both joint types are basically identical and have good accordance with the fatigue class recommended by IIW (FAT_{mean} = 110 MPa). The characteristic values do not correspond fully with IIW value (FAT_{char} = 80 MPa) but it is reasonable since the number of test specimens was minor. When m = 5, the fatigue strength of the X-joints is slightly higher with respect to T-joint but the difference is less than 10%, Figure 40b.

When the bending load case is taken under investigation, Figure 41, it must be noticed that secondary bending stresses due to angular distortion or the mounting of specimen did not occur during the tests. For that reason, nominal stresses are equal to structural stresses which were also verified by strain gage measurements. Additionally, strain gage measurements assigned identical stresses at both weld toes and the testing procedure was successful and both weld toes were as critical for crack initiation.

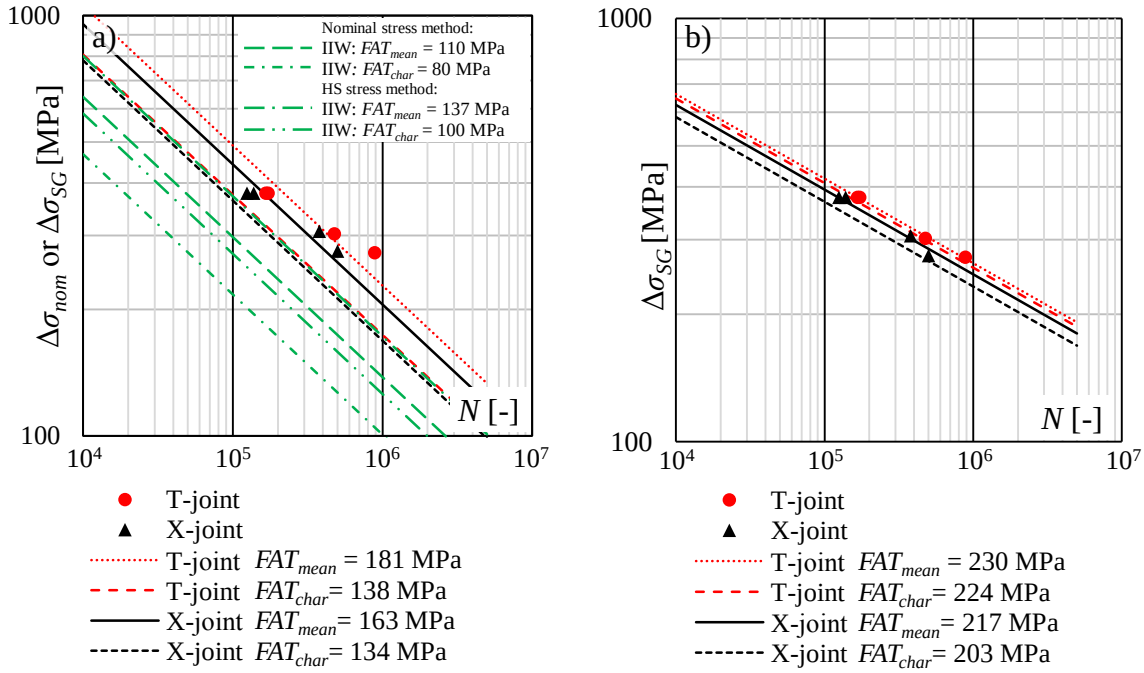

Figure 41. Obtained test results and determined fatigue classes of the bending loaded joints with a slope of (a) m = 3 and (b) m = 5 in terms of nominal stress and HS stress methods.

In the symmetric X-joints, the improvement of fatigue strength is remarkable. When m = 3 is used, the mean fatigue class of X-joints enhances 47 % in terms of HS stress method, Figures 39a and 41a. Related to former studies and results presented in Chapters 4.1-4.2, this

is predicted. On the contrary, Figures 39 and 41 show unexpectedly a distinct improvement in the fatigue strength of T-joints. However, the improvement is not as substantial as in the X-joints but it is still 21 %. The fatigue classes of IIW recommendations are clearly conservative for both joint types when external loading is bending. In nominal stress method, the fatigue strength of T-joints improves more significantly, but the results are not comparable due to a distinguishing secondary bending stress component in tensile loading.

Since bending effect occurred in the tests, it is reasonable to test how the DNV's reduction factor, Equation (10), is suitable for the tested joints. Figure 42 indicates that the reduction factor is excessively high for these joints. The test results subjected to bending distinctly are below the obtained FAT_{mean} = 109 MPa. It appears that FAT_{mean} remain at the low level with respect to FAT_{mean} = 137 MPa suggested by IIW. A reduction factor of 70–80 % for bending stress component would harmonize the test data more clearly on one curve. However, the results fit between a standard deviation of two.

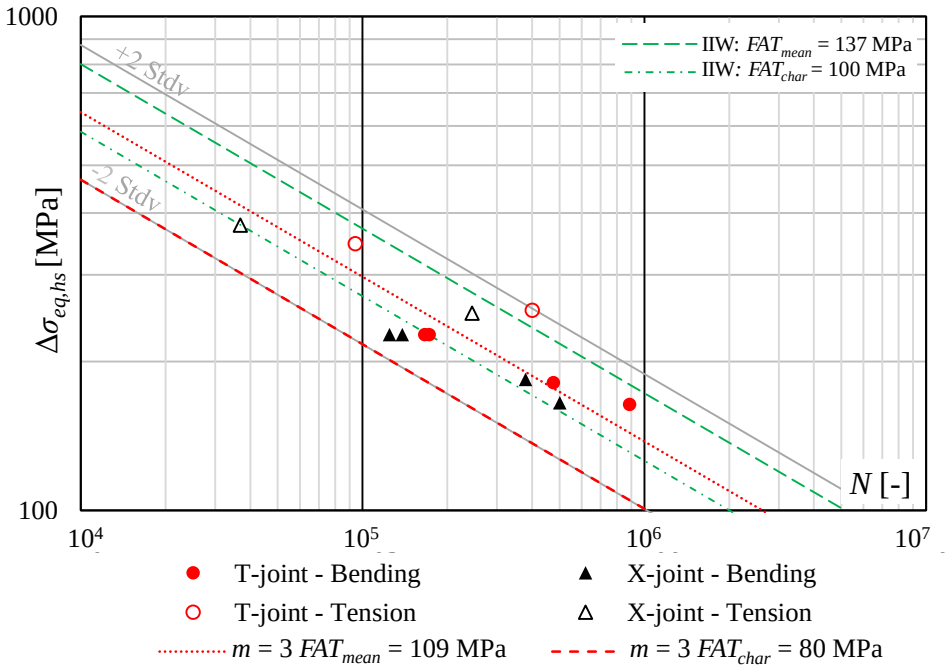

Figure 42. All test data in terms of HS stress method. The bending stress component of each test is reduced by 40 % according to Equation (10).

Figure 43 shows that the test data of tensile loaded both asymmetric and symmetric joints fairly fits on the same FAT class when ENS method is utilized. The recommended m = 3 slope and free m slope curve fittings are applied. For the T-joints, the evaluated FAT_{mean} (m

= 4.93) is slightly conservative and the X-joint test results sets slightly under the curve. If *FAT* classes (m = 4.93) are defined separately for both joint types, $FAT_{mean,asym}$ = 409 MPa and $FAT_{mean,sym}$ = 394 MPa are derived.

In the test results, the analytical formulae of notch stress factors by Tsuji are applied, Appendix V. The membrane and bending stress components of each fatigue test are evaluated by means of strain gage measurements. Notch factors are defined for both stress components to assess the ENS precisely. HS stresses were higher in the T-joints but respectively but higher stress concentration factors in the X-joints compensates it and finally the ENSs are almost identical.

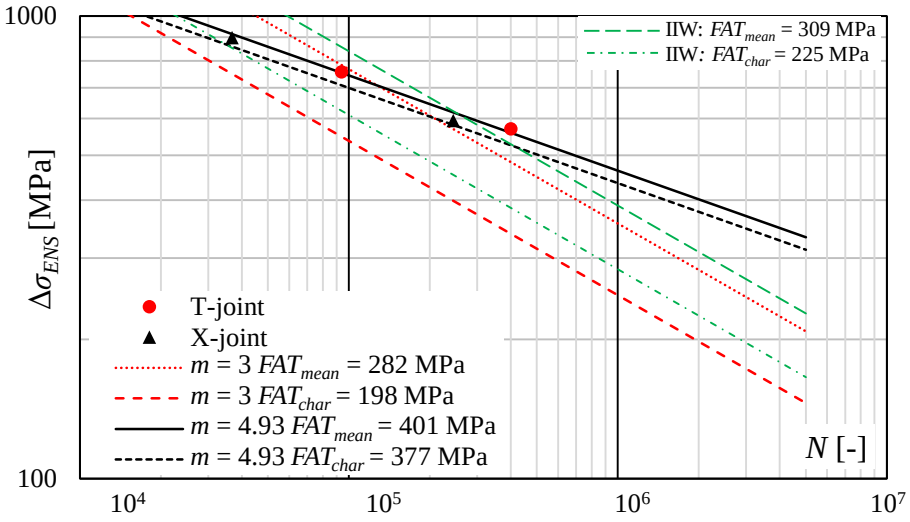

Figure 43. Obtained test results and determined fatigue classes of tensile loaded joints in terms of ENS method.

Due to lack of analytical formulae for bending loaded symmetric joints, ENS method is not utilized in bending loaded joints. Still, ENS method is applied also for bending loaded joints in the numerical analyses of tested specimens, Chapter 4.3.3. Figures 39–41 indicate that the S-N curve slopes of asymmetric and symmetric joints are not similar. Table 10 summarizes the results of standard curve fitting procedure and more comprehensive MSSPD curve fitting for each test series.

Table 10. Summary of mean fatigue classes with various curve fittings and free m in terms of nominal and HS stress systems.

		Standard procedure				MSSPD			
		$\Delta\sigma_{nom}$		$\Delta\sigma_{hs}$		$\Delta\sigma_{nom}$		$\Delta\sigma_{hs}$	
Joint type	Loading type	m	FAT_{mean} [MPa]	m	FAT_{mean} [MPa]	m	FAT_{mean} [MPa]	m	FAT_{mean} [MPa]
T-joint	Bending	4.975	229.5	4.975	229.5	4.995	229.9	4.995	229.9
X-joint	Bending	4.395	204.3	4.395	204.3	4.475	206.1	4.475	206.1
T-joint	Tension	4.105	142.0	5.066	206.7	4.105	142.0	5.066	206.7
X-joint	Tension	4.521	156.0	4.625	159.3	4.521	156.0	4.625	159.3

In each of the fatigue tests, a crack initiated in the desired continuous part of weld, at weld toe. Crack propagated approximately into half of the plate thickness and a final rupture occurred as either ductile failure or the combination of ductile and brittle failure. Figure 44 summarizes the fracture surfaces of all test specimens.

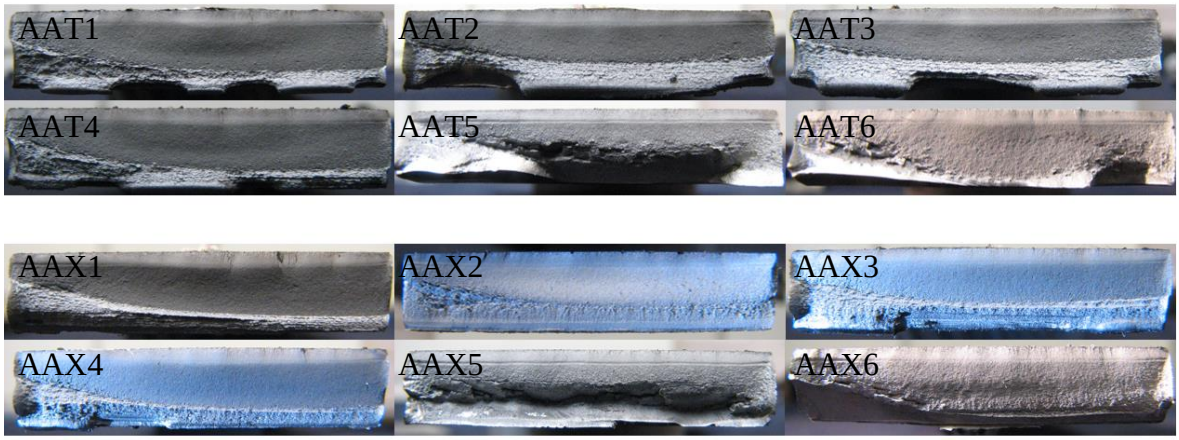

Figure 44. Fracture surfaces of tested specimens. Specimen IDs 1–4 are tested under bending and IDs 5–6 under tensile loading.

Figure 44 illustrates the difference between bending and tensile loading in the final ruptures. In the bending loaded joints, the final fractures were ductile. Under bending loading, the bending effect appears distinctly when crack propagates, as discussed in Chapter 4.1. SIF is lower in the case of bending when SIF does not exceed the fracture toughness of the material. Additionally, when the crack has propagated through the plate width, the section modulus has quadratic dependency on the height and thus, nominal stress increases significantly. For that reason, the yield strength of the material is exceeded and ductile fracture occurs.

When large crack occurs under tensile loading, the SIF values are higher than under bending loading, i.e. crack shape correction term $Y(a)$ gives higher values for membrane stress. Furthermore, cross section area and therefore nominal stress have only linear dependency on the height. Consequently, the yield strength does not exceed primarily and the brittle fracture criteria is fulfilled. This aspect can be seen in specimen IDs 5–6, Figure 44, in which a typical block-shaped surface appears on the edges of fatigue crack.

4.3.3 Numerical Analysis

Numerical analyses were carried out to compare the test results to fatigue assessment methods. All three stress based methods: nominal stress, HS stress and ENS approaches are applied to assess the fatigue life of tested joints. Additionally, LEFM is used to include fracture mechanics in the analyses.

A difficulty appeared in tensile loaded asymmetric joints in which strain gage measurements demonstrated the straightening of specimens, as discussed in Chapter 4.3.2. The measured and evaluated k_m factors are presented in Table 11. Even though the straightening of specimen due to loading was taken into account by utilizing Equation (15) in the analytical evaluation and by using geometrically non-linear FEA, the k_m factors evaluated by strain gage were evidently lower with respect to the corresponding shape laser values. In the strain gage based evaluation, the linear extrapolation is neglected but the used LSE method indicated that the effect of extrapolation is minor when stress at $0.4t$ equals approximately to the extrapolated value. Consequently, the angular distortion was conversely recalculated by means of strain gage measurement, and this value of angular distortion was applied in the ENS and LEFM models. For those models, geometrically linear analyses were finally ran to receive exact DOB. The X-joints were modeled without angular distortion for the same reason.

Table 11. Angular distortions in tensile loaded joints. Indices SG and SL signify strain gage and shape laser, respectively.

ID	α[rad]	$k_{\mathrm{m,analytical}}$ [-]		$k_{m,FEA,SL}$ [-]		$k_{m,FEA,SG}$ [-]	
		SL	SG	LSE	TTWT	LSE	TTWT
AAT5	0.020	1.36	1.26	1.40	1.40	1.29	1.29
AAT6	0.024	1.47	1.35	1.51	1.51	1.39	1.38

The analytical formulas and strain gage measurements had a fine agreement with the k_m factors evaluated by FEA. The values of strain gage measurements were used in the eventual calculation of fatigue lives. The obtained fatigue lives derived by the approaches' mean values are presented with the test results in Figure 45.

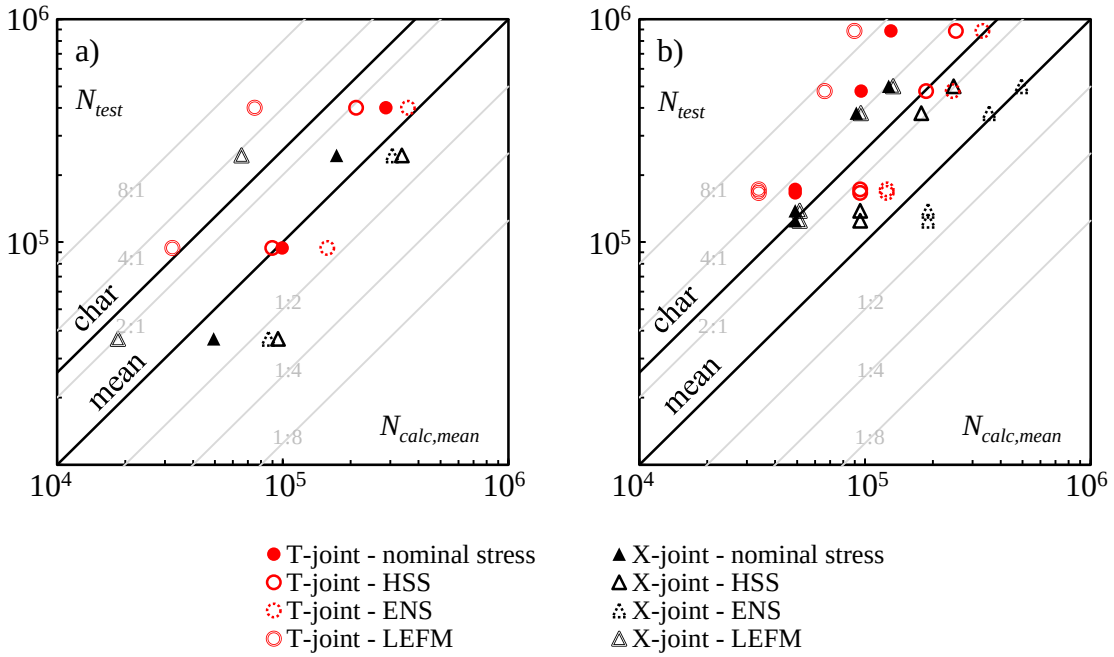

Figure 45. The calculated mean fatigue lives for (a) tensile and (b) bending loaded joints in comparison with the test results.

In the tensile load case, nominal stress and HS stress methods gave the best assessment of fatigue life. Still, fatigue lives of asymmetric and symmetric joints are not on the same curve in terms of HS stress method. ENS method is slightly non-conservative for the tensile load case. In bending load case, ENS method has better agreement with the test results but it overestimates the fatigue life of X-joints, Figure 45b. Both HS stress and nominal stress methods were slightly conservative in bending load case.

LEFM is overly conservative for both joint types. In the fatigue life assessment, initial crack size a_i = 0.05 mm is used but even smaller crack is applied in the model. Figure 46 presents the effect of initial crack size on fatigue life with respect to the fatigue life of a_i = 0.05 mm. In the T-joints, initial crack size more remarkable than in the X-joints. Otherwise, the tensile

load is more sensible for initial crack size. The overview of fatigue life assessment indicates the fact that the slope m = 3 does not fit on the observed joints.

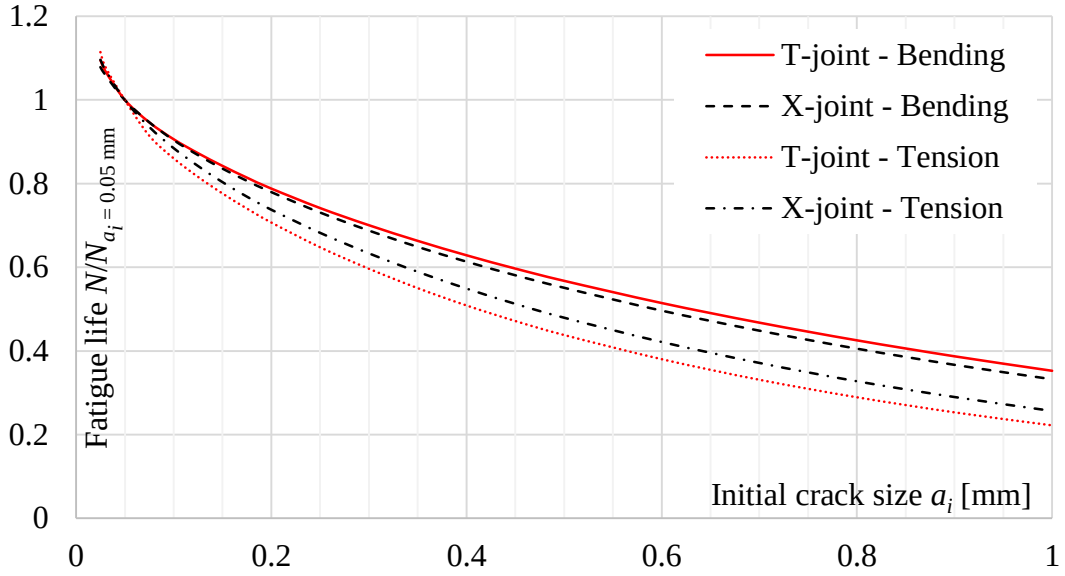

Figure 46. Effect of initial crack size on fatigue life assessed by means of LEFM.

Table 12 summarizes the results of experimental tests compared to numerical analysis. The use of fatigue strength ratios, q_{geom} and q_{load}, removes the conservativeness or non-conservativeness of methods' coefficients. Consequently, the comparability of different fatigue assessment methods is improved.

Table 12. Fatigue strength ratios evaluated by means of used methods. The ratios of the experimental tests are evaluated by using the FAT classes of the slope m = 3. In the tensile loaded T-joints, the angular distortion leading to $k_{m,mean}$ = 1.34 is applied (TTWT, Table 11).

	Experimental		Fatigue assessment			
Ratio	Nom. stress	HS	Nom. Stress	HS	ENS	LEFM
$q_{geom,m}$	1.04	1.36	0.75*	1.00	1.24	1.23
$q_{geom,b}$	1.11	1.11	1.00	1.00	0.87	0.87
$q_{load,asym}$	0.64	0.83	0.75*	1.00	1.09	1.00
$q_{load,sym}$	0.68	0.68	1.00	1.00	0.77	0.71

*If angular distortion considered, otherwise 1.00

Although nominal and HS stress methods agreed well with the test results, Table 12 demonstrate the complexity in the use of nominal and HS stress methods. FAT_{nom} given by

IIW (Hobbacher, 2014, p. 63) covers only k_m = 1.2. In the tests, higher k_m factors were evaluated and hence, it should be taken into account also in nominal stress system. Now, $q_{geom,m} = q_{load,asym}$ = 1.00 / 1.34 = 0.75 are received for nominal stress method. If the effect of angular distortions is neglected, the aforementioned values equal to 1.00. Nevertheless, the fatigue tests indicated a slight improvement (4%) in the fatigue strength of the tensile loaded T-joints. ENS and LEFM have practically identical fatigue strength ratios and the ratios agree fairly with the test results in terms of HS stress method although the effect of symmetry in tensile load case was even greater in the tests.

Compared to the assessed fatigue lives, unexpectedly the fatigue strength of the tested T-joints improved with respect to the X-joints under bending loading. ENS and LEFM methods estimate fatigue strength ratio of 0.87 for bending but the tests indicate a divergent result since fatigue strength ratio is 1.11. Since the angular distortion does not cause secondary bending under bending loading, nominal stress method does not show any distinguishing result between asymmetric and symmetric joints. The test results show that the fatigue strength of transverse attachment joints is consistently higher when the DOB increases. Respectively, ENS gives a value of 1.09 and LEFM a value of 1.00 for the T-joints so the approaches do not fully agree with the test results. In the ENS method and LEFM, the notch effect at weld toe is higher under bending load, which results that the increasing DOB does not give a higher fatigue strength for asymmetric joints. Actually, nominal stress method has better agreement with the test results. However, the ENS method and LEFM agree generally with the test results of X-joints.

5 DISCUSSION

In this thesis, computational and experimental analyses were used to investigate the effect of loading type on the asymmetric and symmetric non-load carrying welded joints. In the joints subjected to tension, both FEA and the conducted fatigue test results pointed out an improvement in the fatigue strength of asymmetric joints compared to symmetric joints. The test results gave an even more remarkable effect of geometrical symmetry than ENS method and LEFM estimated. This result is very essential to take into account in the fatigue designing of welded joints and structures and represents the novelty of this study. The evaluated FAT_{nom} and FAT_{HS} of symmetric joints had relatively good agreement with the IIW values. Consequently, the present recommendations and standards do not utilize completely the fatigue capacity of asymmetric joints in tensile loading.

In the bending loading cases, FEAs estimated that symmetric joints to have lower stress concentration and magnification factors than asymmetric joints. Because of this, the fatigue strength of the tested X-joints should have been higher compared to the T-joints. Nevertheless, the fatigue tests showed unexpectedly that fatigue strength was better in the asymmetric case. On the basis of the conducted FEA and experimental tests, explicit conclusions about fatigue properties of bending loaded joints cannot be drawn. Still, this study is provides notable information about the complexity of bending loading.

Currently, the most ruling European codes (e.g. IIW, EC3 and DNV) consider only the gusset length when fatigue life is assessed for longitudinal gusset joint by means of nominal stress or HS stress methods. Other geometry variations, such as throat thickness and plate width, are neglected. In this study, the effect of the gusset length can be exclusively recognized when the wider plates were analyzed. Respectively, throat thickness and plate width affected on the ENS distinctly. Salehpour (2013, p. 53) presented a similar behavior of plate width's effect on notch stress. In the fatigue designing for engineering purposes, it is not reasonable to consider every single geometrical factor which affects on fatigue properties but it would be necessary to update and refine the current codes. Additionally, the notch stresses were extremely sensitive for the plate width, when the external loading is bending.

In the ENS method, FAT_{mean} = 309 MPa was non-conservative for tensile loaded joints. ENS method estimated also reasonable high values of FAT_{nom} for the transverse attachment joints. Consequently, the recommended FAT_{ens} = 225 MPa might be generally non-conservative for tensile loaded joints and a lower value should be used. This conclusion was made also by Nykänen et al. (2015, p. 308) that proposed FAT_{ens} = 198 MPa. Respectively, under bending loading the mean value had good agreement with the test results because a beneficial bending effect occurred in the experimental tests. In the LEFM, the estimated value $C_{mean} = 1.7 \cdot 10^{-13}$ did not correspond with the test results and the assessed fatigue lives were overly conservative. In general, the evaluated nominal stress and HS stress *FAT* classes of the tests corresponded well with the predictions but characteristic values were relatively low, as predicted, since the number of test specimens was minor.

In nominal stress method, the test results and FEAs of both T-joints and X-joints fit fairly on the same FAT class. In the IIW recommendation (Hobbacher, 2014, p. 63) it is stated that FAT_{nom} = 80 MPa includes an angular distortion leading to k_m = 1.2. In the tensile loaded T-joints, the angular distortions led to k_m = 1.26 and k_m = 1.35, and still any decrease in the fatigue strength compared to X-joints could not be discovered. Consequently, the angular distortion of asymmetric joints, in which it appears commonly due to one-sided welding, may not be as critical as the recommendation implies.

5.1 Conclusions

For now, the standards have mostly concerned asymmetric and symmetric joints as well as loading type consistently. This study shows evidently that both the symmetry of joint and loading type have influence on the fatigue behavior of welded joints. According to the test results and FEAs, the following conclusions can be drawn:

- In the 2D non-load-carrying joints, the fatigue strength of asymmetric joints is higher than the corresponding symmetric joints in tensile loading according to FEA. In bending loading, the fatigue strength of symmetric joint is higher.
- Simultaneously, the fatigue strength of asymmetric joints is higher under tensile loading and the fatigue strength of symmetric joints, on the contrary, under bending loading.
- In longitudinal gusset joints, the plate width increased significantly notch stresses at weld toe in both asymmetric and symmetric cases. Particularly, the plate width have

an extremely major influence on the notch stress values when the external loading is bending.

- Experimental tests supported the theory in the tensile load case but did not work in the bending load case since the increasing DOB obtains consistently higher fatigue strengths.
- The derived FAT classes in terms of nominal stress and HS stress systems had generally good agreement with the fatigue assessments and codes. Still, the consideration of joint's symmetry is challenging by means of nominal stress and HS stress methods without updating the FAT classes of the standards to take symmetry into account.
- ENS method was non-conservative for tensile loaded joints with FAT_{mean} = 309 MPa and LEFM with estimation $C_{char} = 1.7 \cdot 10^{-13}$, was overly conservative for both tensile and bending loaded joints.

In the assessment of the above-mentioned phenomena, it must be noticed that only small-scale specimens were analyzed. In real structures, the magnitude of effect or the effect itself can vary since the actual constraints of structure may have an influence on the stress state at both HS and notch stress levels. For instance, it matters whether a longitudinal gusset is welded on a sheet, rectangular hollow section or the flange of an I-beam. In those structures the stiffness of base plate may vary significantly.

5.2 Further Research

A computational part of this study presented the effect of geometrical symmetry and loading on the fatigue strength of typical non-load carrying joints by using engineering tools. In this respect, the study is completed. More comprehensive and mainly for scientific usage intended fatigue assessment approaches could be utilized. In that case, test data is also required to provide e.g. the knowledge of residual stress state. It would be reasonable to study the effect of bending loading in load-carrying fillet welded joints when also the fatigue of root side must be considered.

According to the test results, this study provides knowledge about normal quality welds. The bending effect occurred evidently in the test results. It is probably one reason for the fact that ENS method was not completely applicable in the bending load case. Further research

about high quality welds is necessary. Quality can be raised by improving the geometry at weld toe, e.g. by means of changing welding position or utilizing post-weld treatments. In that case, the crack initiation time with respect to total fatigue life is emphasized. The residual stresses of the tested joints were measured before testing but the further and more accurate study about the effect of residual stresses might explain why the fatigue strength of asymmetric joints was generally better.

In the longitudinal gusset joints, the width of plate seem to be the most considerable coefficient of geometry variation. It would be reasonable to investigate the effect of plate width more profoundly by means of FEA and experimental tests since the standards do not present any unequivocal guidelines on how to take plate width into account. The codes of IIW, EC3 and DNV pay more attention to the gusset length which, according to this study, affects only on the fatigue of longitudinal gusset joint in the wide plates.

6 SUMMARY

The FEAs of three different non-load carrying joint types along with the experimental tests of transverse attachment joints were carried out in order to clarify the effect of symmetry and loading type on the fatigue of welded joints. In the FEAs, the observed joint types were transverse attachment, cover plate and longitudinal gusset.

Transverse attachment and cover plate joints were modeled and analyzed by using plane strain models. When the fatigue life of a joint was calculated, notch stress system generally predicted that the fatigue strength of asymmetric case is higher than the corresponding symmetric case in the joints subjected to tension. The fatigue strength ratio depended on the dimensions of the joint but the ratios were $q_{geom,m}$ = 1.1–1.3 for the transverse attachment joints and $q_{geom,m}$ = 1.4–1.6 for the cover plate joints. By utilizing LEFM, the effect slightly decreased but still was remarkable, $q_{geom,m}$ = 1.05–1.25 and $q_{geom,m}$ = 1.25–1.45.

In the joints subjected to bending, the effect was reverse. Notch stress system implied that the fatigue strength of symmetric joints is higher than the corresponding asymmetric joints. The fatigue strength ratios were $q_{geom,m}$ = 0.75–0.95 for the transverse attachment and $q_{geom,b}$ = 0.7–0.9 for the cover plate joints. In the transverse attachment case, LEFM even emphasized the effect. For cover plate joints, LEFM gave approximately consistent results with ENS method. Simultaneously, in the 2D models, ENS method predicted that bending load is more harmful for the asymmetric joints and tensile load is more harmful for the symmetric joints in fatigue loading point of view.

The longitudinal gusset case exhibited similar behavior with respect to 2D joint types. The plate width seemed to have an increasing effect on the notch stresses of both asymmetric and symmetric joints subjected to bending. When the width was raised, also the gusset length impacted on the notch stress more distinctly. Additionally, the increase of throat thickness substantially reduced the notch stresses.

The experimental tests were carried out for transverse attachment joints. The test results approved the effect of symmetry in tensile loading, since in terms of HS stress system the

fatigue strength was 36% higher in asymmetric case. By utilizing notch stress system, the results fitted fairly on the same S-N curve. Under bending loading, the fatigue strength of asymmetric joints was higher compared to symmetric joints, on the contrary what FEA predicted. Additionally, in the experimental tests, the increasing DOB enhanced consistently the fatigue strength of both asymmetric and symmetric joints.

REFERENCES

Abaqus. 2014. Abaqus/CAE User's Guide. Dassault Systemes Simulia Corp.

Ahola, A. 2015. Effect of Symmetry on Notch Stress at Weld Toe [in Finnish]. Lappeenranta: 17.1.2015. Bachelor's Thesis. Lappeenranta University of Technology, Laboratory of Steel Structures. 34 p.

Anderson, T. L. 2005. Fracture Mechanics. Fundamentals and Applications. 3rd edition. Boca Raton, Florida, the United States of America: Taylor & Francis Group. 610 p.

Aygül, M., Al-Emrani, M. & Urushadze, S. 2012. Modelling and Fatigue Life Assessment of Orthotropic Bridge Deck Details Using FEM. International Journal of Fatigue, 40. P. 129–142.

Baik, B., Yamada, K. & Ishikawa, T. 2011. Fatigue Crack Propagation Analysis for Welded Joint Subjected to Bending. International Journal of Fatigue, 33: 5. P. 746–758.

Barzoum, Z. & Barzoum, I. 2009. Residual Stress Effects on Fatigue Life of Welded Structures Using LEFM. Engineering Failure Analysis, 16: 1. P. 449–467.

Baumgartner, J. & Bruder, T. 2013. An Efficient Meshing Approach for the Calculation of Notch Stresses. Welding in the World, 57: 1. P. 137–145.

Berge, S. 1985. On the Effect of Plate Thickness in Fatigue of Welds. Engineering Fracture Mechanics, 21: 2. P. 423–435.

Böhler. 2013. Filler Metals Bestseller for Joining Applications [online document]. [accessed: 1.12.2015]. Available from: http://ametist.bg/download/en/967/Weldingguide_ENG.pdf.

Chattopadhyay, A., Glinka, G., El-Zein, M., Qian, J. & Formas, R. 2011. Stress Analysis and Fatigue of Welded Structures. Welding in the World, 55: 7. P. 2–21.

Cornell Fracture Group. 2014. Software [online]. [accessed: 21.10.2015]. Available from: http://www.cfg.cornell.edu/software.html.

DNV-RP-C203. 2011. Fatigue Design of Offshore Steel Structures. Høvik, Norway: Det Norske Veritas. 176 p.

Dowling, N. E. 1999. Mechanical Behavior of Materials. Engineering Methods for Deformation, Fracture and Fatigue. 2nd edition. New Jersey, the United States of America: Prentice Hall. 830 p.

EN 1993-1-8. 2005. Eurocode 3: Design of Steel Structures. Part 1-8: Design of joints. Brussels: European Committee for Standardization. 133 p.

EN 1993-1-9. 2005. Eurocode 3: Design of Steel Structures. Part 1-9: Fatigue. Brussels: European Committee for Standardization. 34 p.

Engesvik, K. M. & Moan, T. 1983. Probabilistic Analysis of the Uncertainty in the Fatigue Capacity of Welded Joints. Engineering Fracture Mechanics, 18:4. P. 743–762.

Fimecc. 2015. BSA – Breakthrough steels and applications [online]. [accessed: 9.6.2015]. Available from: https://www.fimecc.com/programs/bsa.

Fricke, W. 2010. Guideline for the Fatigue Assessment by Notch Stress Analysis for Welded Structures. IIW-document XIII-2240r2-08. 38 p.

Fricke, W. 2013. IIW Guideline for the assessment of weld root fatigue. Welding in the World, 57: 6. P. 753–791.

Hobbacher, A. 2011. The Use of Fracture Mechanics in the Fatigue Analysis of Welded Joints. In: Macdonald, K. A. Fracture and Fatigue of Welded Joints and Structures. Cambridge, UK: Woodhead Publishing. P. 91–112.

Hobbacher, A. 2014. Recommendations for Fatigue Design of Welded Joints and Components. IIW-document XIII-2460-13/XV-1440-13. 164 p.

Iida, K. & Uemura, T. 1996. Stress Concentration Factor Formulae Widely Used in Japan. Fatigue and Fracture of Engineering Materials and Structures, 19: 6. P. 779–786.

Kang, S. W., Kim, W. S. & Paik, Y. M. 2002. Fatigue Strength of Fillet Welded Steel Structure Under Out-of-Plane Bending Load. International Journal of Korean Welding Society, 2: 1. P. 33–37.

Kim, I.-T. & Jeong, Y.-S. 2013. Fatigue Strength Improvement of Welded Joints by Blast Cleaning for Subsequent Painting. International Journal of Steel Structures, 13: 1. P. 11–20.

Laamanen, T. 2013. The Use of FE-analysis in Determining the Ultimate Strength of an S960 QC steel I-profile Beam [in Finnish]. Lappeenranta: 20.9.2013. Master's Thesis. Lappeenranta University of Technology, Laboratory of Steel Structures. 77 p.

Leitner, M., Barsoum, Z. & Schäfers, F. 2015a. Crack Propagation Analysis and Rehabilitation by HFMI of Pre-Fatigued Welded Structures. IIW-document XIII-2583-15. 13 p.

Leitner, M., Mössler, W., Putz, A. & Stoschka, M. 2015b. Effect of Post-Weld Heat Treatment on the Fatigue Strength of HFMI-treated Mild Steel Joints. Welding in the World, 59: 6. P. 861–873.

Lie, S. T., Vipin S. P. & Li, T. 2015. New Weld Toe Magnification Factors for Semi-Elliptical Cracks in Double-Sided T-Butt Joints and Cruciform X-Joints. International Journal of Fatigue, 80. P. 178–191.

Lotsberg, I. & Sigurdsson, G. 2006. Hot Spot Stress S-N Curve for Fatigue Analysis of Plated Structures. Journal of Offshore Mechanics and Arctic Engineering, 128: 4. P. 330–336.

Maddox, S. J. 2015. Allowance for Bending in Fatigue Design Rules for Welded Joints. IIW-document XIII-2580-15. 25 p.

Mbeng, M. 2007. Effective Notch Method Assessment of Misalignment for Fatigue Loaded Welds. Lappeenranta 12.2.2007. Master's Thesis. Lappeenranta University of Technology, Laboratory of Steel Structures. 50 p.

Mettänen, H., Björk, T. & Nykänen, T. 2013. Comparison of Different Methods for Fatigue Assessment of Vibrating Welded Structures. IIW-document XIII-2474-13. 11 p.

Niemi, E. 2003. Levyrakenteiden suunnittelu [in Finnish]. Tekninen tiedotus 2/2003. Helsinki: Teknologiateollisuus. 136 p.

Niemi, E., Fricke, W. & Maddox, S. J. 2006. Fatigue Analysis of Welded Components: Designer's Guide to the Structural Hot-Spot Stress Approach. Cambridge, UK: Woodhead Publishing Ltd. 46 p.

Nykänen, T. & Björk, T. 2015. Assessment of Fatigue Strength of Steel Butt-Welded Joints in as-Welded Condition – Alternative Approaches for Curve Fitting and Mean Stress Effect Analysis. Marine Structures, 44. P. 288–310.

Nykänen, T. Li, X., Björk, T. & Marquis, G. 2005. A Parametric Fracture Mechanics Study of Welded Joints with Toe Cracks and Lack of Penetration. Engineering Fracture Mechanics, 72, 10. P. 1580–1609.

Nykänen, T., Marquis, G., Björk, T. 2007. Effect of Weld Geometry on the Fatigue Strength of Fillet Welded Cruciform Joints. In: Marquis, G., Samuelsson, J., Agerskov, H., Haagensen, P. J. (editors). Proceedings of the International Symposium on Integrated Design

and Manufacturing of Welded Structures, held in Eskilstuna, Sweden 13–14.3.2007. Report 18. Lappeenranta: LTY Digipaino. P. 125–147.

Nykänen, T., Marquis, G., Björk, T. 2009. A Simplified Fatigue Assessment Method for High Quality Welded Cruciform Joints. International Journal of Fatigue, 31: 1. P. 79–87.

Ottersböck, M., Leitner, M. & Stoschka, M. 2015. Effect of Loading Type on Welded and HFMI-treated T-joints. IIW-document XIII-2584-15. 13 p.

Poutiainen, I., Tanskanen, P. & Marquis, G. 2004. Finite Element Methods of Structural Hot Spot Stress Determination – A Comparison of Procedures. International Journal of Fatigue, 26. P. 1147–1157.

Radaj, D. 1990. Design and Analysis of Fatigue Resistant Welded Structures. 1st edition. Cambridge, UK: Woodhead Publishing Ltd. 374 p.

Radaj, D., Sonsino, C. M. & Fricke, W. 2006. Fatigue assessment of welded joints by local approaches. 2nd edition. Cambridge, UK: Woodhead Publishing Ltd. 374 p.

Salehpour, N. 2013. Finite Element Study on Fatigue Strength of Gusset Plate Using Local Approaches. Lappeenranta: 14.8.2013. Master's Thesis. Lappeenranta University of Technology, Laboratory of Steel Structures. 58 p.

Skriko, T. 2014. Väsymiskestävyystutkimukset [in Finnish]. Lappeenranta: 21.3.2014. Research report. Lappeenranta University of Technology, Laboratory of Steel Structures. 36 p.

Sonsino C. M., Fricke W., de Bruyne F., Hoppe A., Ahmadi A. & Zhang, G. 2012. Notch Stress Concepts for the Fatigue Assessment of Welded Joints – Background and Applications. International Journal of Fatigue, 34: 1. P. 2–16.

SSAB. 2015. Strenx 960 MC [online]. [accessed: 30.11.2015]. Available from: http://www.ssab.fi/Products/Brands/Strenx/Products/Strenx-960-MC.

Stresstech. 2014. Xstress 3000 G3 / G3R [online]. [accessed: 21.10.2015]. Available from: http://www.stresstechgroup.com/content/en/1034/74696/Xstress%203000%20G3%20%20%20G3R.html.

Takeuchi, K. 2012. Locations of Strain Gauges for Fatigue Analysis of Welded Joints (1). Welding International, 26: 8. P. 559–566.

Xiao, Z. G., Chen, T. & Zhao, X. L. 2012. Fatigue Strength Evaluation of Transverse Fillet Welded Joints Subjected to Bending Loads. International Journal of Fatigue, 38. P. 57–64.

Fatigue Classifications – Nominal Stress Method (Hobbacher, 2014, p. 63–65).

511	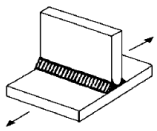	Transverse non-load-carrying attachment, not thicker than main plate K-butt weld, toe ground Two sided fillets, toe ground Fillet weld(s), as welded thicker than main plate	 100 100 80 71	 36 36 28 25	Grinding marks normal to weld toe An angular misalignment corresponding to $\mathbf{k_m = 1.2}$ is already covered
513	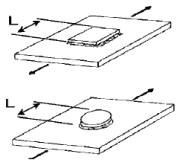	Non-loadcarrying rectangular or circular flat studs, pads or plates. L ≤ 50 mm L >50 and ≤ 150 mm L >150 and ≤ 300 mm L > 300 mm	 80 71 63 50	 28 25 20 18	
521	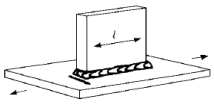	Longitudinal fillet welded gusset of length **l**. Fillet weld around end. l < 50 mm l < 150 mm l < 300 mm l > 300 mm	 80 71 63 50	 28 25 20 18	For gusset on edge: see detail 525. Particularly suitable for assessment on the basis of structural hot spot stress approach.
522	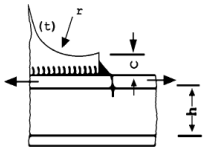	Longitudinal fillet welded gusset with radius transition, fillet weld around end and toe ground, c < 2 t, max 25 mm r > 150 mm	90	32	**t** = thickness of attachment Particularly suitable for assessment on the basis of structural hot spot stress approach.
523	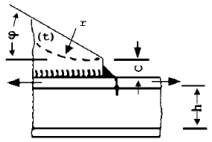	Longitudinal fillet welded gusset with smooth transition (sniped end or radius) welded on beam flange or plate, fillet weld around end. c < 2 t, max 25 mm r > 0.5 h r < 0.5 h or φ > 20°	 71 63	 25 20	**t** = thickness of attachment If attachement thickness < 1/2 of base plat thickness, then one step higher allowed (not for welded on profiles!) Particularly suitable for assessment on the basis of structural hot spot stress approach.
524	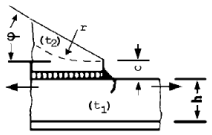	Longitudinal flat side gusset welded on plate edge or beam flange edge, with smooth transition (sniped end or radius), fillet weld around end. c < $2t_2$, max. 25 mm r > 0.5 h r < 0.5 h or φ > 20°	 50 45	 18 16	**t** = thickness of attachment For $t_2 < 0.7\ t_1$, FAT rises 12% Particularly suitable for assessment on the basis of structural hot spot stress approach.

Appendix II

Fatigue Classifications – Hot Spot Stress Method (Hobbacher, 2014, p. 76–77).

3	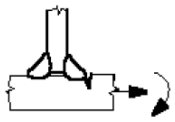	Non load-carrying fillet welds	Transverse non-load carrying attachment, not thicker than main plate, as welded	100	40
5		Cover plate ends and similar joints	As welded	100	40
8	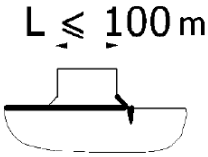	Type “b” joint with short attachment	Fillet or full penetration weld, as welded	100	40
9	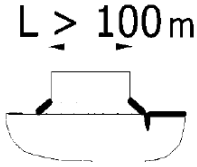	Type “b” joint with long attachment	Fillet or full penetration weld, as welded	90	36

Factors of Effective Notch Stress Method (modified: Radaj, 1990, p. 218–219)

Table III.1. Factor for stress multiaxiality and strength criterion (s). v is Poisson's ratio.

	Tensile and bending loading		Shear and torsional load
	Flat bar	Round bar	
Normal stress hypothesis	2	2	1
Shear stress hypothesis	2	$\frac{2-\nu}{1-\nu}$	1
Octahedral shear hypothesis (von Mises)	$\frac{5}{2}$	$\frac{5-2\upsilon+2\nu^2}{2-2\nu+2\nu^2}$	1
Strain hypothesis	$2+\nu$	$\frac{2-\nu}{1-\nu}$	1
Strain energy hypothesis	$2+\nu$	$\frac{2+\nu}{1-\nu}$	1

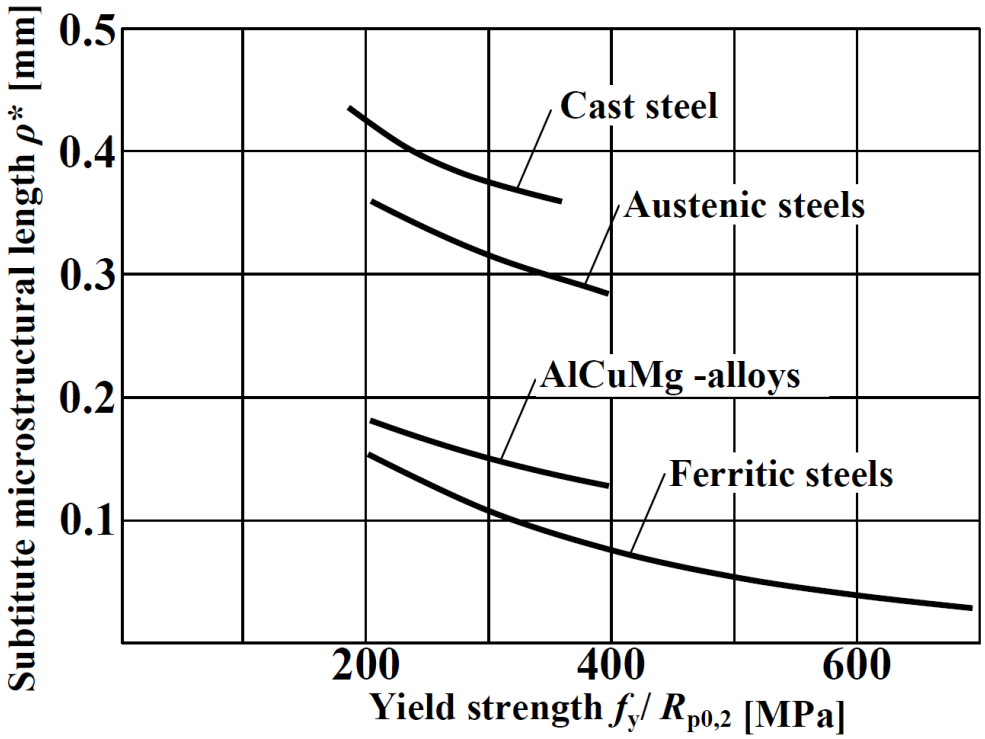

Figure III.1. Substitute microstructural length as a function of yield strength.

Appendix IV

Procedure of Regression Analysis (modified: Hobbacher, 2014, p. 95–96; 149–150)

Determination of fatigue classification by test results ($\Delta\sigma_{test}$, N_{test}).

Basic equation: $\Delta\sigma_{test}{}^{m} \cdot N_{test} = C$

Log-scale: $m \cdot \log \Delta\sigma_{test} + \log N_{test} = \log C$

$x_i = \log C = m \cdot \log \Delta\sigma_{test} + \log N_{test}$

For test results (n<10): fixed slope $m = 3$

Average result for x_i: $x_m = \frac{\sum x_i}{n}$

Standard deviation: $Stdv = \frac{\sum (x_m - x_i)^2}{n-1}$

k factor: as a function of the test data (n). *k* is factor for the calculation of characteristic value

Characteristic value: $x_k = x_m - Stdv \cdot k$

FAT class: mean: $FAT_{mean} = \left(\frac{10^{x_m}}{2 \cdot 10^6}\right)^{\frac{1}{m}}$

characteristic: $FAT_{char} = \left(\frac{10^{x_k}}{2 \cdot 10^6}\right)^{\frac{1}{m}}$

Appendix V

Stress Concentration Factor Formulae by Tsuji (Iida & Uemura, 1996, p. 785–786)

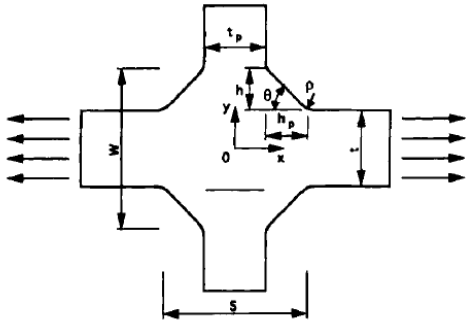

(a) cross joint under tension

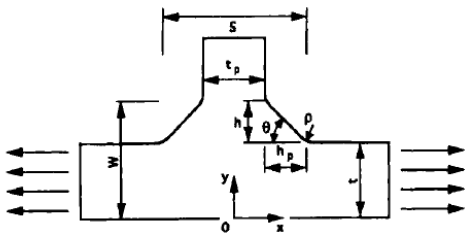

(b) tee joint under tension

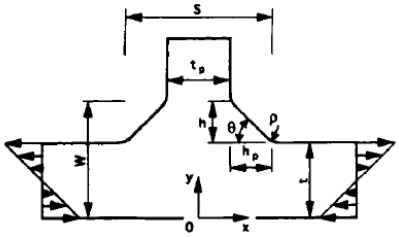

(c) tee joint under bending

k_t factors can be calculated for the presented figures as follows:

$$k_{t,(a)} = 1 + \left[1.347 + 0.397 \ln\frac{S}{t}\right] \cdot Q^{0.467} \cdot f(\theta) \tag{V.2}$$

$$k_{t,(b)} = 1 + 1.015 \cdot Q^{0.446} \cdot f(\theta) \tag{V.3}$$

$$k_{t,(c)} = 1 + \left[0.629 + 0.058 \ln\frac{S}{t}\right] \cdot \left(\frac{\rho}{t}\right)^{-0.431} \cdot \tanh\left(\frac{6h}{t}\right) \cdot f(\theta), \tag{V.4}$$

where

$$f(\theta) = \frac{1 - e^{-0.90 \cdot \theta \cdot \sqrt{W/2h}}}{1 - e^{-0.45 \cdot \pi \cdot \sqrt{W/2h}}} \tag{V.5}$$

$$Q = \frac{1}{2.8 \cdot \left(\frac{W}{t}\right) - 2} \cdot \left(\frac{h}{\rho}\right) \tag{V.6}$$

Bending and Thickness Correction Factor by Maddox (2015, p. 21)

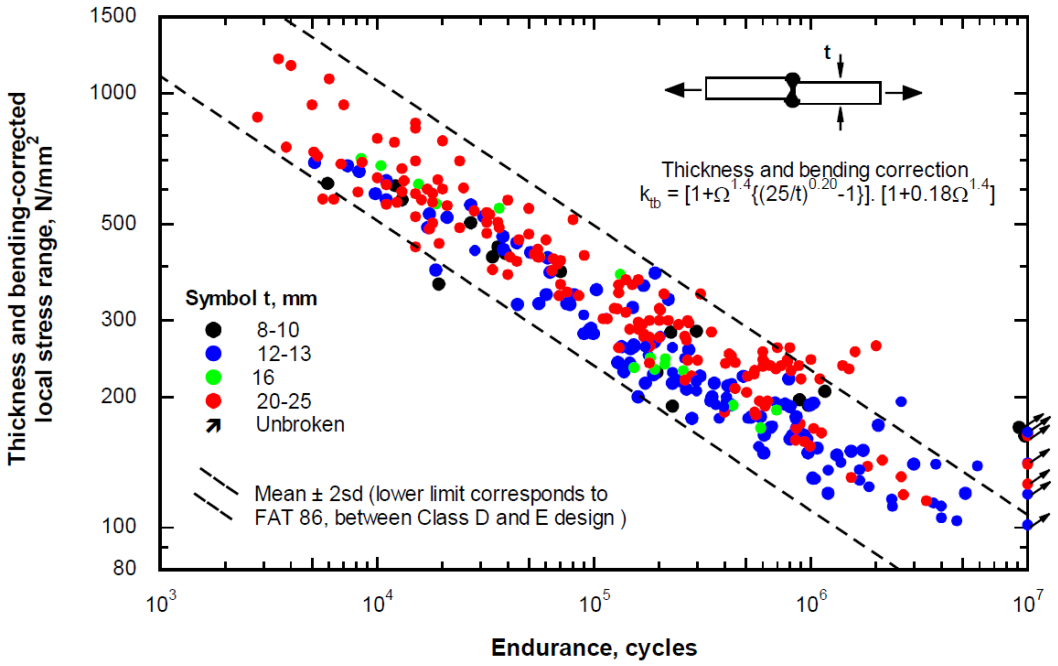

Figure VI.1. Fatigue test results of butt-welded joints.

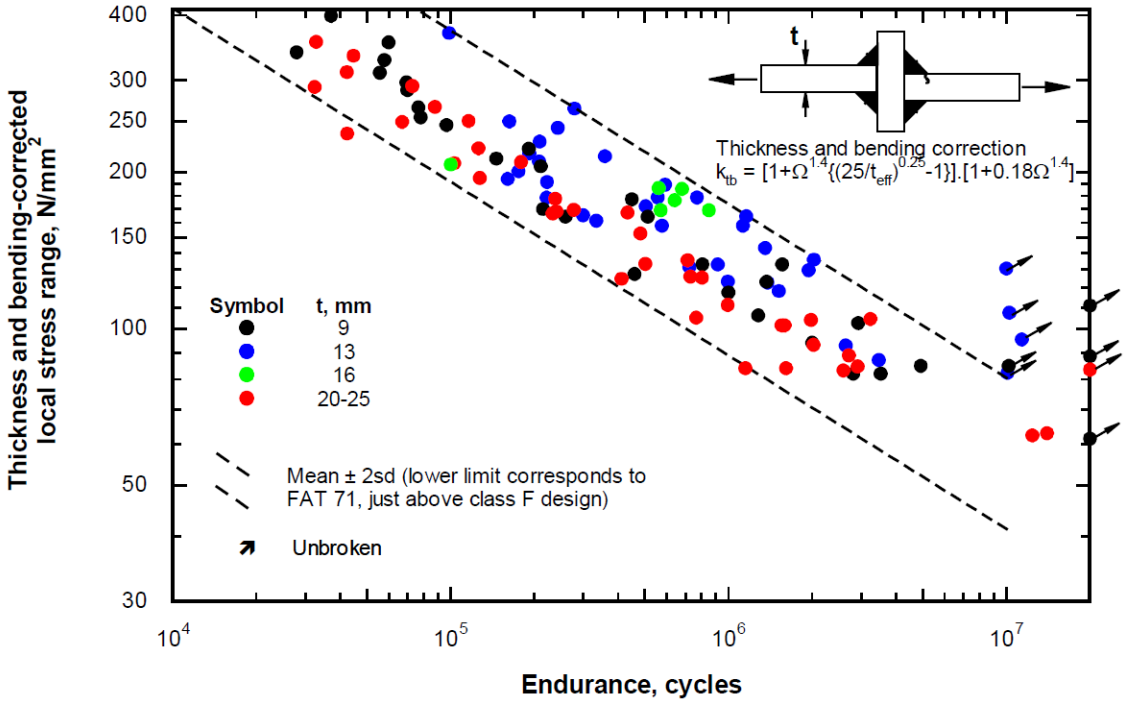

Figure VI.2. Fatigue test results of load-carrying fillet welded joints.

Appendix VII

Welding Parameters of Test Specimens

Table VII.1. Welding parameters of X-joint specimens

Specimen ID	Pass	Current I	Voltage U	[1]Power P	Travel speed v_w	Wire feed speed v_{wire}	Heat input Q	[2]Heat input Q_P	Heat input Q_{loss}	Cooling time $t_{8/5}$
[-]	[-]	[A]	[V]	[W]	[mm/s]	[m/min]	[kJ/mm]	[kJ/mm]	[kJ/mm]	[s]
AAX1	1	230	28.7	6539	5.9	13.2	0.90	0.89	0.79	7.4
	2	229	28.7	6511	5.9	13.2	0.89	0.88	0.79	7.3
	3	231	28.8	6588	5.9	13.2	0.90	0.89	0.79	7.5
	4	229	29	6594	5.9	13.2	0.90	0.89	0.79	7.5
AAX2	1	233	28.8	6661	5.9	13.2	0.91	0.90	0.80	7.6
	2	233	28.7	6649	5.9	13.2	0.91	0.90	0.80	7.6
	3	231	28.9	6623	5.9	13.2	0.91	0.90	0.80	7.6
	4	230	29	6604	5.9	13.2	0.90	0.90	0.80	7.6
AAX3	1	231	28.6	6238	5.9	13.2	0.90	0.85	0.79	7.4
	2	228	28.8	6502	5.9	13.2	0.89	0.88	0.79	7.3
	3	228	28.9	6539	5.9	13.2	0.89	0.89	0.79	7.4
	4	227	29	6523	5.9	13.2	0.89	0.88	0.79	7.4
AAX4	1	232	28.6	6574	5.9	13.2	0.90	0.89	0.79	7.4
	2	231	28.8	6575	5.9	13.2	0.90	0.89	0.79	7.5
	3	227	29	6534	5.9	13.2	0.89	0.89	0.79	7.4
	4	228	28.8	6517	5.9	13.2	0.89	0.88	0.79	7.3
AAX5	1	232	28.6	6581	5.9	13.2	0.90	0.89	0.79	7.4
	2	230	28.9	6580	5.9	13.2	0.90	0.89	0.79	7.5
	3	230	29	6585	5.9	13.2	0.90	0.89	0.80	7.6
	4	230	29	6590	5.9	13.2	0.90	0.89	0.80	7.6
AAX6	1	232	28.6	6590	5.9	13.2	0.90	0.89	0.79	7.4
	2	228	28.7	6481	5.9	13.2	0.89	0.88	0.78	7.3
	3	228	29.1	6576	5.9	13.2	0.90	0.89	0.79	7.5
	4	226	28.9	6469	5.9	13.2	0.89	0.88	0.78	7.3

Table VII.2. Welding parameters of T-joint specimens

Specimen ID	Pass	Current I	Voltage U	[1]Power P	Travel speed v_w	Wire feed speed v_{wire}	Heat input Q	[2]Heat input Q_P	Heat input Q_{loss}	Cooling time $t_{8/5}$
[-]	[-]	[A]	[V]	[W]	[mm/s]	[m/min]	[kJ/mm]	[kJ/mm]	[kJ/mm]	[s]
AAT1	1	231	28.8	6609	5.9	13.2	0.90	0.90	0.79	7.5
	2	230	28.9	6585	5.9	13.2	0.90	0.89	0.79	7.5
AAT2	1	228	28.8	6521	5.9	13.2	0.89	0.88	0.79	7.3
	2	229	28.9	6558	5.9	13.2	0.90	0.89	0.79	7.5
AAT3	1	226	28.7	6447	5.9	13.2	0.88	0.87	0.78	7.2
	2	228	28.9	6528	5.9	13.2	0.89	0.89	0.79	7.4
AAT4	1	229	28.7	6515	5.9	13.2	0.89	0.88	0.79	7.3
	2	229	28.9	6559	5.9	13.2	0.90	0.89	0.79	7.5
AAT5	1	229	28.7	6513	5.9	13.2	0.89	0.88	0.79	7.3
	2	228	28.8	6515	5.9	13.2	0.89	0.88	0.79	7.3
AAT6	1	234	28.8	6672	5.9	13.2	0.91	0.90	0.80	7.7
	2	230	28.9	6598	5.9	13.2	0.90	0.89	0.79	7.5

[1]Power determined by the power unit, which considers losses

[2]Heat input calculated by power ([1])

Table VIII.1. Fatigue classes obtained by LEFM.

			Tensile loading		Bending loading					
	Dimensions		Asymmetric	Symmetric	Asymmetric	Symmetric	Fatigue strength ratio q			
#	Plate thickness t_1	Throat thickness a	$FAT_{m,asym}$	$FAT_{m,sym}$	$FAT_{b,asym}$	$FAT_{b,sym}$	$q_{geom,m}$	$q_{geom,b}$	$q_{load,asym}$	$q_{load,sym}$
	[mm]	[mm]	[MPa]	[MPa]	[MPa]	[MPa]	[-]	[-]	[-]	[-]
1	10	3	78.2	73.4	81.7	88.2	1.07	0.93	0.96	0.83
2	10	5	75.4	68.3	77.3	86.1	1.10	0.90	0.98	0.79
3	10	6	75.2	66.9	76.4	85.8	1.12	0.89	0.98	0.78
4	10	10	75.1	63.5	74.9	85.8	1.18	0.87	1.00	0.74
5	10	12	74.4	62.1	74.3	85.2	1.20	0.87	1.00	0.73
6	10	20	74.9	60.7	74.5	85.4	1.23	0.87	1.01	0.71
7	20	3	74.3	67.3	76.4	84.4	1.10	0.91	0.97	0.80
8	20	5	73.5	64.3	74.2	84.1	1.14	0.88	0.99	0.76
9	20	6	74.1	63.6	73.9	84.4	1.17	0.88	1.00	0.75
10	20	10	75.0	61.9	73.9	85.4	1.21	0.87	1.01	0.72
11	20	12	74.5	61.0	73.7	85.0	1.22	0.87	1.01	0.72
12	20	20	74.9	60.2	74.4	85.3	1.24	0.87	1.01	0.71
13	40	3	70.1	60.2	70.9	81.1	1.16	0.87	0.99	0.74
14	40	5	71.8	59.6	70.5	82.1	1.20	0.86	1.02	0.73
15	40	6	73.0	59.6	70.9	83.0	1.22	0.85	1.03	0.72
16	40	10	75.3	59.7	72.6	84.9	1.26	0.86	1.04	0.70
17	40	12	74.8	59.3	72.8	84.8	1.26	0.86	1.03	0.70
18	40	20	75.0	59.4	74.3	85.1	1.26	0.87	1.01	0.70

Table VIII.2. Fatigue classes obtained by ENS method.

			Tensile loading		Bending loading					
	Dimensions		Asymmetric	Symmetric	Asymmetric	Symmetric	Fatigue strength ratio q			
#	Plate thickness t_1	Throat thickness a	$FAT_{m,asym}$	$FAT_{m,sym}$	$FAT_{b,asym}$	$FAT_{b,sym}$	$q_{geom,m}$	$q_{geom,b}$	$q_{load,asym}$	$q_{load,sym}$
	[mm]	[mm]	[MPa]	[MPa]	[MPa]	[MPa]	[-]	[-]	[-]	[-]
1	10	3	99.6	93.8	93.0	98.7	1.06	0.94	1.07	0.95
2	10	5	94.3	84.6	86.1	95.3	1.11	0.90	1.10	0.89
3	10	6	93.2	81.5	84.5	95.3	1.14	0.89	1.10	0.86
4	10	10	92.2	75.5	82.1	94.5	1.22	0.87	1.12	0.80
5	10	12	92.2	74.0	82.1	95.3	1.25	0.86	1.12	0.78
6	10	20	93.0	72.1	82.1	95.3	1.29	0.86	1.13	0.76
7	20	3	92.2	82.7	82.7	91.5	1.11	0.90	1.11	0.90
8	20	5	91.5	78.1	80.9	92.2	1.17	0.88	1.13	0.85
9	20	6	91.5	76.5	80.4	93.0	1.20	0.86	1.14	0.82
10	20	10	92.2	73.1	80.9	94.5	1.26	0.86	1.14	0.77
11	20	12	92.2	72.6	80.9	94.5	1.27	0.86	1.14	0.77
12	20	20	93.0	71.7	82.1	95.3	1.30	0.86	1.13	0.75
13	40	3	82.7	68.6	71.2	82.7	1.21	0.86	1.16	0.83
14	40	5	87.9	69.4	75.0	88.6	1.27	0.85	1.17	0.78
15	40	6	89.3	69.9	76.0	90.0	1.28	0.84	1.17	0.78
16	40	10	92.2	69.9	78.7	93.8	1.32	0.84	1.17	0.75
17	40	12	93.0	69.9	79.8	94.5	1.33	0.84	1.17	0.74
18	40	20	93.0	70.3	82.1	95.3	1.32	0.86	1.13	0.74

Fatigue Strength Ratios for t_1/t_0 = 0.5 and t_1/t_0 = 1.0

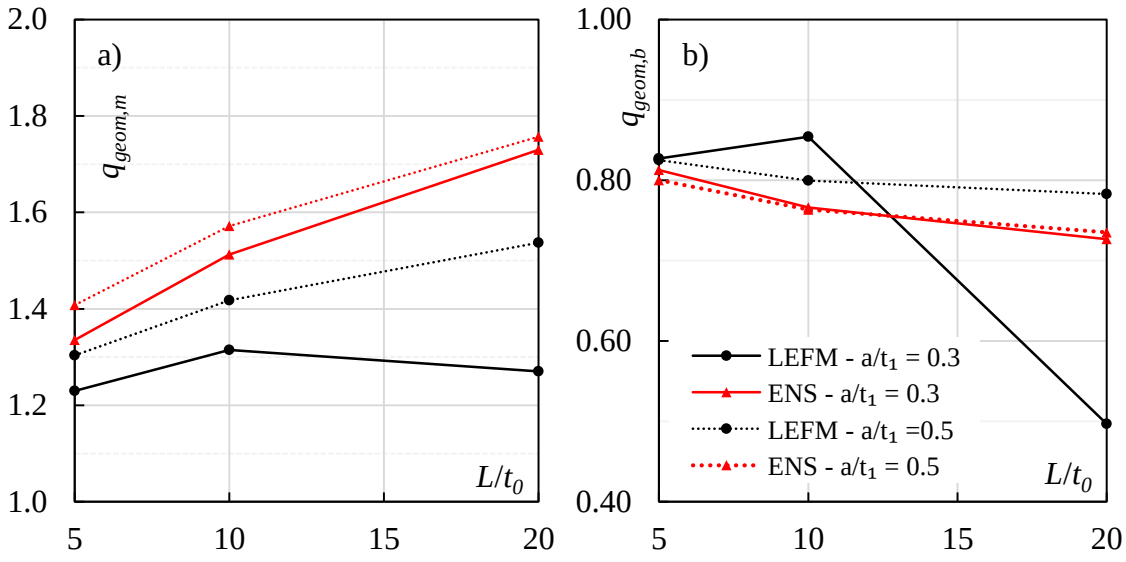

Figure IX.1. Obtained fatigue strength ratios (q_{geom}) of the cover plate joints under (a) tensile and (b) bending loading for t_1/t_0 = 0.5.

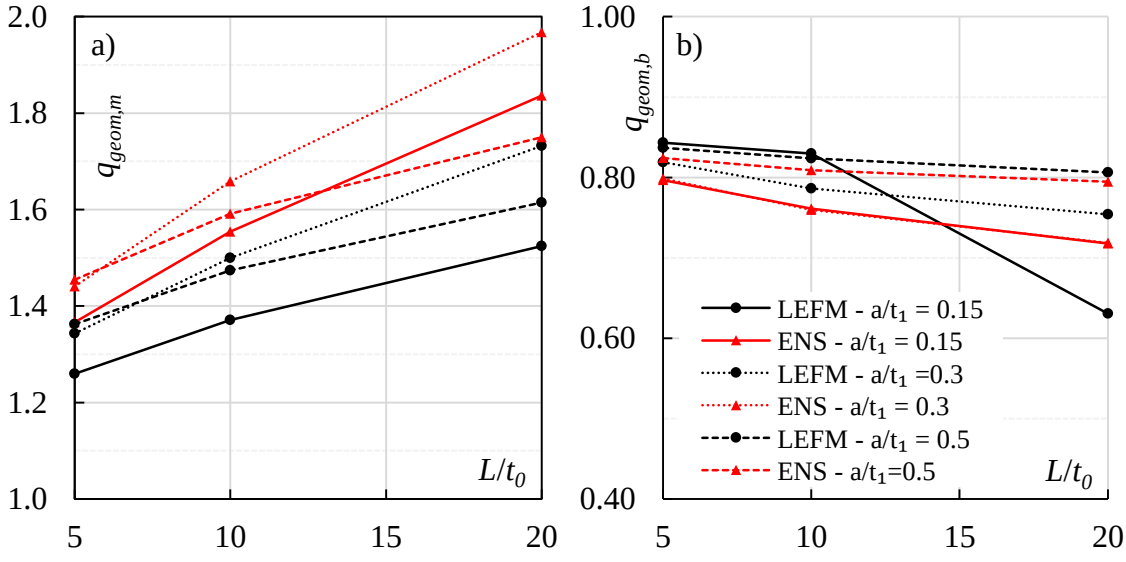

Figure IX.2. Obtained fatigue strength ratios (q_{geom}) of the cover plate joints under (a) tensile and (b) bending loading for t_1/t_0 = 1.0.

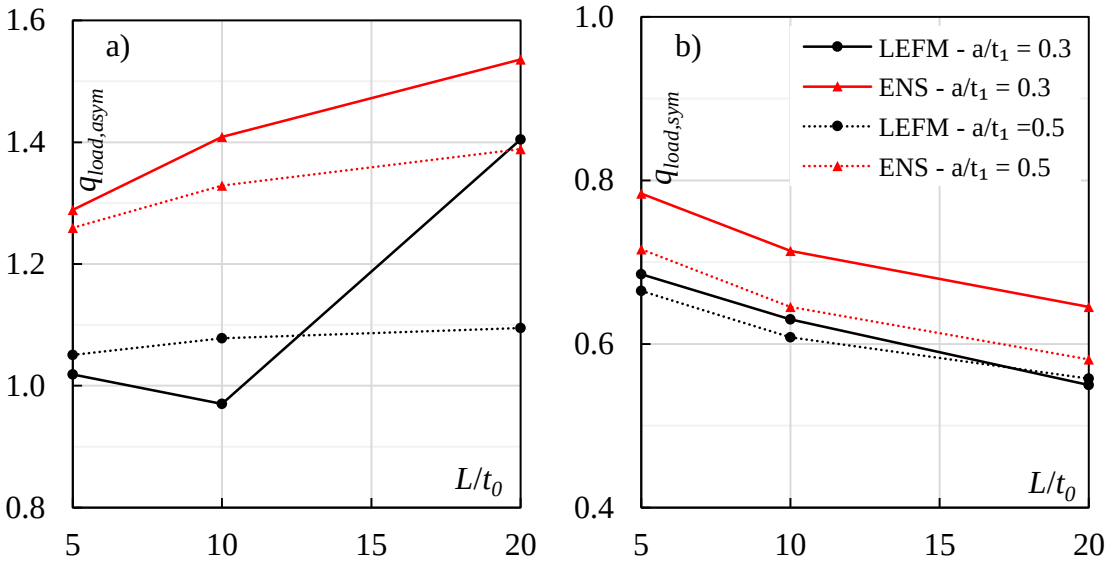

Figure IX.3. Obtained fatigue strength ratios (q_{load}) of the cover plate joints in (a) asymmetric and (b) symmetric joints for t_1/t_0 = 0.5.

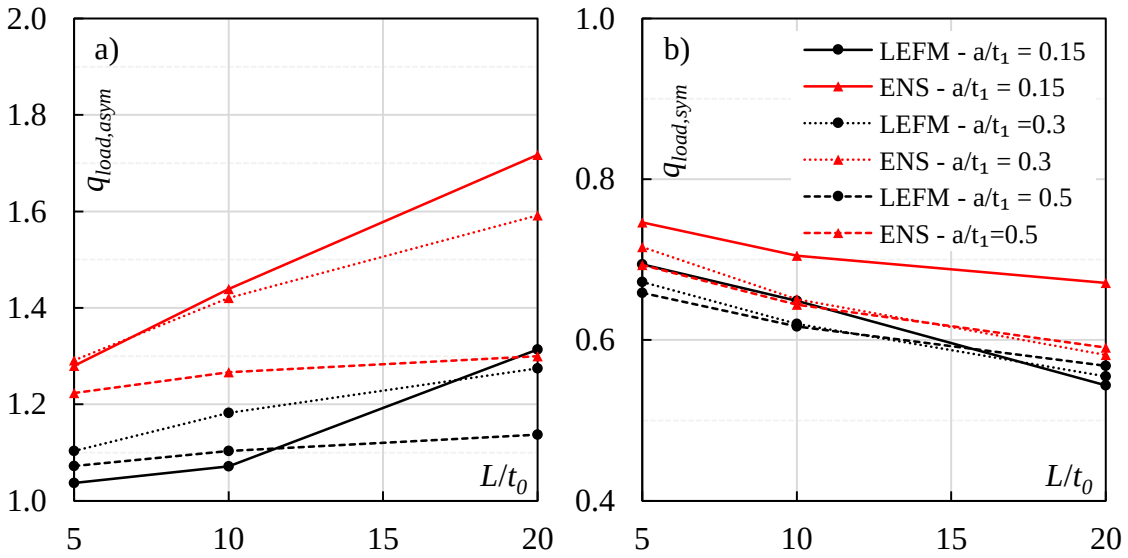

Figure IX.4. Obtained fatigue strength ratios (q_{load}) of the cover plate joints in (a) asymmetric and (b) symmetric joints for t_1/t_0 = 1.0.

Table X.1. Fatigue classes obtained by LEFM.

	Dimensions			Tensile loading		Bending loading		Fatigue strength ratio q			
				Asymmetric	Symmetric	Asymmetric	Symmetric				
#	Plate thickness t_1	Throat thickness a	Length of Attachment L_1	$FAT_{m,asym}$	$FAT_{m,sym}$	$FAT_{b,asym}$	$FAT_{b,sym}$	$q_{geom,m}$	$q_{geom,b}$	$q_{load,asym}$	$q_{load,sym}$
	[mm]	[mm]	[mm]	[MPa]	[MPa]	[MPa]	[MPa]	[-]	[-]	[-]	[-]
1	10	3	100	65.8	53.5	64.6	78.1	1.23	0.83	1.02	0.69
2	10	3	200	61.8	47	63.7	74.6	1.31	0.85	0.97	0.63
3	10	3	400	58	45.67	41.3	83.1	1.27	0.50	1.40	0.55
4	10	5	100	68.3	52.4	65.0	78.8	1.30	0.82	1.05	0.66
5	10	5	200	66.2	46.7	61.4	76.8	1.42	0.80	1.08	0.61
6	10	5	400	64.7	42.1	59.1	75.5	1.54	0.78	1.09	0.56
7	20	3	100	66.9	53.1	64.5	76.5	1.26	0.84	1.04	0.69
8	20	3	200	65.8	48	61.4	74	1.37	0.83	1.07	0.65
9	20	3	400	65.7	43.1	50.0	79.3	1.52	0.63	1.31	0.54
10	20	6	100	72.8	54.2	66	80.6	1.34	0.82	1.10	0.67
11	20	6	200	73.2	48.8	61.9	78.7	1.50	0.79	1.18	0.62
12	20	6	400	73.8	42.6	57.9	76.8	1.73	0.75	1.27	0.55
13	20	10	100	75.5	55.4	70.4	84.1	1.36	0.84	1.07	0.66
14	20	10	200	75.9	51.5	68.8	83.5	1.47	0.82	1.10	0.62
15	20	10	400	76.2	47.2	67	83.1	1.61	0.81	1.14	0.57
16	40	3	100	66	51	63.8	76.5	1.29	0.83	1.03	0.67
17	40	3	200	66.4	46	60.2	74.1	1.44	0.81	1.10	0.62
18	40	3	400	72.1	42.2	63.8	73.3	1.71	0.87	1.13	0.58
19	40	12	100	76.4	56.6	71.2	84.4	1.35	0.84	1.07	0.67
20	40	12	200	77.8	54	70.1	84	1.44	0.83	1.11	0.64
21	40	12	400	79.6	50.2	68.9	83.6	1.59	0.82	1.16	0.60
22	40	20	100	75.3	58.4	74	85.3	1.29	0.87	1.02	0.68
23	40	20	200	75.5	57.1	73.9	85.2	1.32	0.87	1.02	0.67
24	40	20	400	75.7	55.4	73.9	85.2	1.37	0.87	1.02	0.65

Table X.2 Fatigue classes obtained by ENS method.

	Dimensions			Tensile loading		Bending loading		Fatigue strength ratio q			
				Asymmetric	Symmetric	Asymmetric	Symmetric				
#	Plate thickness $t1$	Throat thickness a	Length of Attachment $L1$	$FAT_{m,asym}$	$FAT_{m,sym}$	$FAT_{b,asym}$	$FAT_{b,sym}$	$q_{geom,m}$	$q_{geom,b}$	$q_{load,asym}$	$q_{load,sym}$
	[mm]	[mm]	[mm]	[MPa]	[MPa]	[MPa]	[MPa]	[-]	[-]	[-]	[-]
1	10	3	100	75.5	56.5	58.6	72.1	1.34	0.81	1.29	0.78
2	10	3	200	68.6	45.4	48.7	63.6	1.51	0.77	1.41	0.71
3	10	3	400	62.2	35.9	40.5	55.7	1.73	0.73	1.54	0.65
4	10	5	100	83.3	59.2	66.2	82.7	1.41	0.80	1.26	0.72
5	10	5	200	80.4	51.1	60.5	79.2	1.57	0.76	1.33	0.65
6	10	5	400	78.1	44.5	56.3	76.5	1.76	0.74	1.39	0.58
7	20	3	100	75.0	54.9	58.6	73.5	1.37	0.80	1.28	0.75
8	20	3	200	71.7	46.1	49.8	65.4	1.55	0.76	1.44	0.70
9	20	3	400	70.8	38.5	41.2	57.4	1.84	0.72	1.72	0.67
10	20	6	100	88.6	61.5	68.6	85.9	1.44	0.80	1.29	0.72
11	20	6	200	89.3	53.8	62.8	82.7	1.66	0.76	1.42	0.65
12	20	6	400	90.0	45.7	56.5	78.7	1.97	0.72	1.59	0.58
13	20	10	100	93.0	63.9	76.0	92.2	1.45	0.82	1.22	0.69
14	20	10	200	93.8	58.9	74.0	91.5	1.59	0.81	1.27	0.64
15	20	10	400	93.8	53.6	72.1	90.7	1.75	0.79	1.30	0.59
16	40	3	100	72.1	51.1	56.8	72.6	1.41	0.78	1.27	0.70
17	40	3	200	69.4	42.3	48.7	65.8	1.64	0.74	1.43	0.64
18	40	3	400	72.1	36.4	41.8	59.8	1.98	0.70	1.72	0.61
19	40	12	100	94.5	66.2	78.1	93.8	1.43	0.83	1.21	0.71
20	40	12	200	96.2	62.5	76.5	93.0	1.54	0.82	1.26	0.67
21	40	12	400	98.7	57.7	74.5	92.2	1.71	0.81	1.32	0.63
22	40	20	100	93.0	69.0	81.5	95.3	1.35	0.86	1.14	0.72
23	40	20	200	93.0	67.4	81.5	95.3	1.38	0.86	1.14	0.71
24	40	20	400	93.8	65.0	81.5	95.3	1.44	0.86	1.15	0.68

Appendix XI

Effective Notch Stresses of Longitudinal Gusset Joints

Table XI.1. Effective notch stress factors for b = 50 mm.

		σ_{ENS} / σ_{nom}			
a [mm]	*L* [mm]	$k_{f,asym,t}$	$k_{f,asym,b}$	$k_{f,sym,t}$	$k_{f,sym,b}$
3	75	2.46	3.18	3.05	2.82
3	150	2.46	3.14	3.18	2.82
3	300	2.46	3.14	3.20	2.82
4.5	75	2.37	3.02	2.90	2.72
4.5	150	2.37	3.01	2.96	2.72
4.5	300	2.37	3.01	2.97	2.72
6	75	2.29	2.92	2.81	2.63
6	150	2.30	2.92	2.85	2.64
6	300	2.29	2.92	2.85	2.63

Table XI.2. Effective notch stress factors for b = 200 mm.

		σ_{ENS} / σ_{nom}			
a [mm]	*L* [mm]	$k_{f,asym,t}$	$k_{f,asym,b}$	$k_{f,sym,t}$	$k_{f,sym,b}$
3	37.5	2.70	2.81	4.04	3.89
3	75	2.95	3.38	5.32	4.92
3	150	3.01	3.78	5.67	5.13
3	300	3.02	4.04	5.52	4.99

Measured Shape Laser Data

ID	Throat thickness a [mm]				α_{SL} [10^{-3} rad]	Actual notch radius ρ [mm]			
	*W*1	*W*2	*W*3	*W*4		*W*1	*W*2	*W*3	*W*4
AAT1	4.9	5.0	-	-	23.8	0.2	0.3	-	-
AAT2	5.1	5.3	-	-	19.5	0.2	0.3	-	-
AAT3	5.2	5.2	-	-	25.2	0.3	0.4	-	-
AAT4	5.0	5.1	-	-	22.8	0.4	0.3	-	-
AAT5	5.0	5.2	-	-	20.0	0.4	0.2	-	-
AAT6	5.0	5.0	-	-	24.2	0.3	0.3	-	-
AAX1	5.0	5.1	5.4	5.4	5.1	0.3	0.2	0.3	0.3
AAX2	4.9	5.0	5.1	5.4	3.7	0.3	0.3	0.2	0.2
AAX3	5.0	5.1	5.1	5.4	4.6	0.3	0.3	0.4	0.4
AAX4	5.0	5.0	5.4	5.3	0.8	0.3	0.3	0.3	0.3
AAX5	5.0	5.1	5.4	5.3	5.7	0.2	0.4	0.2	0.3
AAX6	5.2	5.1	5.4	5.3	3.1	0.4	0.2	0.2	0.3

*W*1–*W*4 signify weld pass ID number

Appendix XIII

Fatigue Test Results

Specimen	Joint type	Load type	$\Delta\sigma_{nom}$ [MPa]	$N_{f,test}$ [10^3 cycles]	$k_{m,SL}$	$k_{m,SG}$
AAT1	T-joint	Bending	273	886	-	1.0
AAT2	T-joint	Bending	378	172	-	1.0
AAT3	T-joint	Bending	378	476	-	1.0
AAT4	T-joint	Bending	302	476	-	1.0
AAT5	T-joint	Tension	299	94	1.36	1.26
AAT6	T-joint	Tension	210	400	1.47	1.35
AAX1	X-joint	Bending	275	500	-	1.0
AAX2	X-joint	Bending	378	138	-	1.0
AAX3	X-joint	Bending	378	125	-	1.0
AAX4	X-joint	Bending	307	378	-	1.0
AAX5	X-joint	Tension	378	37	1.10	1.00
AAX6	X-joint	Tension	248	244	1.06	1.01